UiT The Arctic University of Norway

FACULTY OF ENGINEERING SCIENCE AND TECHNOLOGY

A Study of Dynamic Wind Effects on High-Rise Building with Tube-in Tube System in Norway

Son Hoang Pham
Abdelrahman Bassam Abujayyab

Master's thesis in Integrated Building Engineering BYG-3900 May 2023

Acknowledgments

Who knew that a simple Google search could lead to such heights? It's amazing how inspiration can strike in the most unexpected ways. In this case, it was a search about high-rises in Norway that led to the discovery of the spectacular Lilletorget 1 project which became the main inspiration behind this master thesis. After numerous unsuccessful attempts to contact multiple companies and being repeatedly ghosted, we discovered that we were being mistaken for Talkmore telemarketers. Hence, we would like to thank Erlend Nygårdsvoll from Asplan Viak for answering the phone by mistake, which eventually led to a collaboration for this master thesis.

And thus began the seemingly impossible journey to find the one supervisor to rule them all. After fighting against all odds and facing days of relentless hopelessness, Mikhail Khadyko entered chat and decided to take one for the team and get his hands dirty and quickly became the MVP of this thesis.

Therefore, we would like to express our sincere appreciation and deep gratitude to our supervisor, Mikhail Khadyko, for the exceptional guidance provided over the last five months. Your invaluable expertise and experience have allowed us to learn and grow significantly during this time.

In addition to this, we want to thank you for your patience and commitment to helping us, particularly during times when we struggled to learn certain concepts. Your generosity in lending us your dearly personal desktop to run the program, providing motivation when we felt stuck, spending hours assisting us with software-related issues, and offering insightful ideas to solve various problems did not go unnoticed and is highly appreciated.

Besides the academic guidance, Mikhail also provided us with knowledge in music and enlightened us that jazz music indeed has structure and is not as chaotic as it may sound. Lastly, the laughter, the jokes, and the conversations will be missed and remembered.

A special thanks to Mouse Jiggler's overtime dedication so that FEM-Design was able to run analysis smoothly all day without any annoying interruptions from Microsoft's sleeping mode.

On a personal note, we would like to thank our families and friends for the support during these two years. Without them, we wouldn’t be where we are today.

“Jet fuel can’t melt steel beams”-Unknown

Abstract

According to a new high-rise strategy, Norway is expected to have more tall buildings. However, due to a lack of knowledge and experience in high-rise technology, the country has not built many such structures yet. To address this issue, a study was conducted to analyze the response of a high-rise building to dynamic wind load, considering the low seismic activity in the region.

The study is divided into two parts: theoretical and modeling. The theoretical part covers the basics of dynamic structures, FEM-design, material properties, design of wind load, and assessment criteria for high-rise. The modeling part involves constructing a 200-meter-tall high-rise using the tube-in-tube system, with a concrete core and steel frame. The FEM-design was used to construct the structure, and two connection configurations, pinned and rigid, were established for comparison. The design wind load was based on NS-EN 1991 and the wind simulator NOWS.

Based on the results obtained, it was observed that the structure met the serviceability criteria for max top displacement and acceleration comfort criteria. The building also exerted relatively low stresses on structural elements and deformed only elastically when subjected to both quasistatic and dynamic wind load. Furthermore, the results demonstrated NS-EN 1991 as a highly conversative approach for wind design.

Table of contents

List of figures

List of tables

Chapter 1

Introduction

1.1. Background

In Norway, particularly the capital city Oslo, has long been plaguing with the challenge of providing adequate housing for its growing population and for commercial buildings due to limited space. Protecting green spaces is one of the primary reasons behind this challenge. As an urban area with limited space while focusing on preserving green spaces, it is crucial to utilize the available space efficiently. One of the solutions to accommodate this challenge is building higher.

Hence, in the recent years, a new high-rise strategy has been proposed, which allowable buildings height up to 125 meters around Oslo S, while allowing for high-rises up to 70 meters in all other areas. High-rise buildings have been a common feature of central Europe for a long time, but the experience and knowledge of high-rise technology for most contractors, consultants, and advisors in Norway is still limited. To facilitate the construction of new high-rise buildings in Norway, it is crucial to expand knowledge regarding high-rise technology by gathering information from both national and international experiences.

Norway has a low occurrence probability of seismic activity, which makes earthquakes a less significant factor in designing high-rise buildings. Due to the coastal location and varied topography in Norway, wind can be unpredictable and highly variable, which can exert a tremendous pressure on tall buildings. Hence, wind is the dominating factor to consider in the design, and the assessment of wind load will be the main objective of this thesis.

1.2. Problem statement

The primary aim of this thesis to investigate the dynamic behaviour of tall building subjected dynamic wind load. To conduct the parameter study, a tall building at 200 meters in height was constructed using lateral stability system known as tube in tube. The stability system consists of an outer tube made up of a steel frame and an inner tube composed of a concrete core. Two models with different connection configurations were established for the study, one with pinned connection and the other with rigid connection. Quasistatic wind and dynamic wind were applied to assess the following aspects of the two models.

- Does peak value of top displacement satisfy the serviceability limit based on criteria H/500?
- Do stresses in structural elements exceed the yielding limit or eventually the ultimate limit state of the materials?
- What is the peak acceleration of the building at top, and does it satisfy the comfort criteria for acceleration?
- What are differences in wind pressure for quasistatic and dynamic wind?

1.3. Limitation of the study

Due to limited time, the following limitations are imposed to ensure completion of the thesis within the given timeframe:

- The wind data for calculation of quasistatic and dynamic wind is confined to one location, and Trondheim was selected for the parameter study.
- The building is simplified with square shape geometry and to ensure an even and accurate comparison, the same profile of structural elements will be used for both models.
- Tube in tube stability system is supposed to include an outrigger system, which establishes a connection between the outer steel frame and the concrete core, as a mean of transferring most the dead load to the concrete core. The model will be a simplified version without employing outrigger system.
- Steel connection configuration of the two models is confined to pinned with no stiffness and rigid with maximum stiffness. Furthermore, detailed designed of steel connections will not be conducted in this thesis.
- The study does not consider all types of wind loads on surface such as cross wind, shear drag force and turbulence, due to difficulties in obtaining data.

- Power spectral density of wind velocity to produce dynamic wind is limited to one case with a time domain of 180 seconds.
- Approximation of dynamic effects of real wind will be conducted by dividing the building surface into eight sections for different wind loads. Dynamic wind applied will be solely based on this scenario, without additional variations.

Chapter 2

Fundamental dynamic

The chapter is based on Dynamics of Structures: Theory and Applications to Earthquake Engineering (4th Edition) by Anil K. Chopra (Chopra, 2011).

2.1. Equation of motion

Dynamic analysis is the process of analysing the behaviour of a structure or system when subjected to dynamic loads, such as wind and earthquakes. The structure responses to dynamic loads are dependent on the forces that arise within the structure, and these forces are identified as inertia force, viscous force, and elastic force.

The inertia force term is derived from Newtons second law of motion, which states that the net force acting on an object is equal to the mass of the object times acceleration. The mass component in dynamic is considered a constant and depends solely on the amount of material used in the structure. A commonly used technique in structural analysis is the lumped mass method. As the name suggests, this method is based on the assumption that the mass of a given structure is concentrated and assigned at the middle point of the structural elements or nodes rather than being distributed evenly throughout the structure, see figure 2.1 and 2.2.

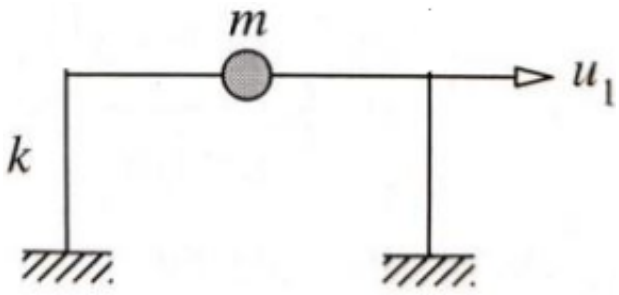

Figure 2.1: Lumping of mass, at middle point of structural member.

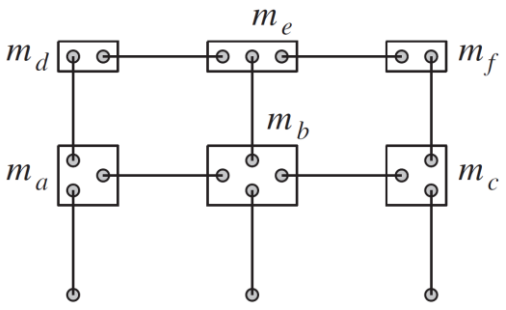

Figure 2.2: Lumping of mass at structural nodes.

Viscous force in general produces damping, which is referred as the energy dissipation of the system, through many mechanisms, such as air resistance, friction at steel connections, opening and closing of microcracks and friction between the structure partition walls. The damping is proportional to the velocity of the system. The final term – the elastic force - is related to the stiffness and displacement. In combination, the three terms describe the dynamic response of the structure when exposed to external excitation force, p(t), and are called the equation of motion, written as equation 2.1.

$$m\ddot{u}(t) + c\dot{u}(t) + ku(t) = p(t) \tag{2.1}$$

The displacement is denoted as u(t), velocity (u̇) and acceleration (ü), where the umlaut represents the differentiation with respect to time. Furthermore, the mass, damping and stiffness of the system are denoted as m, c and k, respectively, and are scalars.

2.2. Single degree of freedom system (SDOF)

Degrees of freedom refer to the number of independent displacements that required to define the motion of all the masses in the structure when disturbed from their static equilibrium position. A single degree of freedom system has one independent displacement, which implies that the mass of the system can only move along one direction. Figure 2.1 is an example of a SDOF system, where the one-story frame has a lateral displacement, u_1. SDOF model is often used to provide a better understanding for analysis of multi-degree of freedom system (MDOF).

2.2.1. Free vibration

Free vibration occurs when a structure undergoes oscillation without any external dynamic excitation. In free vibration, it is idealized that the energy is conserved within the structure and remains the same over time. Therefore, the amplitude of the vibration also stays the same, see figure 2.3. The concept of free vibration provides awareness around the structural response under different conditions and provide optimizing the design of the structure to perform optimally against dynamic excitation. It also provides insight to prevent resonance, which occurs when frequency of external forces matches the natural frequency of the structure. Free vibration of a SDOF can be expressed mathematically as equation 2.2, where external force p(t) and damping c is set to 0.

$$m\ddot{u}(t) + ku(t) = 0 \tag{2.2}$$

The solution to the homogenous differential equation is given as:

$$u(t) = A\cos\omega_n t + B\sin\omega_n t \tag{2.3}$$

where A and B are constants and can be determined by substituting initial displacement u(0) and initial velocity u̇(0) at time zero into equation 2.3. The natural circular frequency of the structure is denoted as ω_n, equation 2.4, and is determined by the mass and stiffness of the structure. The natural circular frequency can be converted to Hz by dividing with 2π, which is referred as the natural cyclic frequency. Both terms are usually referred as natural frequency.

$$\omega_n = \sqrt{\frac{k}{m}}$$
$$f_n = \frac{\omega_n}{2\pi} \tag{2.4}$$

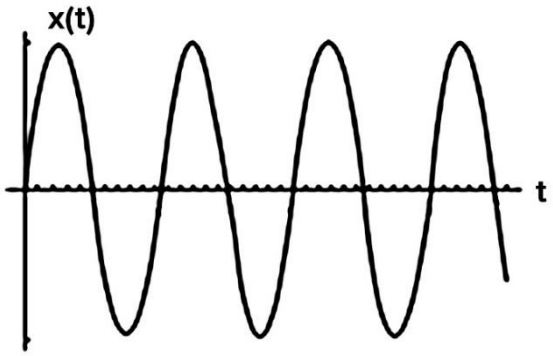

Figure 2.3: Free vibration.

2.3. Damped free vibration

As mentioned earlier, energy conservation in free vibration is a theoretical idea. In real structures, the energy is dissipated by damping mechanisms within the system, which causes the amplitude of vibration to slowly decay over time to equilibrium. Equation 2.1 divides by the mass, gives the governing equation 2.5 for a system with damped free vibration.

$$\ddot{u}(t) + 2\zeta\omega_n\dot{u}(t) + \omega_n^2 u(t) = 0 \tag{2.5}$$

Damping of a system is represented as damping ratio ζ, which is a dimensionless measure depended on the structural mass and stiffness. Damping ratio can be obtained by the damping constant and the critical damping coefficient c_r.

$$\zeta = \frac{c}{c_r} = \frac{c}{2m\omega_n} \tag{2.6}$$

Table 2.1 provides an overview of recommended damping ratios for a variety of structures. Reinforced concrete subjected to stress, which does not exceed halfway of yield point, can be estimated to be to have a damping ratio around 3-5%. The value increases for plastic deformation and the ratio range are estimated to be around 7-10%. For welded steel, bolted and riveted steel, the value is estimated to be the same for linear deformation as in reinforced concrete, and roughly the same for plastic deformation.

Table 2.1 Recommended damping values.

Stress Level	Type and Condition of Structure	Damping Ratio (%)
Working stress, no more than about $\frac{1}{2}$ yield point	Welded steel, prestressed concrete, well-reinforced concrete (only slight cracking)	2–3
	Reinforced concrete with considerable cracking	3–5
	Bolted and/or riveted steel, wood structures with nailed or bolted joints	5–7
At or just below yield point	Welded steel, prestressed concrete (without complete loss in prestress)	5–7
	Prestressed concrete with no prestress left	7–10
	Reinforced concrete	7–10
	Bolted and/or riveted steel, wood structures with bolted joints	10–15
	Wood structures with nailed joints	15–20

There are three types of damping: overdamped, critically damped and underdamped, illustration of the different types of damping is shown in figure 2.4. Critically damped system does not oscillate and returns to its equilibrium system. It represents the transition point between oscillating and nonoscillating motion. In this case $\zeta = 1$. Systems that are overdamped do not oscillate and return to their equilibrium position at a slower rate compared to critically damped system. $\mathrm{Z} < 1$ for

overdamped system. Most structures are underdamped systems, where $\zeta > 1$ and the oscillations with diminishing amplitude occur.

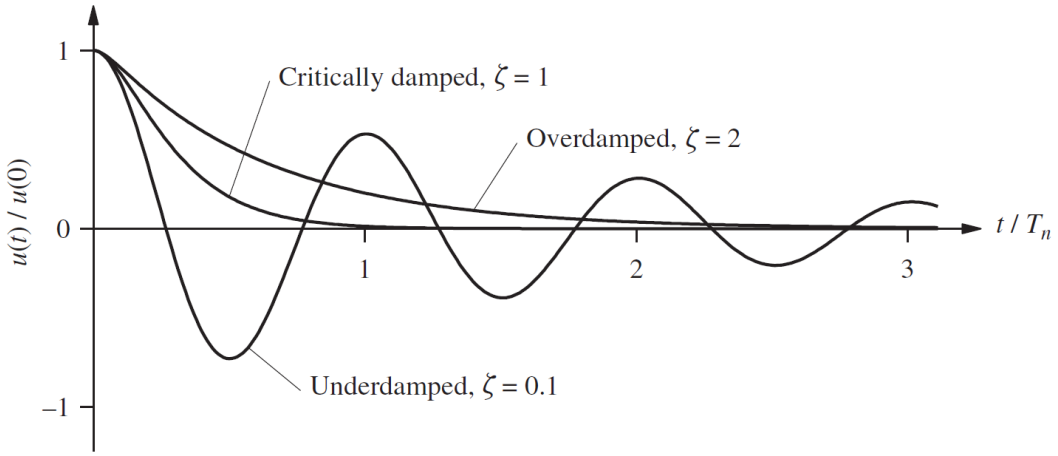

Figure 2.4: Free vibration of underdamped, critically damped, and overdamped systems.

Solution of equation for underdamped structure with initial conditions is given by equation 2.7.

$$u(t) = e^{-\zeta\omega_n t}\left[u(0)cos\omega_D t + \frac{\dot{u}(0) + \zeta\omega_n u(0)}{\omega_D} sin\omega_D t\right] \tag{2.7}$$

Where ω_D is the natural frequency of damped vibration, expressed as equation 2.8.

$$\omega_D = \omega_n\sqrt{1-\zeta^2} \tag{2.8}$$

Damping of a system can be represented theoretically as envelope curves and is given as $\pm\rho e^{-\zeta\omega_n t}$, where ρ is the amplitude of the decreasing oscillation. Figure 2.5 displays the envelope curves of an underdamped system.

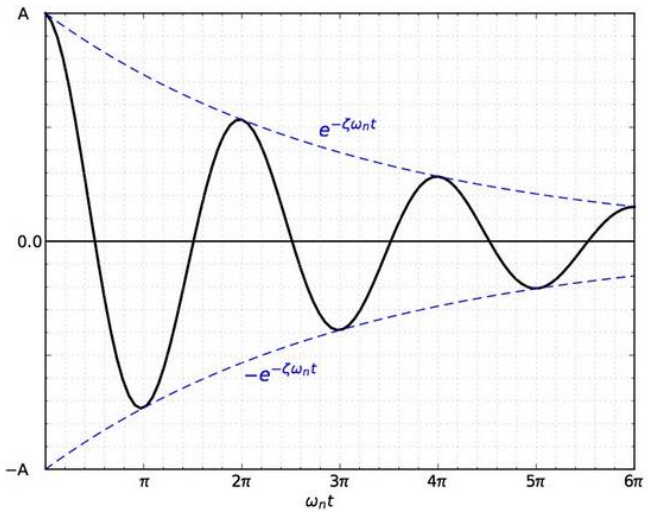

Figure 2.5: Typical response of an underdamped system.

2.4. Multi degree of freedom systems (MDOF)

In multiple degree of freedom systems, there are more independent parameters that dictate the behaviour of the system. In structure, this implies that displacements can occur in multiple directions due to external forces. Hence the involvement of more independent parameters. Scalars in SDOF are reformulated as matrices and vectors in MDOF. The equation of motion can be assembled compactly into matrices and vectors, equation 2.9.

$$\mathbf{m}\ddot{\boldsymbol{u}}(\mathrm{t}) + \mathbf{c}\dot{\mathbf{u}}(\mathrm{t}) + \mathbf{k}\mathbf{u}(\mathrm{t}) = \mathbf{p}(\mathrm{t}) \tag{2.9}$$

The three terms, inertia force, damping forces and elastic forces as matrix and vector form are shown correspondingly in equation 2.10, 2.11, 2.12, where *N* represents the number of DOFs.

$$f_I = \mathbf{m}\ddot{\mathbf{u}} \qquad \begin{bmatrix} f_{I1} \\ f_{I2} \\ \vdots \\ f_{IN} \end{bmatrix} = \begin{bmatrix} m_{11} & m_{12} & \cdots & m_{1j} & \cdots & m_{1N} \\ m_{21} & m_{22} & \cdots & m_{2j} & \cdots & m_{2N} \\ \vdots & \vdots & & \vdots & & \vdots \\ m_{N1} & m_{N2} & \cdots & m_{Nj} & \cdots & m_{NN} \end{bmatrix} \begin{Bmatrix} \ddot{u}_1 \\ \ddot{u}_2 \\ \vdots \\ \ddot{u}_N \end{Bmatrix} \tag{2.10}$$

$$f_D = \mathbf{c}\dot{\mathbf{u}} \qquad \begin{bmatrix} f_{D1} \\ f_{D2} \\ \vdots \\ f_{DN} \end{bmatrix} = \begin{bmatrix} c_{11} & c_{12} & \cdots & c_{1j} & \cdots & c_{1N} \\ c_{21} & c_{22} & \cdots & c_{2j} & \cdots & c_{2N} \\ \vdots & \vdots & & \vdots & & \vdots \\ c_{N1} & c_{N2} & \cdots & c_{Nj} & \cdots & c_{NN} \end{bmatrix} \begin{Bmatrix} \dot{u}_1 \\ \dot{u}_2 \\ \vdots \\ \dot{u}_N \end{Bmatrix} \tag{2.11}$$

$$f_S = \mathbf{k}\mathbf{u} \qquad \begin{bmatrix} f_{S1} \\ f_{S2} \\ \vdots \\ f_{SN} \end{bmatrix} = \begin{bmatrix} k_{11} & k_{12} & \cdots & k_{1j} & \cdots & k_{1N} \\ k_{21} & k_{22} & \cdots & k_{2j} & \cdots & k_{2N} \\ \vdots & \vdots & & \vdots & & \vdots \\ k & k_{N2} & \cdots & k_{Nj} & \cdots & k_{NN} \end{bmatrix} \begin{Bmatrix} u_1 \\ u_2 \\ \vdots \\ u_N \end{Bmatrix} \tag{2.12}$$

The off-diagonal terms in the matrices **m**, **c** and **k** are known as coupling terms, and are dependent on the choice of degrees of freedom to describe the motion. They show the effects of degrees of freedom on each other in terms of mass, stiffness and damping. If there is no coupling relation and DOFs behave completely independently, the terms can be set equal zero, and the equations can be solved independently as single degree of freedom.

2.5. Natural frequencies and mode shapes

Natural frequencies and modes are fundamental concepts in dynamic analysis. Determination of natural frequencies (f_n) and modes (n) of a system is done by modal analysis. A structure has different modes, which describes different deflected shapes during vibration. The vibration of each mode is related to a particular frequency, and it is referred to as the natural vibration frequency of mode shape. Each mode shape is linearly independent of the other mode shapes, which describes a specific way of vibration with a combination of several displacements at the different defined DOF. An example of a two-story frame building with two DOF exposed to horizontal displacements that has two different mode shapes is shown in figure 2.6.

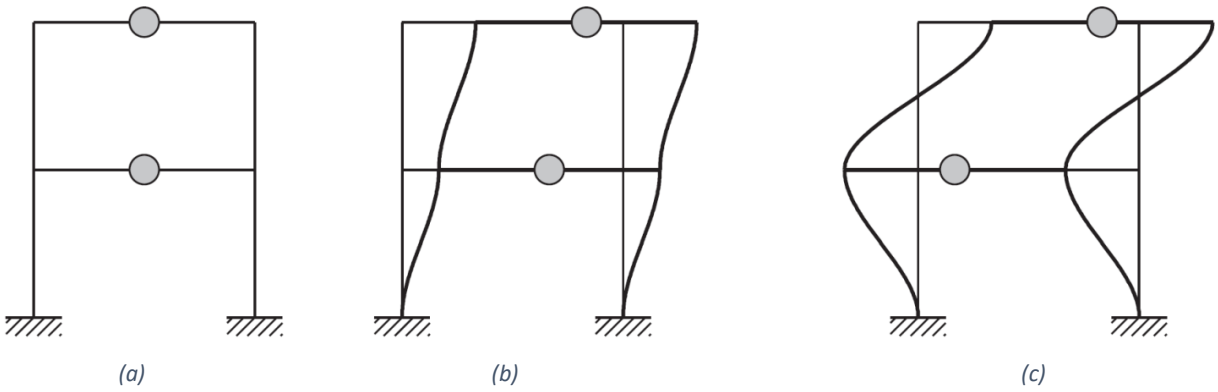

Figure 2.6: a) Static equilibrium, b) First mode shape and c) Second mode shape.

The natural frequencies and mode shapes of the system can be found by solving the governing equation for free vibration given as equation 2.13.

$$\mathbf{m}\ddot{\boldsymbol{u}}(\mathrm{t}) + \mathbf{k}\mathbf{u}(\mathrm{t}) = 0 \tag{2.13}$$

When applied an initial displacement at t= 0, free vibration occurs and is given by equation 2.14, where $q_n(t)$ displays the displacement of the structure at different time instants. Equation 2.15 describes the motion of the structure as simple harmonic function, ϕ_n is a vector describing a combination of displacements in all DOFs that produces mode *n*.

$$\boldsymbol{u}(\mathrm{t}) = q_n(t)\phi_n \tag{2.14}$$

$$\boldsymbol{q_n}(\mathrm{t}) = A\cos\omega_n\, t + B\sin\omega_n\, t \tag{2.15}$$

Equation 2.16 is given by substituting equation 2.15 in equation 2.14, where A and B is determined by the initial conditions as in SDOF.

$$\boldsymbol{u}(t) = \phi_n \left(A \cos \omega_n \, t + B \sin \omega_n \, t\right) \tag{2.16}$$

Furthermore, substituting equation 2.16 in the governing equation 2.13, gives equation 2.17, which is called the matrix eigenvalue problem. Stiffness and mass matrices **k** and **m** are known, while vector ϕ_n and scalar ω_n^2 are unknown.

$$[-\omega_n^2 \boldsymbol{m}\phi_n + \boldsymbol{k}\phi_n] q_n(t) = \boldsymbol{0} \tag{2.17}$$

The equation has a trivial solution, $q_n(t)$=0, which implies that there is no motion in the system. Therefore, the equation can only be satisfied by ω_n and ϕ_n and is rewritten as:

$$[\boldsymbol{k} - \omega_n^2 \boldsymbol{m}]\phi_n = 0 \tag{2.18}$$

The natural frequencies and mode shapes can be obtained by finding the determinant of the characteristic equation 2.19. The equation has one trivial solution, which is $\phi_n = 0$ and implies no motion. Mode shapes are represented as eigenvectors of the matrix.

$$\det[\boldsymbol{k} - \omega_n^2 \boldsymbol{m}] = 0 \tag{2.19}$$

2.6. Rayleigh damping

As mentioned above, the damping properties of a structure involve many mechanisms, which makes it a difficult task to determine the damping ratio of a structure. The damping ratio for existing buildings is determined through experimental data, but this method is costly and time consuming. For new building being designed, the damping property cannot be measured. On that account, modal damping ratio for new buildings is often estimated based on previously measured data on similar structures.

Rayleigh damping is a classical simplified damping model for dynamic structures. This model of damping is a linear combination of the mass and stiffness matrices, which can be expressed as:

$$\boldsymbol{c} = a_0 \boldsymbol{m} + a_1 \boldsymbol{k} \tag{2.20}$$

Where **c, m** and **k** represent the damping, mass, and stiffness matrices, respectively. The damping ratio of *n*th mode can be obtained by equation 2.21.

$$\zeta_n = \frac{a_0}{2}\frac{1}{\omega_n} + \frac{a_1}{2}\omega_n \tag{2.21}$$

The coefficients a_0 and a_1 are constants, with unit sec^{-1} and sec, respectively. The constants are determined by specifying the damping ratios ζ_i and ζ_j for modes i and j of the structure. Equation 2.21 for these two modes can be assembled in matrix form and written as equation 2.22.

$$\frac{1}{2}\begin{bmatrix} 1/\omega_i & \omega_i \\ 1/\omega_j & \omega_j \end{bmatrix}\begin{bmatrix} a_0 \\ a_1 \end{bmatrix} = \begin{bmatrix} \zeta_i \\ \zeta_j \end{bmatrix} \tag{2.22}$$

However, if the damping ratio ζ is estimated to be the same value for the two modes, the constants a_0 and a_1 can be obtained by equation 2.23.

$$a_0 = \zeta\frac{2\omega_i\omega_j}{\omega_i + \omega_j} \qquad a_1 = \zeta\frac{2}{\omega_i + \omega_j} \tag{2.23}$$

The mass and stiffness damping in combination gives Rayleigh damping and can be displayed as a function in figure 2.7. The mass damping component has a greater effect for lower frequencies, while damping for higher frequencies are more dominated by the stiffness damping.

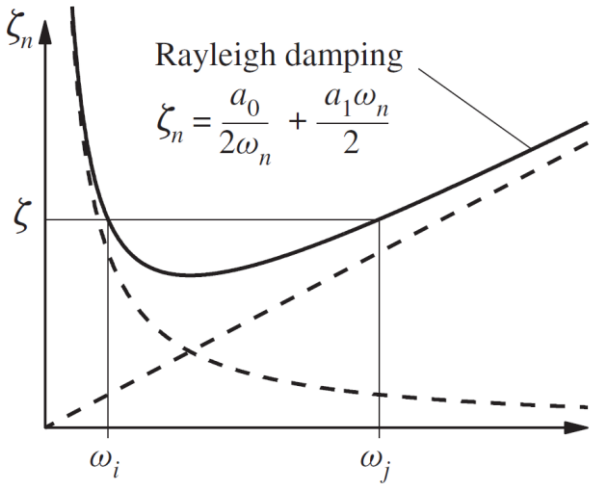

Figure 2.7: Example for Rayleigh damping.

Chapter 3

Mechanical properties

3.1. Stress

Stress is defined as the measure of external force acting on per unit area of an object. The unit of stress is denoted as N/m^2 (SI) and is commonly referred as Pascal with the abbreviation Pa. To fully describe the stress at any point inside the body of a material in a deformed setting, stress tensor is applied. Stress tensor, also known as Cauchy stress tensor, is named after the Augustin-Louis Cauchy.

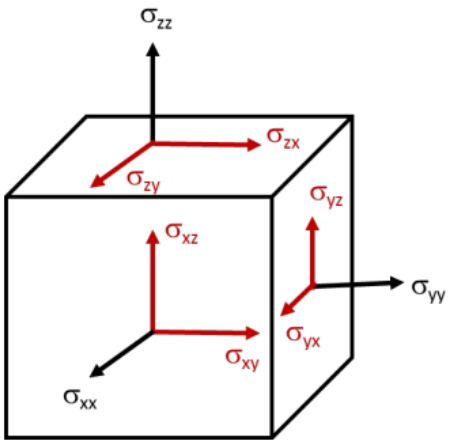

Figure 3.1: The stress components in the coordinate axes (x,y,z).

The stress tensors are of second order and include nine terms, σ_{ij}, where the subscript notation *i* is the direction of the normal to the plane of interest and *j* corresponds to the direction of the stress component (Barbero, 2013). Equation of stress tensor in matrix form is shown in equation 3.1. Since shear stresses across the diagonal that is $\sigma_{xy} = \sigma_{yx} = \sigma_{yz} = \sigma_{zy}$, and $\sigma_{zx} = \sigma_{xz}$ are identical because of static equilibrium. The stress matrix is an assembly of 6 independent components.

$$\begin{bmatrix} \sigma_{xx} & \sigma_{xy} & \sigma_{xz} \\ \sigma_{xy} & \sigma_{yy} & \sigma_{yz} \\ \sigma_{zx} & \sigma_{xx} & \sigma_{zz} \end{bmatrix} \tag{3.1}$$

For a solid body in static equilibrium, the governing differential equation of the stress distribution can be expressed as equation 3.2, where σ is the stress matrix:

$$\begin{matrix} \frac{\partial \sigma_{xx}}{\partial x} + \frac{\partial \sigma_{yx}}{\partial y} + \frac{\partial \sigma_{zx}}{\partial z} = 0 \\ \frac{\partial \sigma_{xy}}{\partial x} + \frac{\partial \sigma_{yy}}{\partial y} + \frac{\partial \sigma_{zy}}{\partial z} = 0 \\ \frac{\partial \sigma_{xz}}{\partial x} + \frac{\partial \sigma_{yz}}{\partial y} + \frac{\partial \sigma_{zz}}{\partial z} = 0 \end{matrix} \quad (3.2)$$

The equation may be derived by considering stress components on the surface of an infinitesimal element. The equation system 3.2 can also be written more compactly as:

$$\mathrm{div}\boldsymbol{\sigma} = 0 \quad (3.3)$$

3.2. Strain

Normal strain is a dimensionless ratio. Given an element that has undergone an infinitesimal deformation, the normal strain can mathematically be expressed by the following equation 3.4 and describes the change in length of the element in the x-direction.

$$\varepsilon_{xx} = \frac{\partial u_x}{\partial x} \quad (3.4)$$

Shear strain occurs when the element undergoes a change in the angle to the original orientation. The shear strain field may be defined from the displacement field by the following relation:

$$\varepsilon_{xx} = \frac{1}{2}\left(\frac{\partial u_x}{\partial y} + \frac{\partial u_y}{\partial x}\right) \quad (3.5)$$

The strain tensors can be assembled in similar fashion as the stress matrix with 6 independent components. The matrix form of strain tensor is given in equation 3.6. The diagonal terms in the matrix represent the normal strains components, while the off-diagonal terms refer to the shear strain components.

$$\begin{bmatrix} \varepsilon_{xx} & \varepsilon_{xy} & \varepsilon_{xz} \\ \varepsilon_{xy} & \varepsilon_{yy} & \varepsilon_{yz} \\ \varepsilon_{zx} & \varepsilon_{xx} & \varepsilon_{zz} \end{bmatrix} \tag{3.6}$$

The strain components are thus partial derivates of the displacement field and the strain tensor can be defined as a displacement gradient and written as:

$$\varepsilon = grad\, \boldsymbol{u} \tag{3.7}$$

3.3. Hooke's Law

The fundamental knowledge in material mechanics is the relationship between stress and strain. This relationship is described by Hooke's Law for linearly elastic materials in certain stress ranges. For small deformation, Hooke's law states that the stress applied to a material is proportional to the strain it experiences. The simplest form of Hooke's law can be represented by the following equation 3.8:

$$\sigma = E\varepsilon \tag{3.8}$$

3.3.1. Anisotropic material

Hooke's law of a three-dimensional elastic body of an anisotropic material can be written in matrix form, equation 3.9 and 3.10, which included 6 components of stress and 6 components of strain that are linearly related to each other. The S is compliance matrix and C represents the stiffness matrix (Barbero, 2013).

$$\begin{matrix} \varepsilon_{xx} \\ \varepsilon_{yy} \\ \varepsilon_{zz} \\ \varepsilon_{yz} \\ \varepsilon_{zx} \\ \lfloor \varepsilon_{xy} \rfloor \end{matrix} = \begin{matrix} S_{11} & S_{12} & S_{13} & S_{14} & S_{15} & S_{16} \\ S_{21} & S_{22} & S_{23} & S_{24} & S_{25} & S_{26} \\ S_{31} & S_{32} & S_{33} & S_{34} & S_{35} & S_{36} \\ S_{41} & S_{42} & S_{43} & S_{44} & S_{45} & S_{46} \\ S_{51} & S_{52} & S_{53} & S_{54} & S_{55} & S_{56} \\ \lfloor S_{61} & S_{62} & S_{63} & S_{64} & S_{65} & S_{66} \rfloor \end{matrix} \begin{matrix} \sigma_{xx} \\ \sigma_{yy} \\ \sigma_{zz} \\ \sigma_{yz} \\ \sigma_{zx} \\ \lfloor \sigma_{xy} \rfloor \end{matrix} \rightarrow \varepsilon = \mathbf{S}\sigma \tag{3.9}$$

$$\begin{matrix} \sigma_{xx} \\ \sigma_{yy} \\ \sigma_{zz} \\ \sigma_{yz} \\ \sigma_{zx} \\ \lfloor \sigma_{xy} \rfloor \end{matrix} = \begin{matrix} C_{11} & C_{12} & C_{13} & C_{14} & C_{15} & C_{16} \\ C_{21} & C_{22} & C_{23} & C_{24} & C_{25} & C_{26} \\ C_{31} & C_{32} & C_{33} & C_{34} & C_{35} & C_{36} \\ C_{41} & C_{42} & C_{43} & C_{44} & C_{45} & C_{46} \\ C_{51} & C_{52} & C_{53} & C_{54} & C_{55} & C_{56} \\ \lfloor C_{61} & C_{62} & C_{63} & C_{64} & C_{65} & C_{66} \rfloor \end{matrix} \begin{matrix} \varepsilon_{xx} \\ \varepsilon_{yy} \\ \varepsilon_{zz} \\ \varepsilon_{yz} \\ \varepsilon_{zx} \\ \lfloor \varepsilon_{xy} \rfloor \end{matrix} \rightarrow \sigma = \mathbf{C}\varepsilon \tag{3.10}$$

Overall, the stiffness and compliance matrix consist of 36 components. Hence the symmetricity in the matrix, there are only 21 components that are independent in Hooke's law.

3.3.2. Isotropic material

Isotropic materials which have the same properties in all direction, because of this symmetry, the only two constants needed to represent the matrix is Young's modulus E and the Poisson's ratio v. The alternative of these two constants K bulk modulus and G shear modulus can also be implemented to in the matrix. These can be derived from equations, by using Young's modulus and Poisson's ratio.

For isotropic material the, the stiffness matrix can be written as:

The compliance matrix form is given by:

$$\begin{matrix}\varepsilon_{xx}\\ \varepsilon_{yy}\\ \varepsilon_{zz}\\ \varepsilon_{yz}\\ \varepsilon_{zx}\\ \lfloor\varepsilon_{xy}\rfloor\end{matrix} = \frac{1}{\mathrm{E}}\begin{bmatrix} 1 & -v & -v & 0 & 0 & 0\\ -v & 1 & -v & 0 & 0 & 0\\ -v & -v & 1 & 0 & 0 & 0\\ 0 & 0 & 0 & 1+v & 0 & 0\\ 0 & 0 & 0 & 0 & 1+v & 0\\ 0 & 0 & 0 & 0 & 0 & 1+v \end{bmatrix}\begin{matrix}\sigma_{xx}\\ \sigma_{yy}\\ \sigma_{zz}\\ \sigma_{yz}\\ \sigma_{zx}\\ \lfloor\sigma_{xy}\rfloor\end{matrix} \tag{3.11}$$

$$\begin{matrix}\sigma_{xx}\\ \sigma_{yy}\\ \sigma_{zz}\\ \sigma_{yz}\\ \sigma_{zx}\\ \lfloor\sigma_{xy}\rfloor\end{matrix} = \frac{E}{(1+v)(1-2v)}\begin{bmatrix} 1-v & v & v & 0 & 0 & 0\\ v & 1-v & v & 0 & 0 & 0\\ v & v & 1-v & 0 & 0 & 0\\ 0 & 0 & 0 & 1-2v & 0 & 0\\ 0 & 0 & 0 & 0 & 1-2v & 0\\ 0 & 0 & 0 & 0 & 0 & 1-2v \end{bmatrix}\begin{matrix}\varepsilon_{xx}\\ \varepsilon_{yy}\\ \varepsilon_{zz}\\ \varepsilon_{yz}\\ \varepsilon_{zx}\\ \lfloor\varepsilon_{xy}\rfloor\end{matrix} \tag{3.12}$$

3.4. Boundary value problem

In engineering, determination of materials behaviours under different loading conditions are an essential aspect for the design and analysis process. In order to determine all the forces and displacements of a material body, certain conditions around the boundary of the body must be specified and considered, to find the internal stresses and strains. This is also known as the boundary value problem (BVP). In other words, this structure analysis problem involves finding the solution to a differential equation, with specified boundary conditions.

In material mechanics, there are two types of boundary conditions, which is displacement boundary condition and traction boundary condition. The displacement boundary conditions specify the geometric constraints that are imposed on some portion of total boundary surface of the material, and deformation of the body is dependent on these constraints (P.A., n.d.). The boundary condition is denoted as $\mathbf{u} = \bar{\mathbf{u}}$, where the overbar indicates the prescribed constraint portion. Traction boundary condition is the prescribed distribution of forces on the boundary of the material and is expressed as $\mathbf{t} = \boldsymbol{\sigma}\mathbf{n} = \bar{\boldsymbol{t}}$, where ***n*** is the normal vector of the surface. Figure 3.2 illustrates boundary conditions of

a body. For a body with specified displacements and tractions over a certain portion of the surface $s_u$and s_σ, the boundary conditions of the body are given as:

$$\begin{aligned} \mathbf{t} = \boldsymbol{\sigma}\mathbf{n} = \bar{\boldsymbol{t}}, \qquad & \text{on } s_\sigma \\ \mathbf{u} = \bar{\mathbf{u}}, \qquad & \text{on } s_u \end{aligned} \tag{3.13}$$

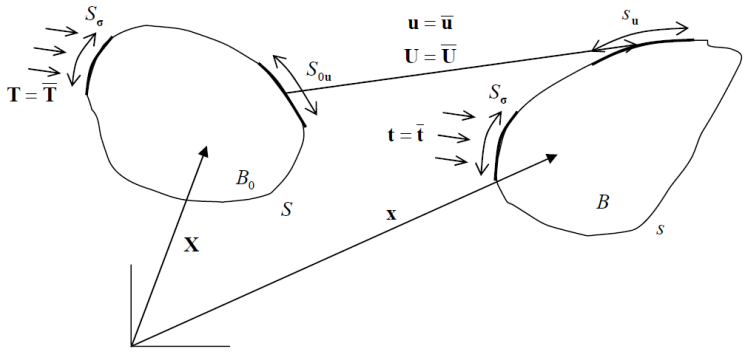

Figure 3.2: Displacement and traction boundary conditions of a domain (P.A., n.d.).

The stress field in the body must satisfy the equilibrium equation 3.2, which is the main differential equation of the material mechanics. The equation must be solved for the aforementioned boundary conditions. The displacement is implicitly included in the equation because the stress depends on the strain and therefore the displacements through the elasticity and plasticity laws (constitutive equations).

3.5. Concrete

Concrete has a long history and has been used as a building material for thousands of years throughout history. Concrete is one of the most common materials used in construction, which is typically consists of cement, sand, and aggregates such as stone and gravel. Cement is produced by burning limestone and acts as the glue that binds the sand and aggregates together, while the sand is used to fill the gaps between the aggregates. The choice of aggregates can affect the strength, stiffness, and durability of the concrete. The strength and durability of concrete can be affected by various factors during the production process. Some of these factors include the quality of the materials and the amount of water used in the concrete mixture, additionally to the time and temperature during the curing process. Concrete strength is usually measured in terms of compressive strength, which indicates the amount of pressure the concrete can withstand before cracking occurs (Thue, 2019).

There are several types of concrete used in structures, and each type has different properties. Some of the most common types include normal, lightweight and heavyweight concrete. Normal concrete is

the most used type, with a density ranging from 2000 - 2600 kg/m³. While heavyweight concrete has a density between 2600 kg/m³ - 5600 kg/m³ and can be achieved by using heavy aggregates. Additionally, concrete has several classes based on its strength and durability properties. Concrete in class C30/37, for example, should withstand a characteristic compressive strength of 30 MPa and a maximum compressive strength of 37 MPa (Kontrollbetong, n.d.).

3.6. Steel mechanical properties

Steel is amongst the most common building material used in structures. Therefore, understanding steel mechanical properties is essential to comprehend steel constructions behaviours during deformation. Parameters such as elastic modulus, elasticity, plasticity, and ductility are especially in interest when it comes to designing steel elements.

3.6.1. Elasticity properties

Steel is an elastoplastic material, which indicates the material have both elastic properties and plastic properties. Elastic properties refer to the ability of the material to return to its original shape after being deformed. In the process deformation, the initial deformation phase is called elastic deformation, where the relationship of stress and strain is linear, figure 3.3.

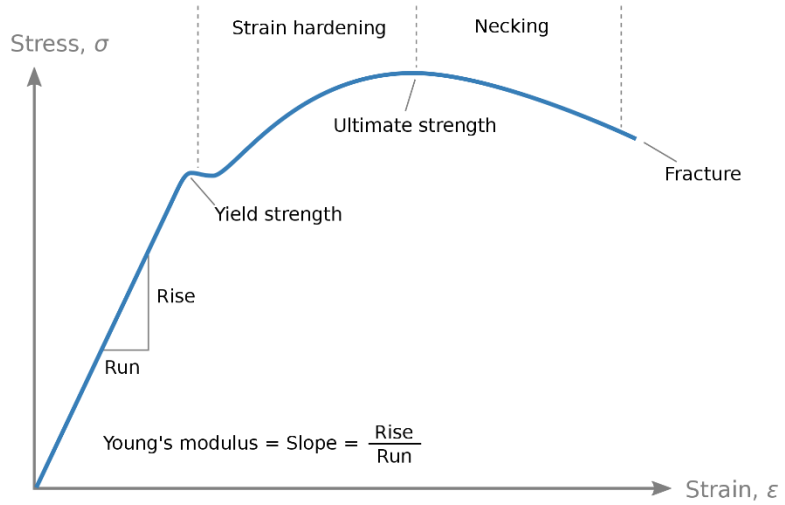

Figure 3.3: Stress–strain curve (Wikipedia, 2023).

3.7. Plasticity properties

Plastic properties refer to a ability of the material to permanently deform without breaking. Plastic deformation occurs when the material exceeds its elastic limit. At the time when the steel element is deformed beyond its elastic limit, the stress and strain is no longer proportional and will develop a non-linear relationship curvature as shown in figure 3.3.

The most important plastic property of steel is its yield strength, which is the stress at which a material begins to deform plastically. The yield strength of steel can vary depending on the type and grade of steel. Deformation after the yield point makes the metal gradually stronger and it requires an increase in stress for further plastic deformation, this process is called work hardening, see figure 3.3.

3.8. von Mises yield criterion

For mechanics problem that involves complex loading conditions of a ductile material, von Mises yield criterion σ_{vm} can be implemented to estimate when yielding will occur and ultimate limit state of the material. The von Mises yield criterion can be expressed mathematically as equation 2.36, where σ is the normal stresses and τ is the shear stresses.

$$\sigma_{vm} = \sqrt{\sigma_{xx}^2 + \sigma_{yy}^2 + \sigma_{zz}^2 - (\sigma_{xy} + \sigma_{yz} + \sigma_{zx} + 3\big(\tau_{xy}^2 + \tau_{yz}^2 + \tau_{zx}^2\big)} \qquad (2.36)$$

3.9. Connections

Joints are locations where two or more bars meet and are fastened together. Joints are an important construction detail that bind the structure together and consist of several components. Joints can transfer load between the fastened construction components, such as a joint between a beam and a column transfers a shear force in the beam to the axial force in the column. Joints are of great importance for the behaviour of the construction; therefore, it is important to determine the capacity and stiffness of the joints in relation to design moments and loads. Steel connections can be made with screws, nails, bolts, or welding (Norsk Standard, 2009b, 2015).

The design of steel structures in Norway is carried out according to NS-EN 1993 Eurocode 3, where Part 1 covers general rules and rules for buildings, and Part 8 covers joints and connections.

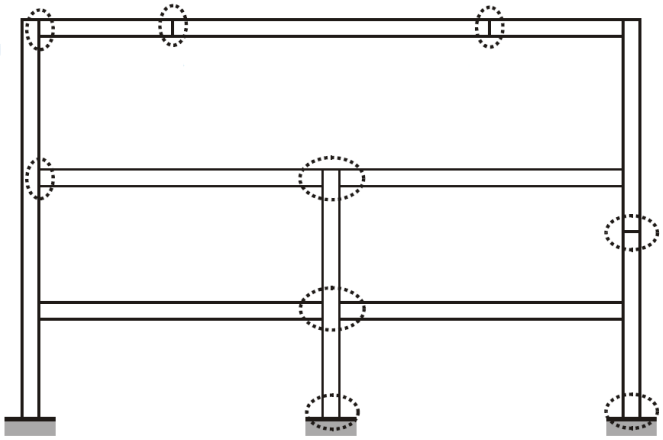

Figure 3.4: Different types of joint configurations (Norsk Standard, 2009b).

3.9.1. Classification of joints

Norwegian Standard distinguishes between three joint models: pinned, rigid (continuous), and partially rigid (semi-continuous), as illustrated in figure 3.5. The choice of joint model determines whether the moment-rotation relationship at the joint should be included in the global analysis or not. In NS-EN 1993 part 8, the joints are classified according to their stiffness and strength (Norsk Standard, 2009b).

A joint can be defined as pinned, rigid or semi-rigid based on its rotational stiffness. Joint configuration is determined by comparing the initial rotational stiffness, $S_{j,ini}$, of the joint with the classification limits displayed in figure 3.5. A pinned joint should be able to transfer load effects without creating moments that can affect the connected members or the structure. Hence the pinned joint should not transfer bending moments, and the initial rotation stiffness $Sj \leq 0{,}5 * EI_b/L_b$. Rigid joints are fixed and stiff, which should not undergo substantial deformation under applied moments. Joint must have sufficient rotational stiffness to be considered as fully rigid in the analysis. The joint is classified as rigid if $Sj \geq k_b EI_b/L_b$. In the case where the joint does not meet the criteria for either pinned or rigid, it can then be classified as a partially rigid joint. The different variables for the classification formula are defined in figure 3.5.

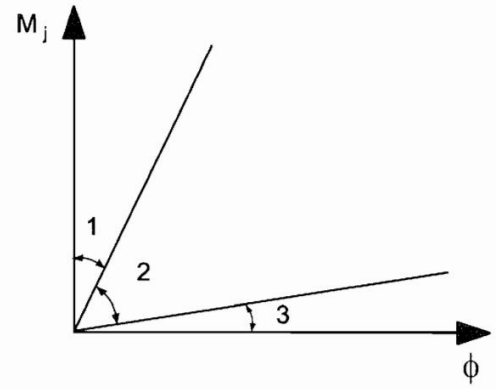

Zone 1: rigid, if $S_{j,ini} \geq k_b EI_b / L_b$

where:

$k_b = 8$ for frames where the bracing system reduces the horizontal displacement by at least 80 %

$k_b = 25$ for other frames, provided that in every storey $K_b/K_c \geq 0,1$ *)

Zone 2: semi-rigid

All joints in zone 2 should be classified as semi-rigid. Joints in zones 1 or 3 may optionally also be treated as semi-rigid.

Zone 3: nominally pinned, if $S_{j,ini} \leq 0,5 EI_b / L_b$

*) For frames where $K_b/K_c < 0,1$ the joints should be classified as semi-rigid.

Key:

K_b	is	the mean value of I_b/L_b for all the beams at the top of that storey;
K_c	is	the mean value of I_c/L_c for all the columns in that storey;
I_b	is	the second moment of area of a beam;
I_c	is	the second moment of area of a column;
L_b	is	the span of a beam (centre-to-centre of columns);
L_c	is	the storey height of a column.

Figure 3.5: Classification of joints according to stiffness (Norsk Standard, 2009b).

When joints are classified by strength, the design moment capacity, $M_{j,Rd}$, for the joint is compared to the design moment capacity for the members connected at the joint. For the design of pinned joint, the moment capacity should be less than 25% of the members connected to the joint. Pinned joints should be able to accommodate the rotation created by the design loads. The design capacity for rigid joints should be equal to or greater than the beam or column meeting at the joint, so they can transfer moments. Partially rigid joints should transfer all resulting load effects including partially the moments, and these partial moments should be considered in the global analysis (Norsk Standard, 2009b).

Capital 4

Finite element method (FEM)

As mentioned earlier, the boundary value problem involves finding solution to a set of differential equations with that are constraint by boundary conditions. For 2D and 3D problems that involve complex geometries, boundary conditions and nonlinear material properties, which include many variables and unknowns, which makes it challenging to obtain the analytical solution. Hence the suitable approach to solve such problems is to acquire approximate solution by FEM. The basic idea behind FEM is to divide the complex structure into many small elements, as shown in figure 4.1, and then solving the problem within each element independently. The solutions within the individual elements are then combined to give an overall solution for the entire problem (Kurowski, 2016).

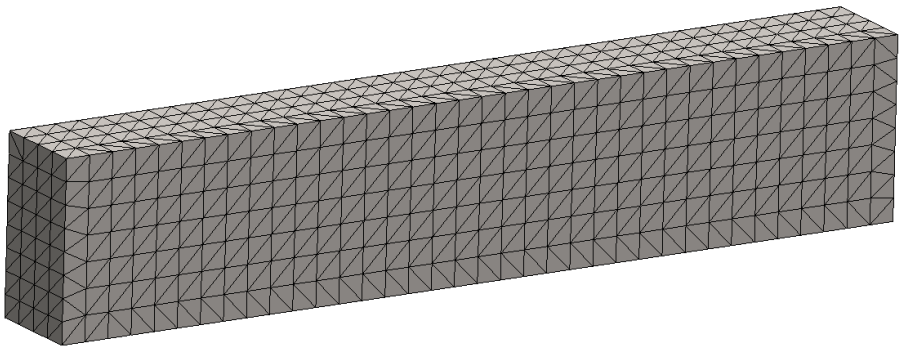

Figure 4.1: Mesh of simple beam.

4.1. Principle of virtual work

FEM utilizes the principle of virtual work to solve governing differential equations with specified boundary conditions. By this method, the virtual displacements and deformations resulted by forces that are acting on the body can be determined. Virtual displacement $\delta \boldsymbol{u}$ is considered an infinitesimal deformation of a body and is referred as arbitrary or hypothetical displacement. The principle of virtual work states that the total external virtual work subjected to a body must be equal to the virtual work done by internal forces. In other words, the work that results in deformation by external loads and

body forces is equivalent to work by the internal stresses over the strains that occur in the body. The principle of virtual work in spatial form is expressed as:

$$\int_{s_\sigma} \boldsymbol{t} \cdot \delta\mathbf{u} ds + \int_{V} \boldsymbol{b} \cdot \delta\mathbf{u} dV = \int_{V} \boldsymbol{\sigma} : \mathrm{grad}(\delta\mathbf{u}) dV + \int_{s_\sigma} \rho\ddot{\mathbf{u}} \cdot \delta\mathbf{u} ds \tag{4.1}$$

Where first term is the work of external forces $\boldsymbol{t}$ on the virtual displacement $\delta\mathbf{u}$, second term is the work of body forces $\boldsymbol{b}$ on the same virtual displacement, third term is the internal work of the stress field $\boldsymbol{\sigma}$ on the virtual strain field $\mathrm{grad}(\delta\mathbf{u})$ and last term is the work of the inertial forces $\rho\ddot{\mathbf{u}}$ on the virtual displacement.

In instances where the traction acting on a body is significantly greater than its body force and body dynamic, the latter mentioned two terms is insignificant. Thus, the equation 4.1 can be reduced to:

$$\int_{s_\sigma} \boldsymbol{t} \cdot \delta\mathbf{u} ds = \int_{V} \boldsymbol{\sigma} : \mathrm{grad}(\delta\mathbf{u}) dV \tag{4.2}$$

It may be shown that the work equation, 4.1, and stress equilibrium equation 3.2, are equivalent and may be derived from each other.

The discretized work concept is about dividing the body into smaller elements which are interconnected with nodes at the end point of the elements. These nodes represent the degree of freedom in which the nodes can translate, also referred as nodal displacements. The total displacement *u* of the body in any point between the nodes can be expressed by the sum of the defined shape functions N_i of each degree of freedom times the defined nodal displacements d_i of the defined nodes (Kurowski, 2016).

$$u = \sum N_i d_i \tag{4.3}$$

The shape functions are most often polynomial function used to interpolate the displacement field over each element and may be first order, second order and rarely higher. In first order, shape function is linear and is defined as a straight line which connects the two nodes of the element. In contrast, second-order shape function is quadratic polynomial which offers better accuracy of the approximated solution, because the quadratic shape function can capture the curvatures of the element (Kurowski, 2016), figure 4.2.

(a) *(b)*

Figure 4.2: a) First order element b) second order element.

When the shape function has been established, it is further used to assemble the stiffness matrix component. As mentioned above, strain is defined as the gradient of displacement u. Therefore, the definition of strain can be rewritten as:

$$\varepsilon = \text{grad}\ \mathbf{u} = \text{grad}\ \mathbf{Nd} = \mathbf{Bd} \tag{4.4}$$

The gradient of the shape function matrix, $\text{grad}\ \mathbf{N}$ is denoted as **B** and the nodal displacement vector is taken out of the gradient function as it is independent on the coordinates. The strain here is written as a vector in Voigt notation for convenience. Furthermore, stress tensor from equation 4.2 (reduced virtual work equation) can be replaced by the product of strain and compliance stiffness matrix or the elastic law, hence it can be rewritten as:

$$\int_{s_\sigma} \boldsymbol{t} \cdot \delta\mathbf{u} ds = \int_{v} \boldsymbol{\varepsilon^T C} : \text{grad}(\delta\mathbf{u}) dv \tag{4.5}$$

Substitute equation 4.4 in equation 4.5 and replacing the integral of tractions over displacement field with a equivalent sum of work of the forces in the nodes over the nodal displacements gives:

$$\sum \mathbf{r} \cdot \delta\mathbf{d} = \int_{\mathbf{v}} \mathbf{B^T}\ \mathbf{d}\ \mathbf{C}\ \mathbf{B}\ \delta\mathbf{d}\ \text{dv} \tag{4.6}$$

Where $\mathbf{r}$ is the nodal forces and $\delta\mathbf{d}$ is the virtual displacement. Summation is over the nodal DOFs. Infinitesimal displacements is arbitrary and therefore can be removed, and the previous equation can be rewritten as:

$$\mathbf{r} = \int_V \mathbf{B}^T \boldsymbol{C}\ \mathbf{B}\, dV\mathbf{d} \tag{4.7}$$

Where $\mathbf{d}$ is the nodal displacements and volume integral $\int_V \mathbf{B}^T \boldsymbol{C}\ \mathbf{B}\, dV$ is the stiffness matrix. Once the element stiffness matrices are assembled, it is used to construct the global stiffness matrix for the entire system. The global stiffness matrix is then used to solve the system of equations for the unknown nodal displacements and forces, which gives the final solution for the problem. The volume integral in the stiffness matrix is found by numerical integration with Gauss method. The strains are then found from equation 3.7 and the stresses from equation 3.12.

4.2. Linear/ non-linear

Finite element analysis differentiates between linear and non-linear analysis. Parameters such as material properties, boundary conditions, and magnitude of displacements will influence which analysis is performed for the issue. In linear analysis, these parameters are linear, and the analysis is confined to solving problems with small strains and infinitely small displacements. Non-linear models consider large displacements and non-linear elastoplastic materials as well as dynamic problems. During a non-linear analysis, the stiffness matrix does not remain constant throughout the problem. (Kim, 2014)

4.3. Explicit and implicit analysis

Explicit and implicit methods is numerical computation methods in FEM used to solve for the governing equation that dictates the behaviour of a given system.

The explicit procedure, as in the name suggest, uses numerical computation to obtain values that are explicitly at each time step. This implies that solution at a particular time step is derived solely by using the data from the previous time step. The method is simple and computationally efficient, because it does not involve iterative procedures, and therefore works well with highly nonlinear problems, but it

requires a very small timestep to be stable. The other drawback involves deficiency in accuracy of the results at increasing timestep (Sun et al., 2000).

In contrast, the implicit method involves determining the solution at each time steps. The values at a given time step are derived by utilizing the values from the current and previous time steps through many iterations. The used timestep can be thus significantly larger without a loss of accuracy or stability. Therefore, this method is arguably more accurate than the explicit method for many relevant problems. The implicit method is computational demanding within the given timestep, which implies that it may require a lot a time and memory to solve some types of problem (Sun et al., 2000).

Capital 5

Wind load

The chapter is based on Norwegian standard - Eurocode 1: Actions on structures - Part 1-4: General actions - Wind actions (Norsk Standard, 2009a), unless otherwise will be specified in text.

5.1. Design of wind load

The effect of wind on high-rise buildings is significant and the effect will vary with time and position. Wind speed and wind load will vary with different terrain categories. Terrain categories can be classified into five categories according to NS-EN 1991-1-4, se figure 5.1. Where the first category including buildings in open terrain and the last category including complex terrain with many tall buildings. Open terrain refers to areas without obstacles that can affect the flow of wind, such as open fields or coastlines. Tall buildings located in open terrain will have higher wind speeds and forces compared to other types of land.

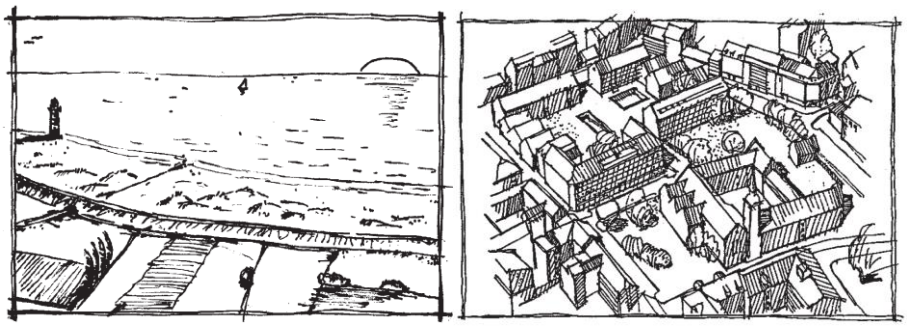

(a) *(b)*

Figure 5.1: a) shows Terrain Category 1, b) shows Terrain Category 5 (Norsk Standard, 2009a).

The impact of wind on the response of a structure depends on the size, shape, and material properties of the construction. The geometry of a building plays an important role in determining the wind impact on it. Tall buildings with irregular shapes and curves will experience more significant wind forces compared to buildings with regular shapes. The reason being irregular shape of the building creates turbulence that increases the wind pressure on the building. For example, a tall rectangular building

will have less wind pressure compared to a building with an L- or C-shaped plan. This is because a rectangular building provides a smaller surface area for the wind, reducing wind loads.

On wide buildings, wind will create friction forces on the surfaces of the structures. Friction forces act tangentially on the building surface and can be significant, especially on tall structures. Wind pressure acts perpendicular to the surface of the building. It also creates suction forces on the roof and sidewalls, respectively. Wind pressure is the force per unit area and depends on various factors, but primarily on the wind speed.

In Norway, the European standard NS-EN 1991-1-4, "Eurocode 1: Actions on structures - Part 1-4: General actions - Wind actions", is used to calculate wind loads on buildings. This standard is utilized in this thesis to assess the wind loads that impact the constructed model. The standard considers several factors that affect wind loads, including terrain categories, building geometry, and exposure to wind. NS-EN 1991-1-4 also provides comprehensive guidance for calculating wind pressures on different building components, such as roofs, walls, and facades. Moreover, the standard accounts for variations in wind speed and pressure along the height of the building.

To calculate the wind pressure on surfaces according to wind standards, it is necessary to first determine the basis velocity pressure and the peak velocity pressure as shown below.

Basis velocity pressure: $$q_b = \frac{1}{2} * \rho * v_b^2 \quad (5.1)$$

where

- ρ = the air density, recommended value is 1,25 kg/m3
- v_b = The fundamental wind speed that depends on the time of year and wind direction, measured at a height of 10 meters above the ground for terrain category II

Peak velocity pressure: $$q_p(z) = c_e(z) * q_b \quad (5.2)$$

where

- c_e = is the exposure factor given in figure (5.2)

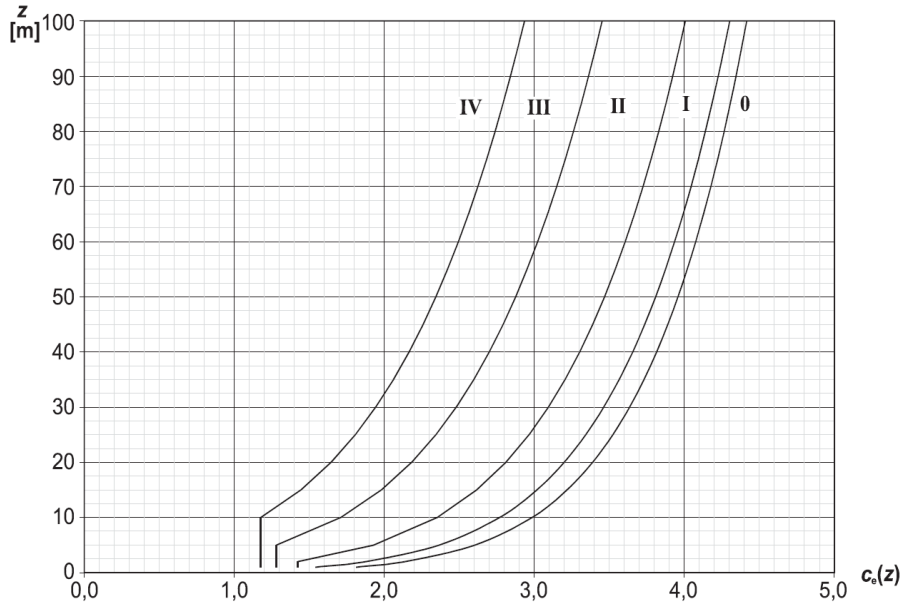

Figure 5.2: Illustrations of the exposure factor ce(z) (Norsk Standard, 2009a).

Wind pressure on surfaces: $$w_e = q_p(z) * c_{pe} \quad (5.3)$$

where

c_{pe} = the external pressure coefficient, table 5.1

Table 5.1: Recommended values of external pressure coefficients, of rectangular plan buildings (Norsk Standard, 2009a).

Sone	A		B		C		D		E	
h/d	$c_{pe,10}$	$c_{pe,1}$	$c_{pe,10}$	$c_{pe,1}$	$c_{pe,10}$	$c_{pe,1}$	$c_{pe,10}$	$c_{pe,1}$	$c_{pe,10}$	$c_{pe,1}$
5	-1,2	-1,4	-0,8	-1,1	-0,5		+0,8	+1,0	-0,7	
1	-1,2	-1,4	-0,8	-1,1	-0,5		+0,8	+1,0	-0,5	
≤ 0,25	-1,2	-1,4	-0,8	-1,1	-0,5		+0,7	+1,0	-0,3	

Wind can create three dynamic movements of the building: along-wind, crosswind, and torsion. Along-wind occurs when wind forces cause the structure to sway back and forth along its longest axis. Crosswind occurs when wind forces the structure to sway perpendicular to its longest axis. Torsional movements occur when wind forces the structure to rotate around its vertical axis.

With high-rise buildings, it is important to consider the dynamic response of the building under wind loads. The dynamic response is calculated according to the Australian standard AS/NZS 1170.2. In the case of high-rise buildings, the Australian standard is based on more knowledge and experience than the Norwegian standard. The Australian standard is used to find the dynamic factor. The dynamic factor takes into account dynamic properties of the building, including natural frequencies, damping factors, and wind spectral factor (Australian/New Zealand Standard, 2021), as shown in formula 5.4.

$$C_{dyn} = \frac{1 + 2I_h\sqrt{g_R^2 B_S + \frac{H_s g_R^2 S E_t}{\zeta}}}{(1 + 2g_v I_h)} \tag{5.4}$$

Where

s = the height at which external forces acting on a structure are calculated.

h = the average height of a structure's roof above ground level

Ih = the level of turbulence intensity, obtained from Table 5.2, by setting the height

gv = peak factor for the upwind velocity fluctuations, taken as 3.4 in calculations

Bs = background factor that measures the slowly varying background component of the response to low-frequency wind speed variations and can be determined using Equation 5.5.

$$B_s = \frac{1}{1 + \frac{\sqrt{0.26(h-s)^2 + 0.46b_{sh}^2}}{L_h}} \tag{5.5}$$

b_{sh} = the average width of a structure that spans between heights s and h

Lh = is a measure of the turbulence length scale at a certain height "h" in meters. It's calculated using Equation 5.6

$$L_h = 85(h/10)^{0.25} \tag{5.6}$$

Hs = the height factor for the resonant response of a structure, which is equal to 1 + (s/h)2

gR = the peak factor for the resonant response of a structure with a period of 10 minutes. It's calculated using Equation 5.7

$$= \sqrt{1.2 + 2log_e(600n_a)} \tag{5.7}$$

S = is the size reduction factor for a structure. It's calculated using Equation 5.8, where "na" is the first mode natural frequency of vibration of a structure in the along-wind direction in Hertz, and b0h the average width of a structure that spans between heights 0 and h

$$\frac{1}{1 + \frac{3.5n_a h(1 + g_v I_h)}{V_{des,0}} 1 + \frac{4n_a b_{0h}(1 + g_v I_h)}{V_{des,0}}} \tag{5.8}$$

Et = (π/4) multiplied by the spectrum of turbulence in the incoming wind stream, as defined by Equation 5.9

$$= \frac{\pi N}{(1 + 70.8N^2)^{5/6}} \tag{5.9}$$

where

N = the reduced frequency of a structure, which is dimensionless.

$$= \frac{n_a L_h [1 + (g_v I_h)]}{V_{des,0}} \tag{5.10}$$

na = The natural frequency of vibration in Hertz, corresponding to the first mode of vibration of a structure in the along-wind direction.

Vdes,θ = the design wind speed of a building at a height "h"

ζ = The ratio of a structure's damping coefficient to its critical damping coefficient

Table 5.2: Turbulence intensity (Australian/New Zealand Standard, 2021).

Height (z) m	Terrain Category 1	Terrain Category 2	Terrain Category 2.5	Terrain Category 3	Terrain Category 4
≤ 5	0.128	0.196	0.234	0.271	0.342
10	0.117	0.183	0.211	0.239	0.342
15	0.112	0.176	0.201	0.225	0.342
20	0.109	0.171	0.193	0.215	0.342
30	0.104	0.162	0.183	0.203	0.305
40	0.101	0.156	0.178	0.195	0.285
50	0.099	0.151	0.170	0.188	0.270
75	0.095	0.140	0.158	0.176	0.248
100	0.092	0.131	0.149	0.166	0.233
150	0.089	0.117	0.134	0.150	0.210
200	0.087	0.107	0.123	0.139	0.196

Capital 6

Lateral stability system

In tall building design, one of the main challenges is limiting lateral displacement when the building is subjected to lateral loads, such as wind and earthquakes. Therefore, achieving sufficient stiffness to withstand these forces is the main priority in the design process. In addition to considerations of wind- and seismic loading, vibrations induced by wind which affects comfort of the residents is another major issue that needs to be considered in the design. Among the different lateral stability systems, tube system is the conventional design for tall buildings. Figure 6.1 shows an overview of the different design of tube systems for tall buildings (Fu, 2018).

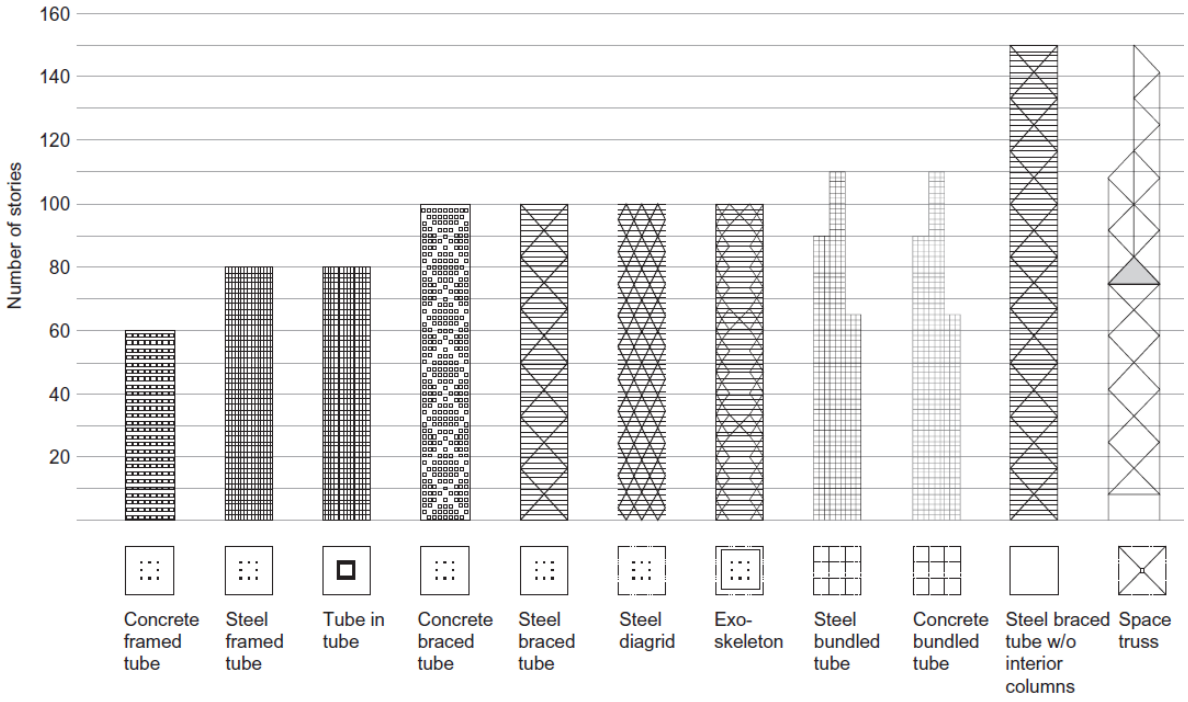

Figure 6.1 List of different lateral stability system in tall buildings (Fu, 2018).

6.1. Tube in tube

Tube in tube was chosen system for the case-study. The design of tube in tube system consists of an interior tube and an exterior tube, as shown in figure 6.2. The inner tube can be made as a concrete core wall or steel framed tube. Concrete core is the conventional solution for the inner tube since it provides a stiffer core structure. Steel core is lighter and therefore offers a cheaper cost for the foundation design. However, steel core is less preferably after 9/11 attack on the Twin Towers. The core system used in the Towers was a framed tube system, which was made by steel. The fire caused by the crashed, the structure starts sagging and failed because of the high temperature and led to the collapse of the Twin Towers. Hence, concrete core becomes a major choice for consideration due to increased stiffness and fire resistance, which makes the design safer (Fu, 2018). The One World Trade Center replaced the previous steel framed tube with a concrete core, see figure 6.3.

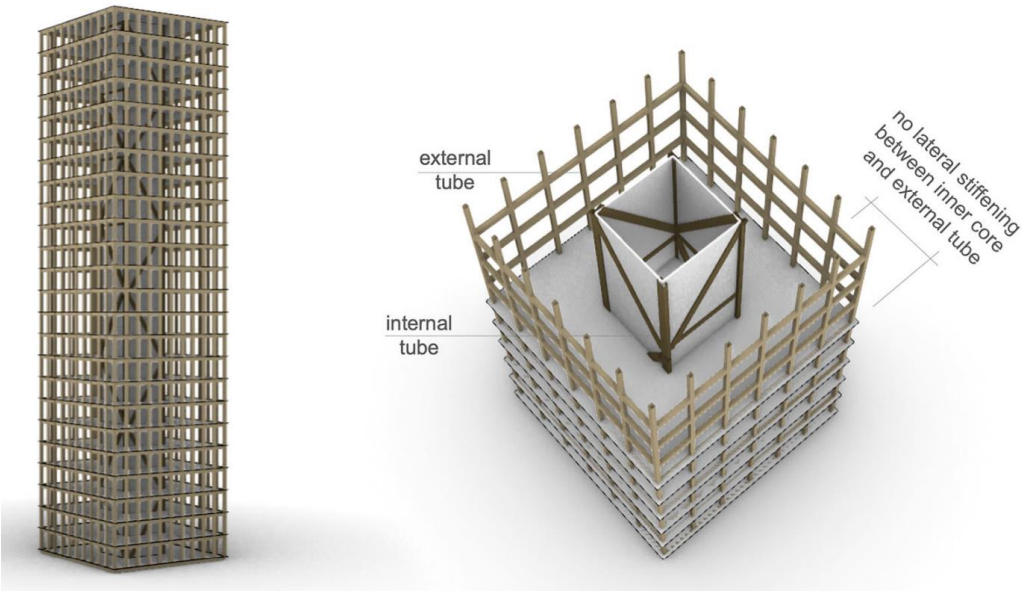

Figure 6.2: Illustration of Tube-in-tube system (Binck et al., 2022).

Figure 6.3: One World Trade Center (Flickr, n.d.).

The exterior tube has more structural depth and is an assembly of rigid beams and columns. The perimeter of the exterior tube includes closely placed columns and spandrel beams with through moment connection to resist lateral loads. To enhance the overall integrity and stiffness of the exterior tube to withstand wind loads, implementation of bracing is needed, which transfers the forces from the exterior tube down to soil beneath the foundation. The concrete core provides structural stability and primarily provides vertical load bearing for the building.

The two tubes are interconnected through floor diaphragm and outriggers. They work together as a pair of soft tubes, which means both would have approximately same stiffness, but since the exterior tube is more exposed to the lateral load from the wind, the exterior tube should be made a little stiffer than the inner tube. The tube in tube design is effective against resisting overturning due to lateral loads (Fu, 2018).

Chapter 7

Assessment criteria

7.1. Comfort design criteria for high-rise building

The tall and slender characteristics of high-rise buildings make them vulnerable to wind-induced vibrations. The acceleration generated by these horizontal oscillations can have a significant effect on the occupant discomfort and even provoke fear. Fear can be evoked by experiencing an extreme wind event which causes the building to vibrate at a noticeable rate, combined with the belief that a building should remain in a fix position without any movement. Discomfort is the result from vibrations that are sustained throughout an extended timeframe or occurrences on a regular basis and may trigger motion sickness (Burton, 2015). Therefore, one of the primary aims in designing high-rise buildings is to mitigate the discomfort and fear factor and create an environment that is comfortable and satisfactory for working and living.

Tolerance level of acceleration in high-rise is complicated and must include various factors in consideration, such as measurement of acceleration, selected return period and natural frequencies of the building. Acceleration of a building can be represented as peak acceleration, which is the largest value that occurred during a certain timeframe. Another alternative is root-mean-square (rms) acceleration, which is the median of the acceleration values experienced during a period. Peak acceleration is more common used in guidelines. Furthermore, the acceptable level for acceleration is usually based on a selected return period, for example 1 year, 5-years, 10-years and more. This factor again is dependent on the wind occurrence probability at different regions. Occupants may have a higher tolerance for vibrations that rarely occur or for a short duration, but not the opposite. Design that is based on longer period of reoccurrence such as 10-year period does not tackle the discomfort for vibrations that occurs regularly. Therefore, it is more reasonable to design for a smaller return period based on 1 year, which is more appropriate for the daily lives of the occupants (Burton, 2015). People perceive motion differently at certain frequencies, which leads to varied tolerance levels for

each individual. Some might feel discomfort with acceleration at 0.1 Hz, while others do not and otherwise (Mendis, 2017). Table 7.1 is an overview for human perception at different accelerations.

Acceptable limit of peak acceleration as a function of frequency corresponding to different selected return period developed by Irwin (1978) and Melbourne (1989) and Cheung is given in figure 7.1. It can be observed that the acceptable peak acceleration limit for tall building ranges from 0.02 to 0.2 m⁄s^2.

Table 7.1: Overview of human perception at different acceleration levels (Mendis, 2017).

LEVEL	ACCELERATION (m / sec^2)	EFFECT
1	< 0.05	Humans cannot perceive motion
2	0.05 - 0.1	a) Sensitive people can perceive motion; b) hanging objects may move slightly
3	0.1 - 0.25	a) Majority of people will perceive motion; b) level of motion may affect desk work: c) long - term exposure may produce motion sickness
4	0.25 - 0.4	a) Desk work becomes difficult or almost impossible; b) ambulation still possible
5	0.4 - 0.5	a) People strongly perceive motion; b) difficult to walk naturally; c) standing people may lose balance.
6	0.5 - 0.6	Most people cannot tolerate motion and are unable to walk naturally
7	0.6 - 0.7	People cannot walk or tolerate motion.
8	> 0.85	Objects begin to fall and people may be injured

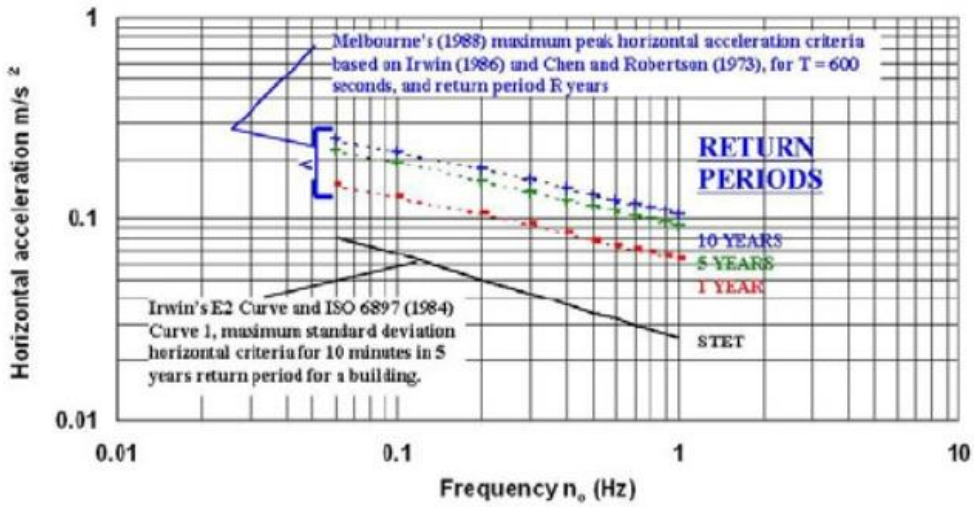

Figure 7.1: Acceptable limit of peak acceleration as a function of frequency corresponding to different selected return period developed by Irwin (1978) and Melbourne (1989) and Cheung (Mendis, 2017).

7.2. Maximum allowable drift limits in tall buildings

Excessive lateral drift (deflection) could cause damage to non-structural elements, such as partition walls, cladding, lifts and interior finishes. To mitigate this outcome, total building drift ratio and inter-story drift ratio was introduced as an assessment to serviceability of a structure when subjected to lateral loads.

The total building drift ratio refers to the peak lateral deflection at the top level of a building, divides by the height of the building *H*. This method in not commonly used and there is only few standards or codes that include guideline for the calculation. However, equation 7.1 is commonly used to calculate the maximum permitted limit for total building drift, which is derived from design data of existing buildings, see table 7.2 (Smith, 2011).

$$H/500 \tag{7.1}$$

Table 7.2: Peak lateral deflection criteria of existing buildings (Smith, 2011).

Name of building	Lctn	Source of data	Ht (m)	Structural System	Max Lateral Deflect	Max Interstorey Drift
Central Plaza	Hong Kong	Arup	374	perimeter tube core	H/785	
West Tower	Guangzhou	Arup	432	RC Core + CFT Diagrid	H/575	h/500
Jin Mao Tower	Shanghai	Taranath	421	RC Core + SRC Column frame	H/575 (Chinese code wind)	
International Commerce Centre	Hong Kong	Arup	480	RC Core + Outrigger + SRC Column frame	H/400	h/300
2IFC	Hong Kong	Arup	420	RC Core + Outrigger + SRC Column frame	H/466	h/315
Petronas Tower	Kuala Lumpur	Taranath	452	RC Core + Outrigger + SRC Column frame	H/560 (50 year wind)	
Elysian Hotel	Chicago	Taranath	208	RC Core + outrigger + RC Mega columns	H/800	
Pinnacle	London	Arup		Braced steel perimeter with viscous dampers		h/300
St Francis Towers	Manila	Arup	210	RC core, moment frame, Damped outrigger	H/230	h/250
Al Bateen Towers	Dubai	Taranath	204	Coupled shear wall		h/300 (reported as 10 year wind)
SRZ Tower	Dubai	Taranath	265	RC Core + outrigger + frame		Approx h/350 (10 year wind)

Chapter 8

Methodology

8.1. FEM-Design

The software used in this thesis was FEM-design, which is specialized for designing and analysing structures based on finite element method. There is a manual for the software available online, which was utilized for the design process and conducting of analysis.

FEM-design includes a wide range of engineering functions, such as static both static and dynamic analysis, linear and nonlinear calculations, design, and optimization of structures based on diverse specifications. A comprehensive library of different materials and profiles is included in the software, in addition to a wide range of standards and codes. The program provides an efficient way to design steel structures, such as standard steel connections in accordance with chosen design code. Design of concrete and timber structures are also included in the software.

8.2. Control of FEM-design

The finite element method employs numerical calculations that produce approximations solutions, which may contain errors from various sources. The sources include discretization errors and convergence errors (Kurowski, 2016). Therefore, it is essential to conduct a control of FEM software by performing analyses for simpler cases before proceeding to more advanced and complex cases. This step is crucial as it can provide valuable insights into how the software works and quickly detect errors and issues early on. By analysing simpler cases, it is possible to validate the accuracy of the software by comparing the numerical results with analytical solutions. This approach ensures accurate numerical calculations of the software and establishes a solid foundation for analysing more complex cases.

8.2.1. Case 1: Control of internal forces of structural elements

Case 1 aims to validate internal forces of the structural members when exert to external loading. A one-story frame with three different types of bracing was constructed and subjected to 20 kN horizonal load, illustrated in figure 8.1. The frame consists of 3.5 meters long column and beam. Pinned and roller support was implemented for the structure.

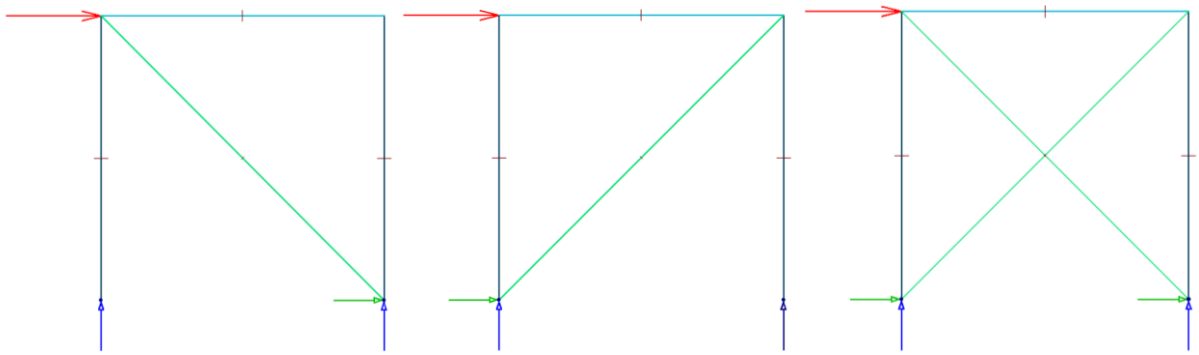

Figure 8.1: One story frame with different bracing subjected to horizontal loading.

Result from manual calculation is shown in appendix A and internal forces for the different members of the three cases are displayed in figure 8.2. The results provided by the software was consistent according to results obtained through manual calculation.

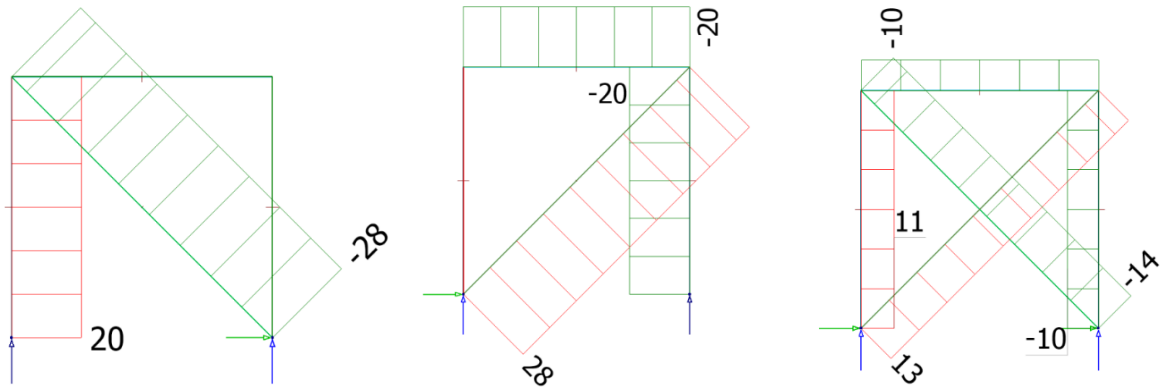

Figure 8.2: Stresses of different bracing configurations of one-story frame model.

8.2.2. Case 2: Control of natural frequency and mode shape

In case 2, a simple two-story shear frame with fixed support will be used to verify natural frequencies and mode shapes obtained by numerical solutions by the software, as shown in figure 8.3.

The steel properties of frame are listed in table 8.1

Table 8.1: Properties and dimensions of steel members.

Young's modulus	210 GPa
Story height	3.5 meters
Beam length	3.5 meters
Column length	3.5 meters

The profile of steel beams used to construct the frame is HE-A 160 and has the following material properties given in table 8.2.

Table 8.2: Properties and dimensions of HE-A 160.

Moment of Inertia, I_X	1.644 cm^4
Weight	30.1 kg/m
Beam length	3.5 meters
Column length	3.5 meters

With the given material properties and dimensions, the global stiffness matrix and mass matrix of the frame can be assembled. Analytical solution can be obtained by solving for equation 2.19, detailed calculation is shown in appendix B.

The setup of the frame in FEM-design must approach the simplified model used to obtain the analytical solution as extensively as possible. The results obtained by manual calculation is circumscribed to two DOFs and only translation along x-axis, hence two natural frequencies and mode shapes can be acquired. The following boundary conditions are imposed on the idealized frame, where horizontal beams are considered indefinitely rigid, thus no deformation, and the stiffness of the structure relies entirely on stiffness of the columns. Thus, the horizontal beam is replaced with a more robust profile, HE-A 220.

Furthermore, the story stiffness is the sum of the lateral stiffnesses of the total columns in the story (Chopra, 2011). It is assumed that the connection at joints is rigidly clamped, hence the total story stiffness is represented as the summation:

$$k_j \sum_{columns} \frac{12EI_C}{h^3} \left(N/m\right) \tag{8.1}$$

The numerical model does not represent the analytical model exactly. The horizontal elements are not infinitely stiff, and the columns can rotate in the joints although very little. Therefore, the stiffness matrix for the numerical system is going to be slightly different. The mass distribution in the numerical system is mostly similar to the analytical one, but instead of single lumped masses in the horizontal plates, the masses are assigned to the nodes/joints according to the total mass of beams/columns that they connect, see figure 8.3. Since natural frequency is sensitive to the exact mass and stiffness matrices of the structure, the natural frequency obtained from the software will differ somewhat from that was obtained through manual calculation.

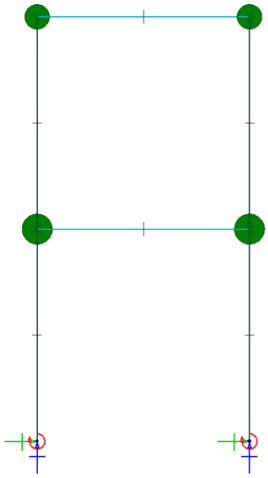

Figure 8.3: Structural mass assigned at nodes.

Based on the information provided above, the eigenvalue analysis was conducted. Natural frequencies and mode shapes obtained from FEM-design are displayed in figure 8.4.

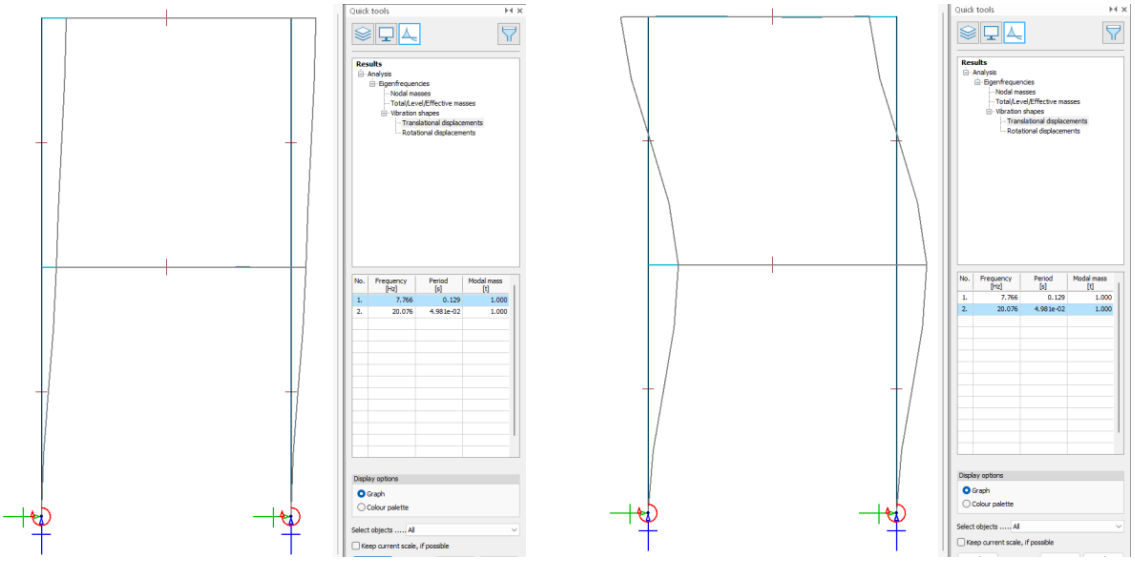

(a) *(b)*

Figure 8.4: a) 1st bending mode, b)2nd bending mode.

Table 8.3: Results obtained from FEM-design and manual calculation.

Results	Natural frequency 1st mode	Natural frequency 2nd mode
FEM-design	7.766	20.076
Manual calculation	7.710	20.200

Upon reviewing the results of the numerical and manual calculations depicted in table 8.3, an expected discrepancy was observed. The magnitude of this discrepancy is quite small considered the employed approximations. Therefore, the case study validated the accuracy and reliability of the program. It can be concluded that the software can be used to conduct analysis for more complex cases.

8.2.3. Case 3: Analysis of tube in tube system

The upcoming chapters will provide a comprehensive description of the model configuration in FEM-design. The lateral stability system of the building will be based on tube in tube system, which consists of an outer tube made up by steel elements with implemented bracing trusses and a concrete core.

In order to simplify the analysis, a square shape geometry was utilised for the model with each side equates 40 meters. The outer tube consists of columns with 8 meters spacing interconnected with steel beams. The columns are produced from several profiles with consecutively reducing cross sections. The joints between the profiles fully transfer the moment. Concrete floors were implemented and served primarily as the connection of the steel frame and the concrete core. The building is composed of 50 stories, with each story measures 4 meters in height, resulting a total height of 200 meters.

Connection configuration

Two models with different connection stiffness configurations are established for the analysis of horizonal displacement when subjected to wind load, which are pinned and rigid connection. The primary aim is to assess how these types of connection affect the horizontal displacement when the building is subjected to wind and other aspects of static and dynamic structure behaviour. Pinned connection is established between foundation and the building for both cases.

In both cases the structure is in principle statically determinate, including the pinned connection case, due to the columns being designed as continuous throughout the length. In pinned connection, the attached structural members are allowed to rotate and do not generate moments in the connection. The pinned connection model is thus supplied with bracing in the outer perimeter to provide more stability to the structure. Belt truss, as the name suggest, is a type of steel bracing installed around the outer frame at selected heights. For this instance, the belt trusses are positioned at the pinned

connection, where the transition to smaller column profile occurs. Figure 8.5 displays the position of belt truss in the model.

For rigid configuration, the connection is fixed, and no relative rotations are allowed, which results the same moment capacity in the connection as in the corresponding members. Due to no allowed rotations in this instance, the structure in principle requires less to no bracing than the other types. Through iteratively optimizing the structure, it was revealed that bracing was needed for the rigid model to reduce the horizontal displacement to acceptable levels, as the no-bracing structure was deflecting excessively at the top.

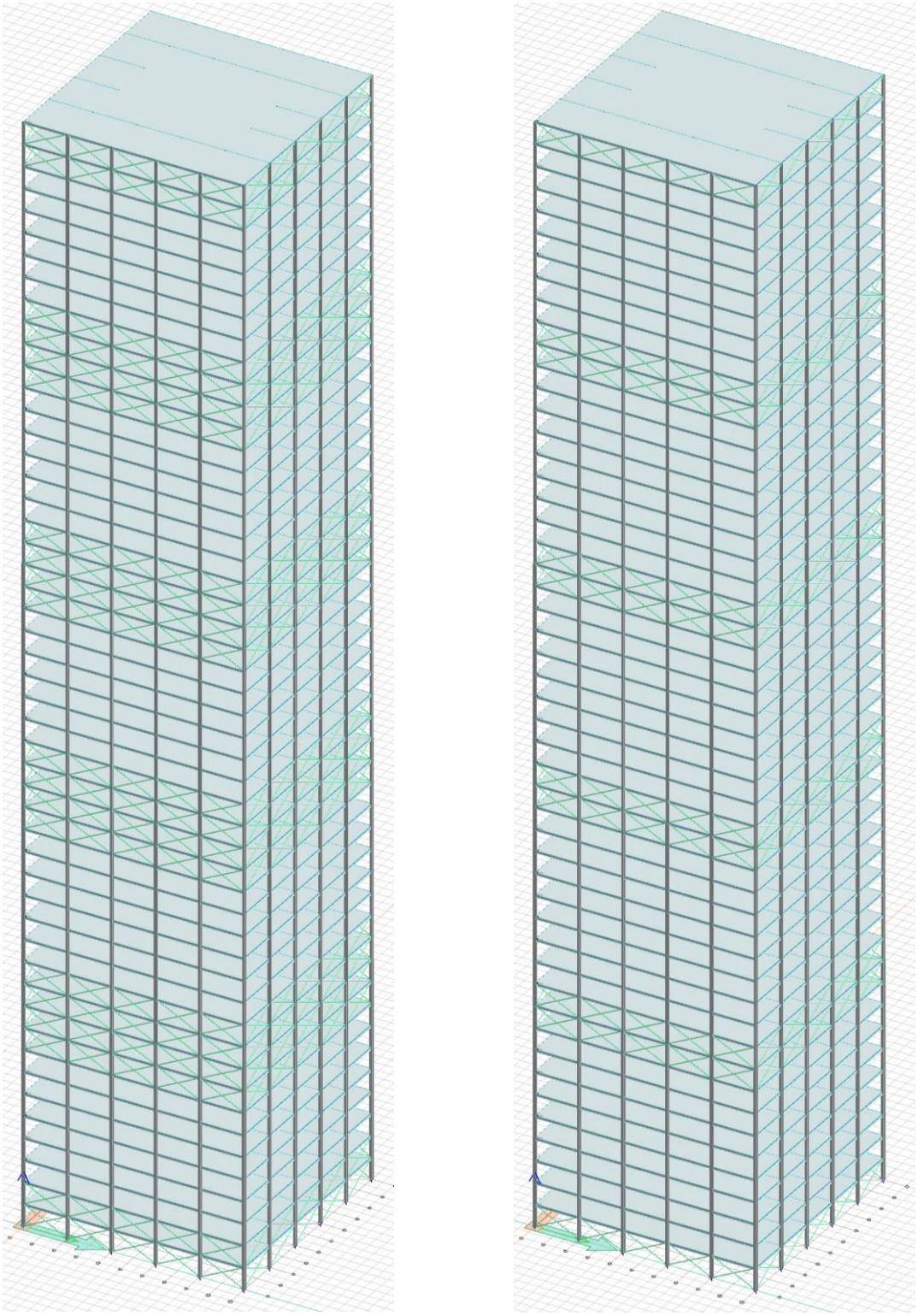

(a) *(b)*

Figure 8.5: a) Pinned connection configuration b) Rigid connection configuration.

Steel elements

Due to higher stiffness and resistance in tension, steel columns were selected for the case study. High-strength steel used for the structure is S450. The selected profile for columns is HD400 with H-sections, see figure 8.6.

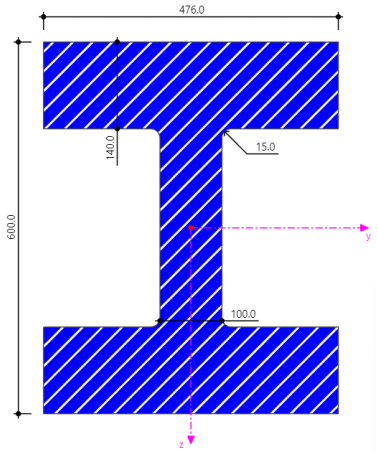

Figure 8.6: Cross section of HD 400x1299.

Columns located in the upper levels are exposed to substantially lower vertical and horizontal loads compared to the columns at the ground level. Therefore, the columns profile is modified and replaced with smaller ones with increasing height. The concept is displayed in figure 8.7. Table 8.4 displays an overview of profiles used for columns at different floors level.

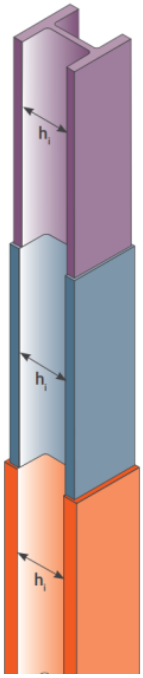

Figure 8.7: Stacking up HD 400 columns.

Table 8.4: Overview of columns profiles at different heights.

Columns profile	Floor
HD 400 x 1299	1-10
HD 400 x 900	11-20
HD 400 x 592	21-30
HD 400 x 421	31-40
HD 400 x 287	41-50

The primary function of horizontal beams in the structure will be handling the live loads design for the story. Hence, the profile for beams will remain the same for every floors. The selected profile for beams is HE-B 340. The H-profile provides efficiency when it comes to assembly of connection. Additionally, in-situ concrete floors with strength class B35/45 are chosen as the resolution, which is interconnected with the concrete core, displayed in figure 8.8.

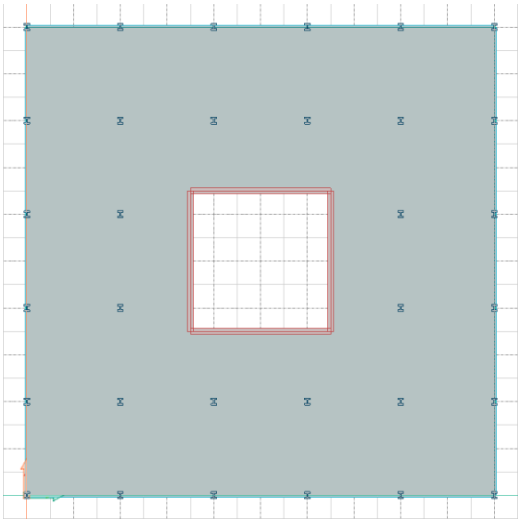

Figure 8.8: Concrete floors connected to the core structure.

Concrete core

The core structure is an assembly of four coupled shear walls and primarily accountable for bearing vertical loads of the structure. The concrete core is square shape with each side equalling to 12 meters in length. The strength class of concrete utilised in the core is B40/50 with an initial thickness of 500mm. The thickness reduces as the building height increases as the same with the columns. Change in thickness of the core is displayed in table 8.5.

Table 8.5: Overview of concrete core thickness at different heights.

Concrete thickness (mm)	Height (m)
500 mm	0 - 50 m
400 mm	50 - 100 m
300 mm	100 - 150 m
200 mm	150 - 200 m

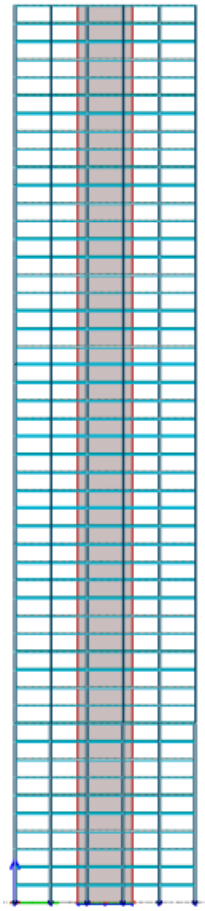

Figure 8.9: Concrete core as inner tube.

Load case combination

In this study, the selected load case consists of the following loads. Firstly, the dead load accounts for the weights from structural elements. Once the model is configured, FEM-design will automatically generate the dead load based on the model configuration. Secondly, live load is set to be 3 kN/m^2, which is derived from NS-EN-1991 for office building. This load was defined as distributed load over each floor.

The last component is wind load. The wind load will be modelled separately as two cases, first as a quasi-static load with dynamic effects accounted for through dynamic coefficients, and then as a time dependent varying load, which will allow for a more accurate account of the various dynamic effects. The purpose of quasi-static wind load is to establish a baseline model that will be able to withstand all the expected loads without going over capacity in the structural elements and remaining within serviceability limits in terms of displacements. The dynamic wind load will be employed to assess the vibrational response of the structure induced by the inherently periodic nature of the real wind load.

Quasi-static wind load

The input values for quasi-static wind load are derived from NS-EN 1991-1-4:2005+NA:200. It should be noted that quasistatic wind calculation based on NS-EN 1991 is limited, hence Australian standard AS/NZS 1170.2:2021 was utilised to determine the dynamic factor of wind load. Detailed manually computation is given in appendix C.

Trondheim is the selected location for the case study. The mean wind velocity is set to be 26m/s adhering to the standard specifications. Wind velocity was multiplied with designated air density of 1.2kg/m^3 to obtain the wind pressure. A height factor was introduced to account for the amplified wind pressure that increases with heights. The factors provided in the standard are confined to a height of 100 meters, and therefore not sufficient for the case study. Interpolation was utilised to obtain the set data of height factors beyond 100 meters and is displayed in figure 8.10. The input of wind pressures is modelled as distributed load exerted on the surface area for every 10 meters in height.

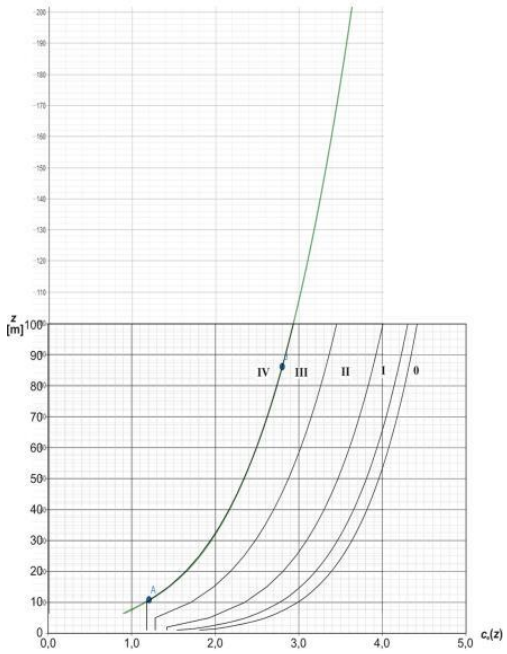

Figure 8.10: Interpolation of exposure factor.

Wind loads exert different pressures on surfaces of the building, which is divided into different zone as seen in figure 8.11. When determining the wind pressure on a specific surface, it is taken into account using a factor shown in table 8.6. To simplify the complexity of this matter, only wind pressure that affects the front and rear surfaces, of the building are included in the analysis due to the same direction of effect. Hence, the total wind pressure of along wind is the sum of these two surfaces. To account for the dynamic effect, the wind pressure is multiplied with a dynamic factor, equation 5.4, to obtain the final values that was used in the model.

Table 8.6: Recommended values of external pressure coefficients.

Zone	A	B	D	E
	- 1,2	- 0,8	0,8	- 0.7

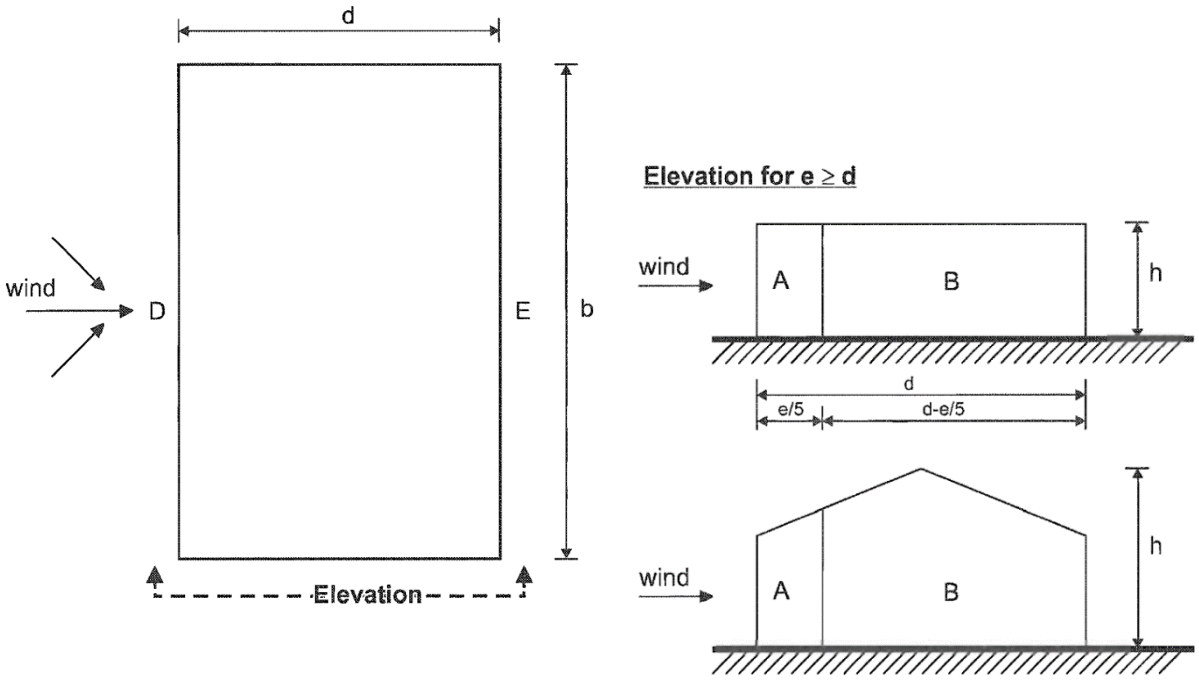

Figure 8.11: Zones of external pressures on vertical walls (Norsk Standard, 2009a).

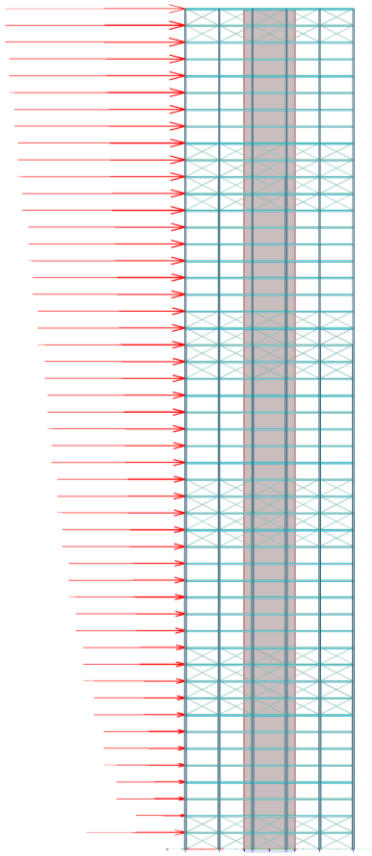

Figure 8.12: Illustration of quasistatic wind load.

8.3. NatHaz On-line Wind Simulator (NOWS)

Dynamic wind is a signal varying in time, which can be treated as a complex periodic signal consisting of multiple harmonic signals and is thus often represented in the form of power spectral density (PSD) – distribution of power into the frequency components. These PSD are often created based on field measurement data, which is difficult to execute. For certain locations and heights, there are no data available. For high-rise buildings, wind tunnel test is the primary practice to obtain the dynamic wind data for analysis.

NOWS is an online wind simulator developed by NatHaz (Natural Hazards) Modeling Laboratory at University of Notre Dame. The simulator offers a simple and effective way to simulate PSD of wind velocity fluctuations at a given time domain, which possesses a close resemblance of real wind characteristics. The simulator was previously used in a master thesis "Verification of the Wind Induced Dynamic Response of the Svinesund Bridge in the Time Domain by the use of Autoregressive Simulations", (Fiskum, 2012). The wind fluctuation data generated by NOWS was compared to wind data measurements registered from sensors implemented on the bridge. The results indicate a solid resemblance of the real time wind. Based on this, NOWS is implemented to simulate wind fluctuations for dynamic wind analysis in this thesis. For readers who are interested in the theory used in NOWS can consult (NatHaz, n.d.).

It should be noted that NOWS generates wind pressure that arises due to wind velocity on a flat front surface of a structure positioned normal and towards to the wind direction. It does not provide information about the wind pressure on the opposite side of the building with negative pressure or the sides, where the turbulence and shearing effects are relevant. This information is quite difficult to estimate and was thus left out of the present work.

The input needed to generate the PSD of wind are the following: locations in vertical and horizonal directions for wind speed simulation, total number of frequencies to be generated, cut-off frequency, exposure category, and 3-sec gust wind speed. The online user interface is displayed in figure 8.13. In depth explanations for the simulation inputs are described in the upcoming chapters.

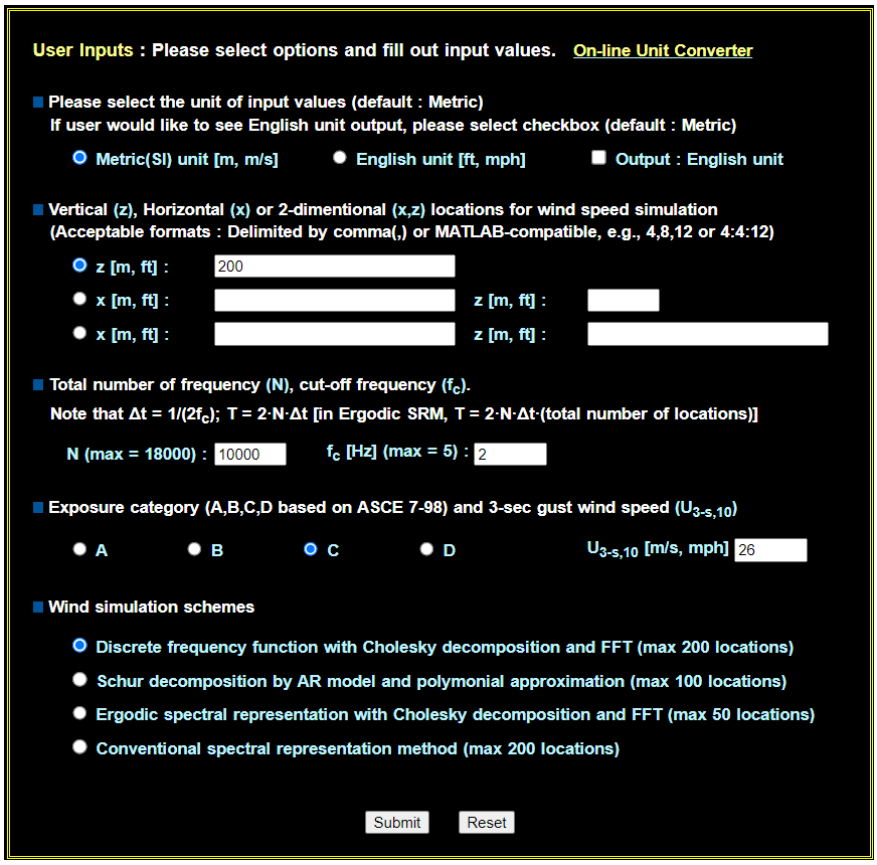

Figure 8.13: User interface of NOWS (NatHaz, n.d.).

8.3.1. Cut of frequency and number of frequencies

Based on eigenvalues analysis displayed in tables 9.3 and 9.4, it is observed that the first eight natural frequencies of the building are smaller than 2 Hz. Hence, the input for cut of frequency f_c is set to be 2Hz. The physical meaning is that the components with higher frequency are not likely to incite any significant structural response.

As for total number of frequencies, it will be two simulations time domains, one with 180 seconds. NOWS provides equation 8.2 to calculate the total number of frequencies.

$$T = 2 * N * \Delta t \tag{8.2}$$

Where T is time frame of wind simulation in seconds, is the total number of frequencies, and Δt is the time step of the simulation and can be obtained through the cut of frequency with equation 8.3.

$$\Delta t = \frac{1}{2f_c} \tag{8.3}$$

For the wind simulation with the time domain of 180 seconds, the total number of frequencies obtained by the equations above is 360.

8.3.2. Wind velocity

The input for wind velocity is based on ASCE7-98, which is 3-sec gust wind that is measured at 10 meters height. Wind velocity 26 m/s according to NS-EN 1991-1-4:2005+NA:2009 is measured over 10 minutes period at 10 meters height. Thus, the wind velocity must be converted to 3-sec gust wind. The conversion of wind velocity can be done by utilizing equation 8.4, which is provided from Simiu and Miyata (Simiu, 2011).

$$V_t(z) = \bar{V}(z)\left[1 + \frac{\eta c(t)}{2.5\ln\left({}^{z}/_{z_0}\right)}\right] \tag{8.4}$$

where $V_t(z)$ is the mean wind velocity over t seconds, and $\bar{V}(z)$ is the mean wind velocity within a record of approximately one hour over surface roughness z_0. Coefficients z_0, η and c(t) are provided in table 8.7 (Simiu, 2011).

Table 8.7: Factors $\eta\ (z_0)$ and $z_0\ (m)$. (Simiu, 2011)

		$\boldsymbol{z_0\ (m)}$		0.005		0.03		0.30		1.00		
		$\boldsymbol{\eta\ (z_0)}$		2.55		2.45		2.30		2.20		
t	1	10	20	30	50	100	200	300	600	1000	3600	
$\boldsymbol{c\ (t)}$	3.00	2.32	2.00	1.73	1.35	1.02	0.70	0.54	0.36	0.16.	0.00	

Due to the uncertainty regarding which values are suitable for case study, different values were experimented with to obtain 3-sec gust wind velocities. The highest wind velocity will be selected for the case study. The values used in calculation for the wind velocity are shown in table 8.8. The 3-sec gust wind velocity input was set to be 29.57 m/s.

Table 8.8: Values used in wind velocity calculation.

$\boldsymbol{\eta}$	$\boldsymbol{c(t)}$	$\boldsymbol{z\ (m)}$	$\boldsymbol{z_0\ (m)}$	$\boldsymbol{V_t(z)\ (m/s)}$	$\boldsymbol{\bar{V}(z)\ (m/s)}$
2.55	0.36	10	0.005	26	27.26
2.2	0.36	10	1	26	29.57

8.4. Exposure category

Exposure category used in NOWS are based on the American standard ASCE 7-98. The newest revision of the standard is ASCE7-22 and is assumed to have the same definition for the exposure categories as

the ASCE7-98. The standard specifies three different exposure categories B, C and D and stated the following definitions (American Society of Civil Engineers Staff, 2021):

Exposure C*. Exposure C shall apply for all cases where Exposure B or D does not apply.*

Exposure B*. For buildings or other structures with a mean roof height less than or equal to 30 ft (9.1 m), Exposure B shall apply where the ground surface roughness, as defined by Surface Roughness B, prevails in the upwind direction for a distance greater than 1,500 ft (457 m). For buildings or other structures with a mean roof height greater than 30 ft (9.1 m), Exposure B shall apply where Surface Roughness B prevails in the upwind direction for a distance greater than 2,600 ft (792 m) or 20 times the height of the building or structure, whichever is greater.*

Exposure D*. Exposure D shall apply where the ground surface roughness, as defined by Surface Roughness D, prevails in the upwind direction for a distance greater than 5,000 ft (1,524 m) or 20 times the building or structure height, whichever is greater. Exposure D shall also apply where the ground surface roughness immediately upwind of the site is B or C, and the building or structure is within a distance of 600 ft (183 m) or 20 times the building or structure height, whichever is greater.*

Exposure categories are dependent on the selected Surface Roughness category, which according to ASCE7-22 are defined as follow (American Society of Civil Engineers Staff, 2021):

Surface Roughness B*. Urban and suburban areas, wooded areas, or other terrain with numerous, closely spaced obstructions that have the size of single-family dwellings or larger.*

Surface Roughness C*. Open terrain with scattered obstructions that have heights generally less than 30 ft (9.1 m). This category includes flat, open country and grasslands.*

Surface Roughness D*. Flat, unobstructed areas and water surfaces. This category includes smooth mud flats, salt flats, and unbroken ice.*

As mentioned earlier the case study is based on building in Trondheim which is an urban area. Given this condition, surface roughness B is selected. Furthermore, both exposure categories B and D is suitable for urban areas, where the exposure category B has a relative smoother and more open areas compared to exposure category D, which is denser. Since the building is 200 meters tall, which is significantly taller than the mean roof height for buildings in Trondheim. Hence, the exposure category B was selected.

8.5. Horizontal coordinates vertical coordinates

Based on results obtained from modal analysis, it has been observed that the building may display torsional deformation at certain frequencies. The wind load in a quasi-static case is defined as a distributed load over a surface that varies with height, however, it remains consistent in the horizontal axis. With this wind pressure distribution, the building will only exert mode shapes that sways back and forth in one direction, and torsional deformation due to dynamic wind is not possible to assess. Therefore, it is necessary to modify the wind load to better approach real wind fluctuations that can exert torsional deformation of the building.

To achieve this, the surface that the wind encounters are divided into eight sections, each with height of 50 meters and 20 meters in width, as illustrated in figure 8.14. A mean distributed load is defined for each of these eight sections, which is then combined with a fluctuating wind factor that varies with time. Each section of the surface is equally divided, with each point located in the middle of the section. NOWS generates 8 corresponding PSDs for each of the points. The input parameters for the program along the x-axis are set at the 10-meter and 30-meter marks, while the input parameters for the z-axis are set at heights of 25, 75, 125, and 175 meters.

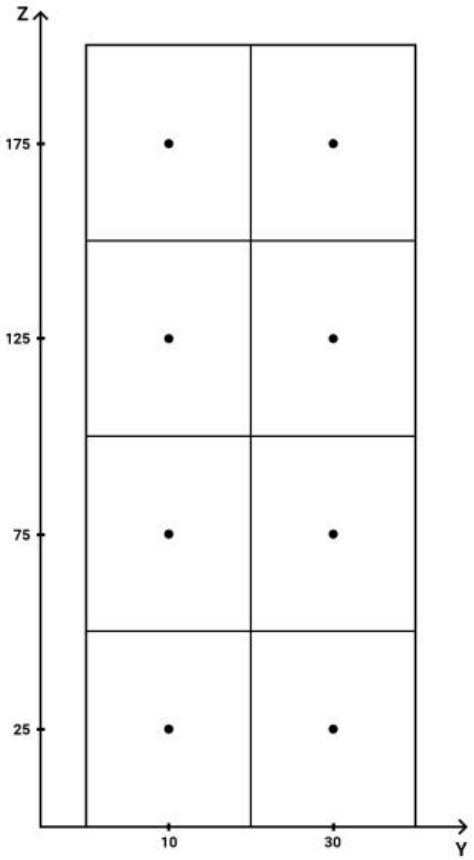

Figure 8.14: Surface divided into sections to better represent real wind.

This approach results a difference in loading on the defined sections, which provides a better representation of real wind. With the dynamic wind load setup described above, different pressures will be established on the surface, creating a pulling back and forth effect at the edge of the surface. Through analysis, it is possible to assess whether these wind forces will exert a torsional moment on the building.

8.6. Output of dynamic wind data

The generated PSD of wind velocity based on the previous mentioned inputs are presented below as the plots of fluctuating wind velocity in time. For a time domain of 180 seconds, the following PSD wind velocity are generated.

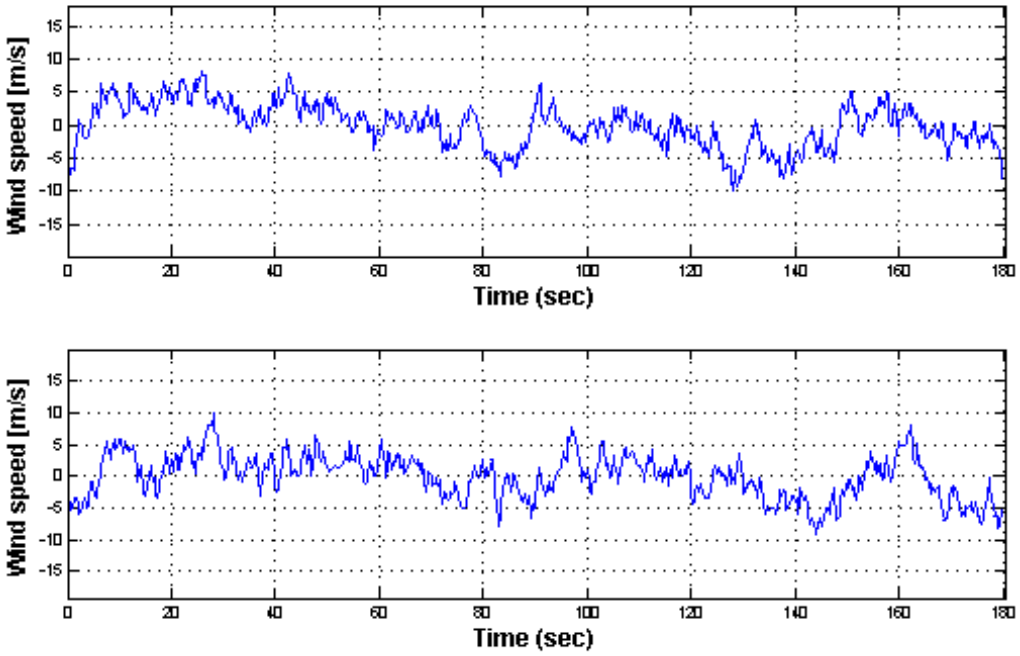

Figure 8.15 Wind at 25 meters height. Section 1 (above) and section 2 (below).

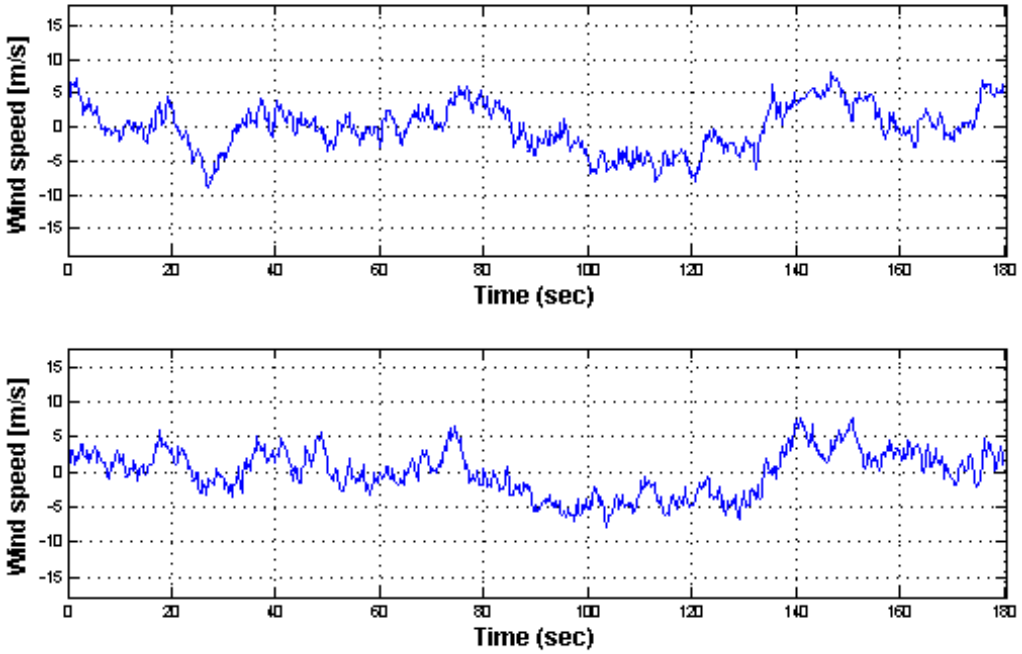

Figure 8.16: Fluctuating wind speed at 75 meters height. Section 3 (above) and section 4 (below).

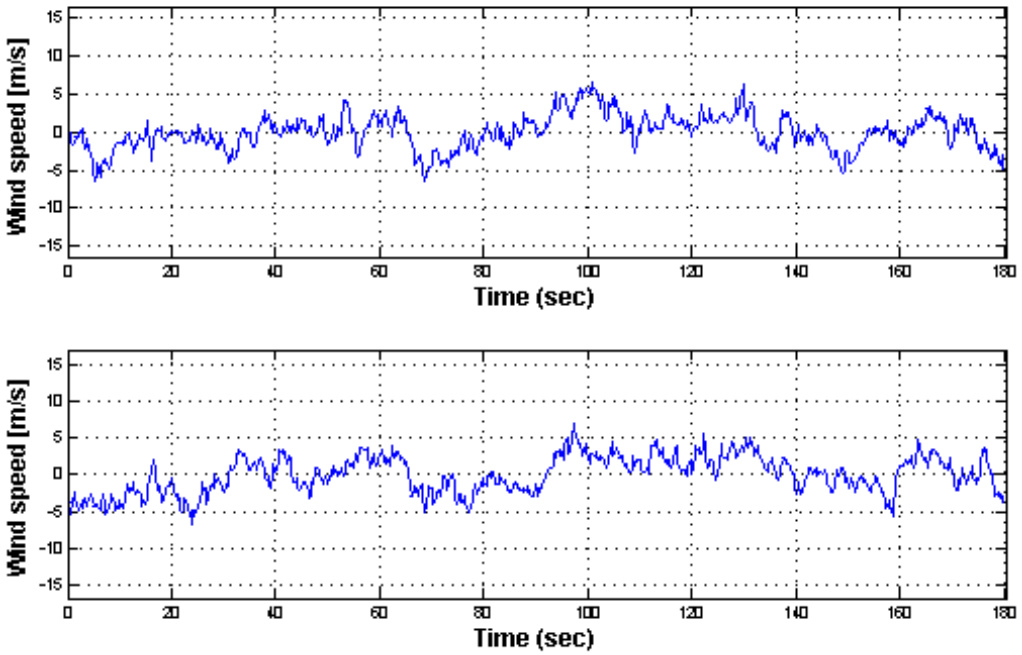

Figure 8.17 Fluctuating wind speed at 125 meters height. Section 5 (above) and section 6 (below).

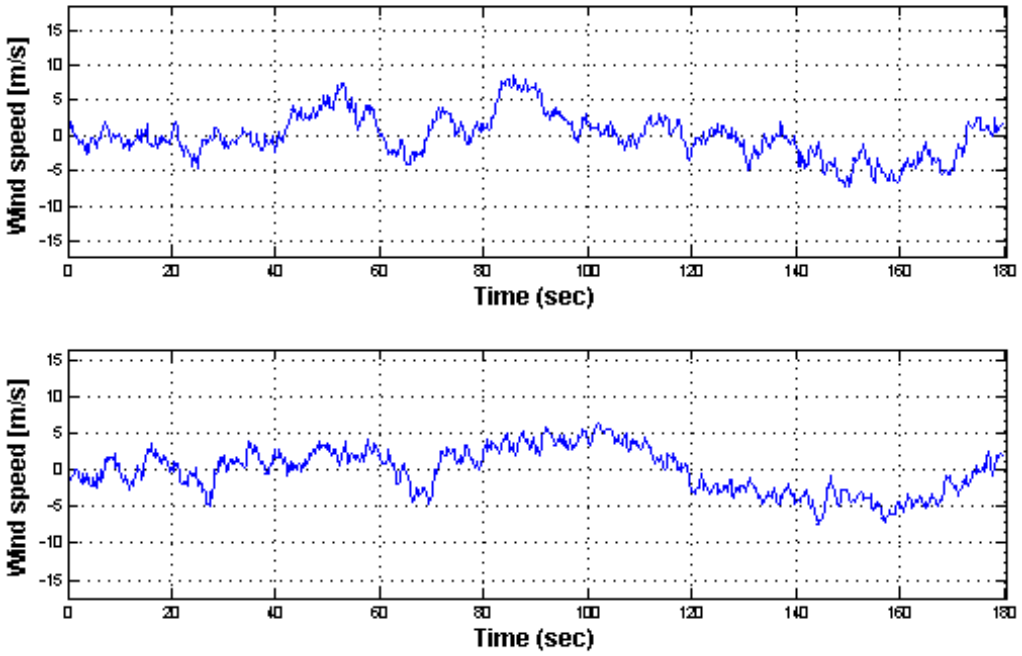

Figure 8.18 Fluctuating wind speed at 175 meters height. Section 7 (above) and section 8 (below).

These PSD of fluctuating wind velocity can then be converted to fluctuating wind force by equations 8.5.

$$q(t) = \rho * C_D * U * u(t) \tag{8.5}$$

Where F(t) is fluctuating wind force, ρ is air density, CD is drag coefficient, A, U is mean wind velocity and u(t) is fluctuating wind speed. Moreover, the final wind pressure inputs are determined by combining the fluctuation values with the mean wind velocity. The mean wind velocity is calculated by equation 8.6.

$$\bar{q}(t) = \rho * C_D * U^2 \tag{8.6}$$

Drag coefficient for high-rise is determined based on experimental data through wind tunnel testing. For high-rise with square shape with similar plan aspect ratio and height aspect ratio to the model used in this thesis, the value is set to be 1.4 (Nair et al., 2020).

In FEM-design, dynamic wind load is modelled as an excitation force. The wind pressure must be converted to a dimensionless factor for the input in the software. The factor has a maximum limit of 1 and -1. Therefore, the highest wind pressure is defined as factor 1, which lay the basis for adjusting of the remaining wind pressures. Detailed calculations are given in appendix D.

8.7. Determination of Rayleigh damping ratio and damping coefficients of the model

When performing dynamic analysis, inputs of damping ratio and coefficient are required. These values must be determined separately for each connection configuration, due to differences in natural frequencies. Rayleigh damping ratio can be obtained from table 2.1. Since the building is constructed with both steel and concrete elements, the approximated damping ratio utilised is set to 5% and is applied for both models.

As mentioned earlier, the first eight natural frequencies of the building are considered the most important and will be employed for calculation of the damping coefficients. Given that the damping ratio is assumed to be the same for all the modes included in the analysis, mass and stiffness damping coefficients can be obtained from equation 2.23. To avoid over-damping of the building response, it is suggested to use to lowest and the highest natural frequency in the calculation (Orcina, n.d.). The natural frequencies obtained from modal analysis were converted from hertz to rad/s for the calculation. Converted natural frequencies and obtained damping coefficients are displayed in table 8.9.

Table 8.9: Employed natural frequencies used in calculations and obtained damping coefficients of both models.

	Lowest natural frequency (rad/s)	Highest natural frequency (rad/s)	a_0	a_1
Pinned connection model	0.188	1.768	0.0169	0.0511
Rigid connection model	0.172	1.722	0.0156	0.0527

It is important to note that the use of Rayleigh damping in the dynamic calculation may not accurately represent the damping of the system. Hence, the effect of damping on displacement cannot be accurately assess and will not be included in the discussion.

Chapter 9

Results and discussion

9.1. Design of the structure based on quasistatic load

In designing the structure, an iterative approach was employed that involved refining the design over several stages, a rough design was created based on intuition and estimation. The following step involves testing static loads to gauge the stress levels and maximum displacement of the structure. Subsequently, these findings were utilised as criteria for optimization of the structure. Ultimately, the final structure was chosen from among various options involving steel beams, columns, and bars, in addition to how much bracing would be needed and where it should be placed.

9.2. Quasistatic load and responses of models

Max lateral deflection was one criterion used in assessment of safety and integrity of the structure. The maximum lateral deflection for a 200-meter-tall building, as determined by equation 7.1, is 400 mm. According to the results displayed in figure 9.1, the pinned model satisfies the deflection criteria, while the rigid model in figure 9.2 exceeds the limit to a small extent. It should be noted that the formula used to calculate the maximum allowable top deflection is a generalized and simplified assessment criteria and certainly conservative. Hence, the limit of lateral deflection for tall building can be extended to a greater extent, compared to the calculated value. While the formula can serve as a helpful guideline, it is important to do due diligence in determining what is permissible for the specific building.

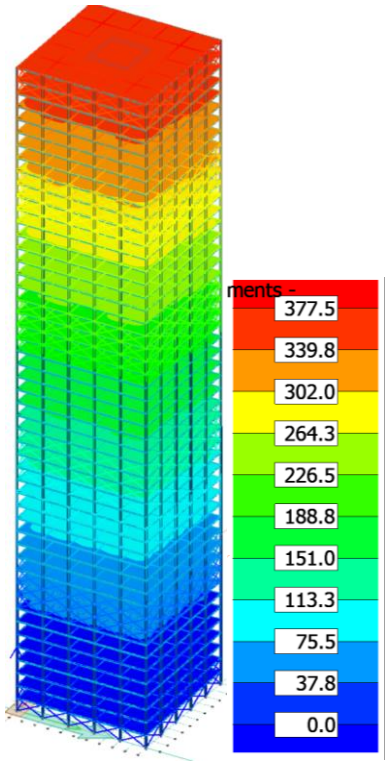

Figure 9.1: Horizontal displacement of pinned connection model subjected to quasi-static wind load.

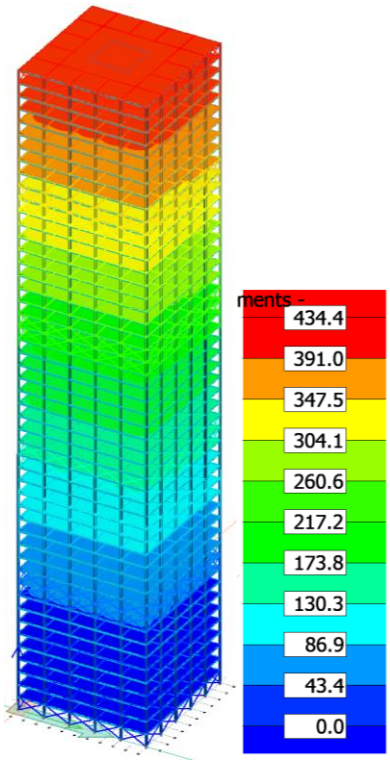

Figure 9.2: Horizontal displacement of rigid connection model subjected to quasi-static wind load.

The assessment of von Mises stresses in concrete elements are done separately for dead load and wind load. Figures 9.3 and 9.4 illustrate the von Mises stress resulted from dead load. The pinned model displayed a maximum value of 38.02 N/mm^2, while the rigid model exhibits a slightly lower maximum value of 26.18 N/mm^2. For the wind load case displayed in figures 9.5 and 9.6, the maximum stresses are 16.211 N/mm2 for the pinned model and 13.718 N/mm^2 for the rigid model, respectively. The results from the two cases revealed an interesting finding, which is, the stresses that occurred in the concrete elements is primarily generated by the dead load of the structure. Wind load contributions are approximately half the vale of the dead weight.

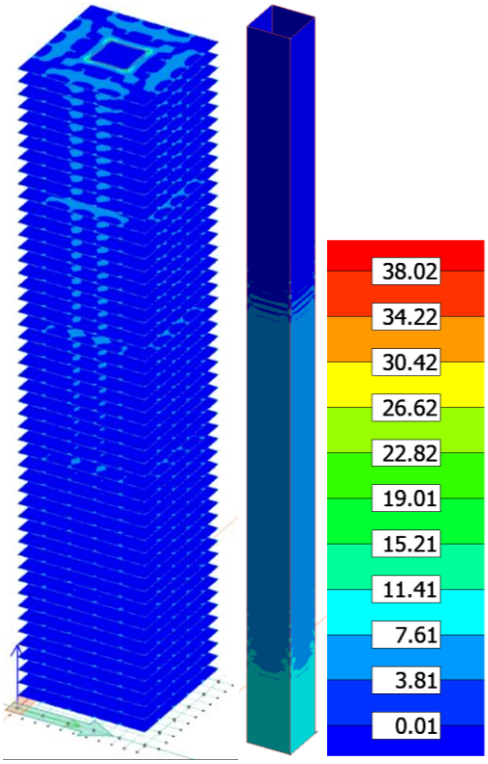

Figure 9.3: von Mises stress in shell elements of pinned connection model generated by dead load.

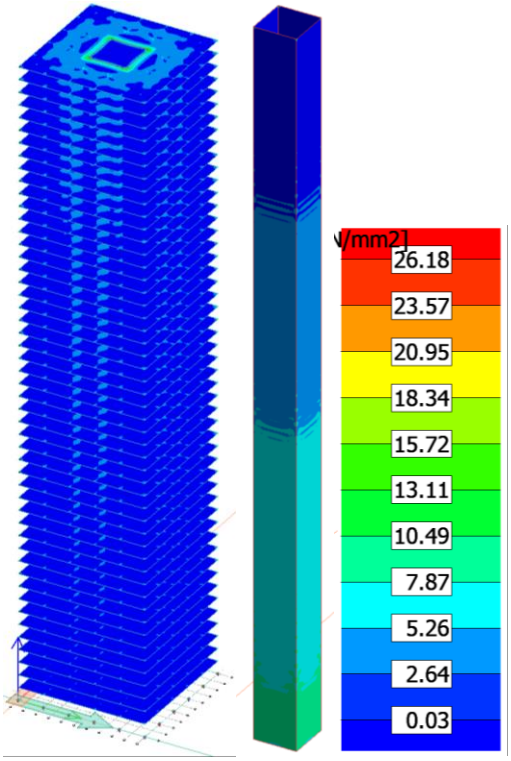

Figure 9.4: von Mises stress in shell elements of rigid connection model generated by dead load.

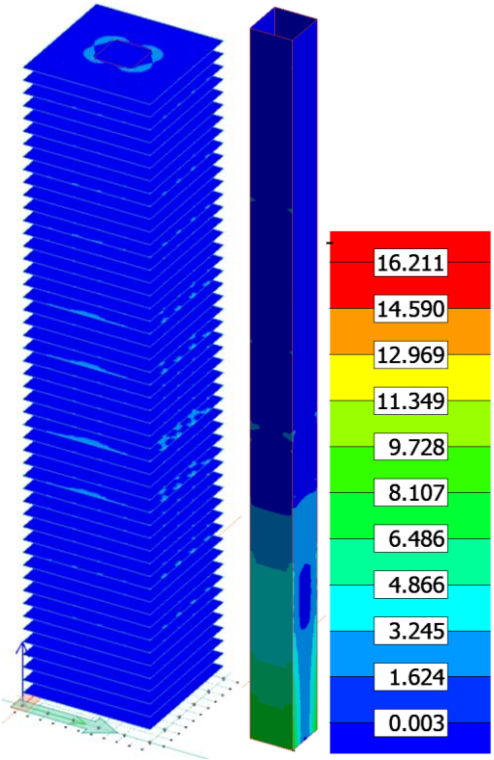

Figure 9.5: von Mises stress in shell elements of pinned connection model generated by wind load.

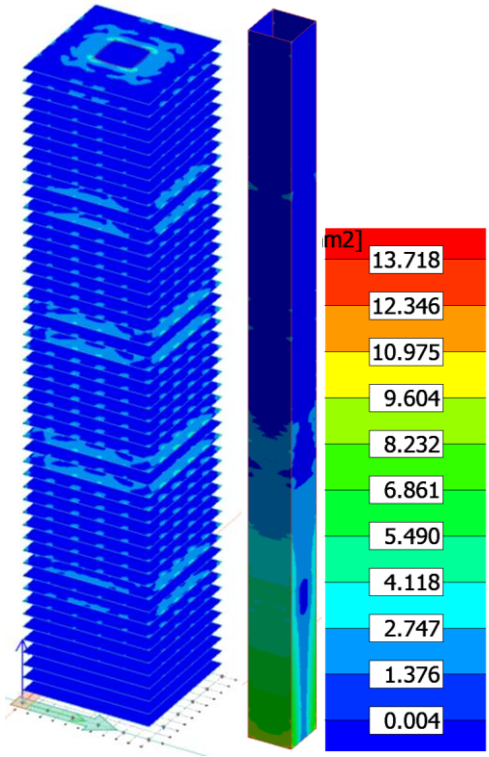

Figure 9.6: von Mises stress in shell elements of rigid connection model generated by wind load.

Stresses in concrete elements for combined load case are displayed in figures 9.7 and 9.8 for both models. Overall, the stress values for concrete floors were relatively small as for the tube structure, which could suggest that these elements are overdesigned. The floors experience the highest stress values specifically at the interface between the tube structure and the floors. The stress there exceeds the concrete strength locally. Nevertheless, considering the simplified modelling of the joint here and the complexity of the stress fields around wall to floor connections in concrete structures it was chosen to neglect this local stress concentration. It has no effect on the dynamic behaviour of the structure. The rigid model displayed a higher displacement, but lower stress values, in contrast to the pinned model, which is an interesting result of the internal force redistribution by the rigid connection system. The tube structure exhibits high stress values at one side of the tube in the bottom, which indicate that the tube is partially contributing to withstanding the wind force, which may be expected for the tube in tube system, but most of the lateral force is naturally resisted by outer tube.

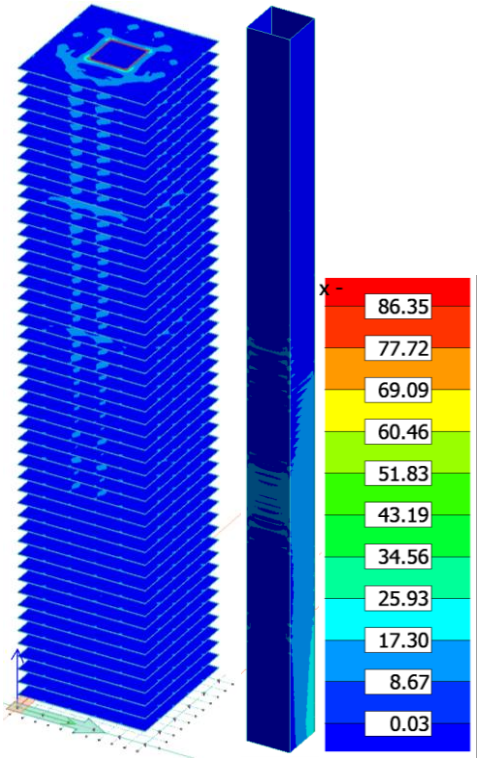

Figure 9.7:. von Mises stress in shell elements of pinned connection model from combined load.

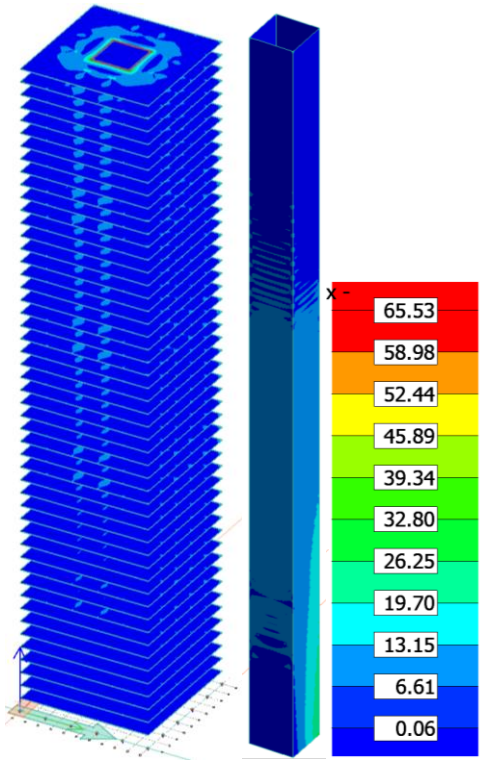

Figure 9.8: von Mises stress in shell elements of rigid connection model from combined load.

Figures 9.9 and 9.10 depicts the peak stress value observed in the combined load case. It is evident that the stress occurred locally at the interface between the corner columns and the concrete floors. Hence, localized stress can be negligible as it has no effect on the dynamic behaviour of the structure.

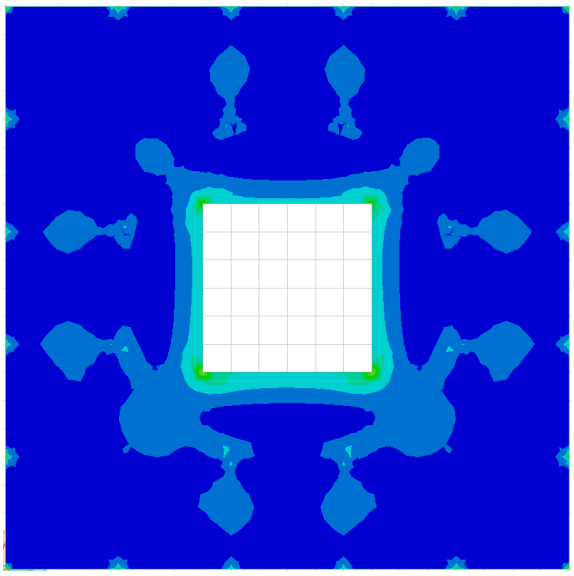

Figure 9.9: von Mises stress in the concrete floor from combined load case.

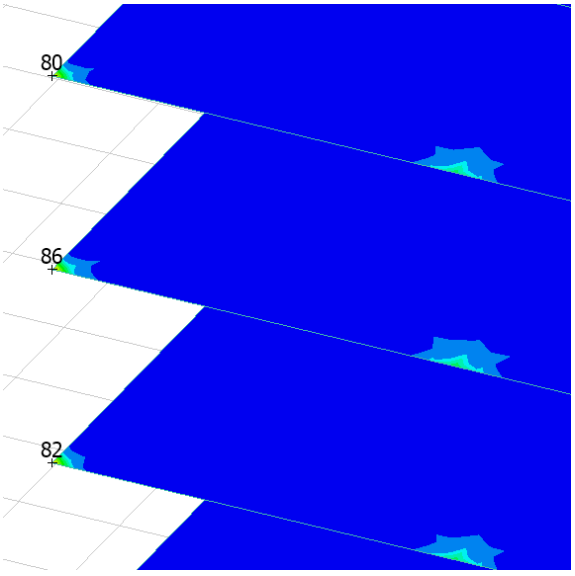

Figure 9.10: Peak von Mises stress at the interface between the corner columns and the concrete floors.

Stresses of steel bars were assessed separately for the different types of loading. Stresses from dead load are displayed in figures 9.11 and 9.12. The outer columns displayed moderate stress value ranges from 50.83 N/m^2 to 70,99 N/m^2 for pinned model, while stresses values for rigid model ranges from 58.20 N/m^2 to 81,39 N/m^2. For wind load, the highest stresses are concentrated at the belt trusses in the middle section for both models, which indicate that some additional optimization could reduce maximum local stresses in the steel parts even more, see figures 9.13 and 9.14.

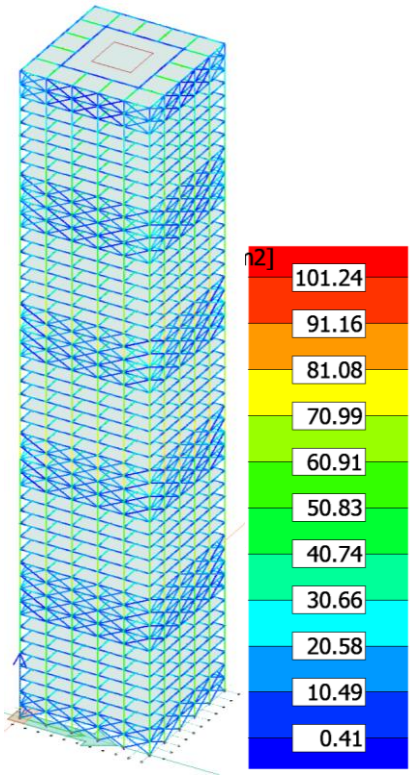

Figure 9.11: von Mises stress in bar elements of pinned connection model generated by dead load.

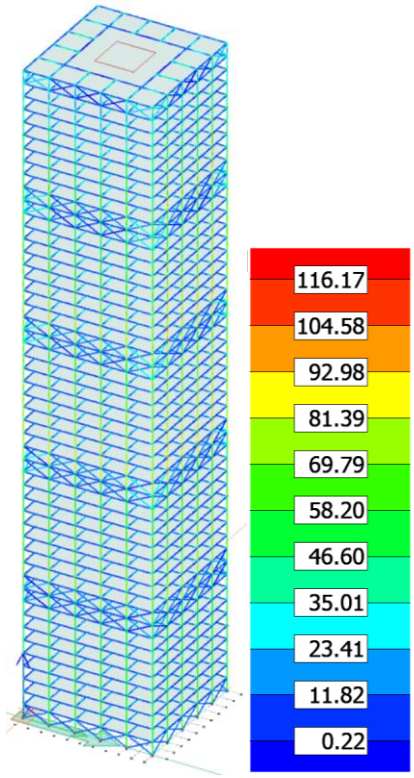

Figure 9.12 von Mises stress in bar elements of rigid connection model generated by dead load.

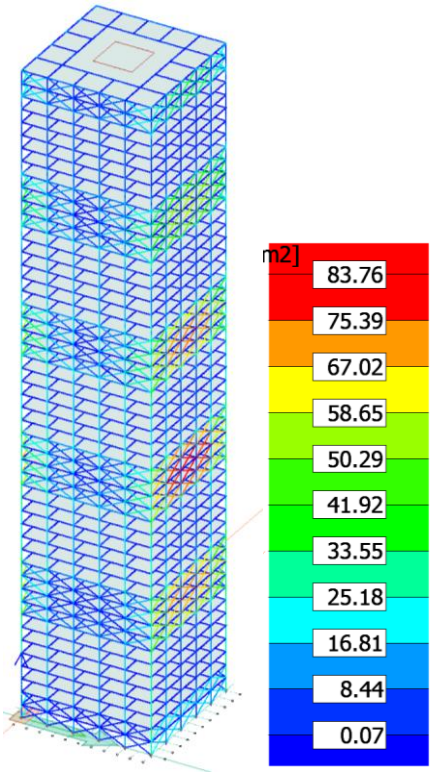

Figure 9.13: von Mises stress in bar elements of pinned connection model generated by wind load.

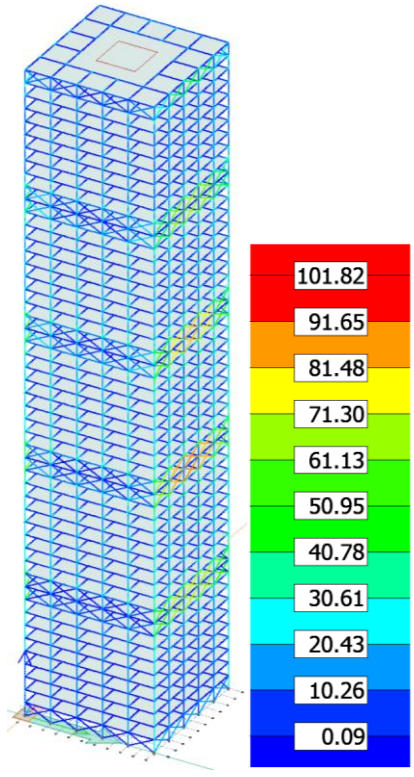

Figure 9.14: von Mises stress in bar elements of rigid connection model generated by wind load.

For the total stress assessment of the combined load cases, it is observed that the columns and bracing are more susceptible to wind loading compared to the horizontal beams. The perimeter columns display moderate level of stresses, and it is concentrated in the middle section of the structure as displayed in figures 9.15 and 9.16. Columns displayed stresses that has varies from a range of 111.2 N/mm^2 to 177.7 N/mm^2 for the pinned model, which is somewhat lower than rigid model with a range of 167 N/mm^2 to 266.9 N/mm^2.

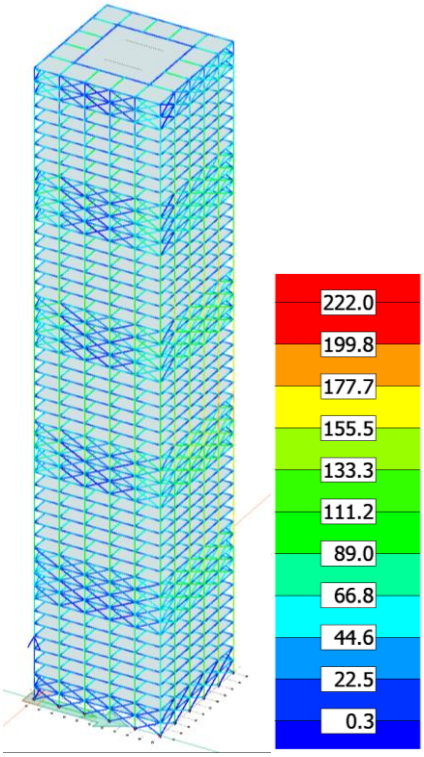

Figure 9.15: von Mises stress in bar elements of pinned connection model from combined load.

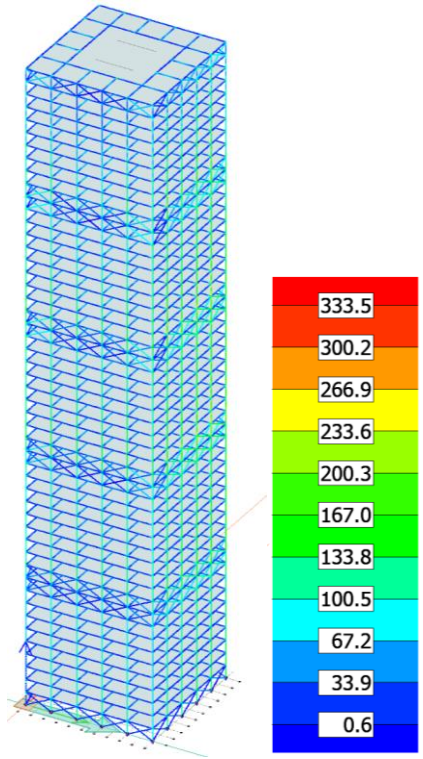

Figure 9.16: von Mises stress in bar elements of rigid connection model from combined load.

The highest level of stresses is observed locally at transition between profiles in the structure, specifically at the end of column and the start of the new profile, which is displayed in figure 9.17. The axial force only gradually changes by increasing on every floor, but the profile cross section changes abruptly to a smaller one, leading to sudden increase in stress. The high stress value displayed in the inner columns is due to the dead load of the building and the live load. As mentioned earlier, the core structure is supposed to provide assistance with bearing of the dead and live load, while the columns will primarily withstand most of the wind load. The approach can only be done by implementing outrigger beams which is the interface between the columns and the concrete core, which ensures the weight of the structure is transferred to the core. Since the model is simplified and outrigger beams were not employed in the model, which causes the columns to bear a lot of dead and live load as well.

Since the columns now bearing both dead and live load it is evident that, they will display the highest stress values compared to the rest of the structure.

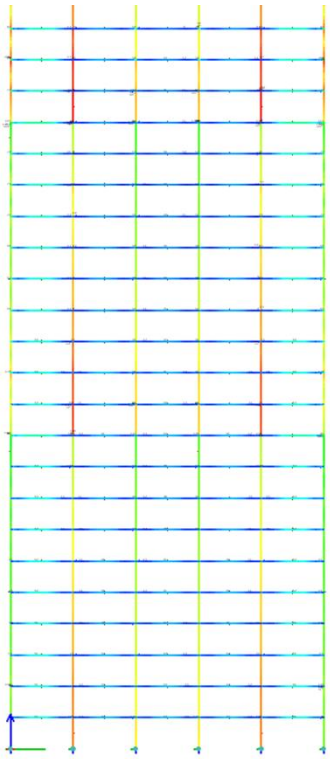

Figure 9.17: Peak von Mises stress in inner columns.

Still, the highest stress value does not exceed the yielding limit of steel, and the structure only deformed elastically. For concrete, stress concentration occurs locally at the connections, which have not undergone detailed design. Thereby it is expected that these stresses will not have any significant impact on the global dynamics of the structure. Hence, stresses are not in this case a critical parameter, but displacement are the more limiting factor for critical assessment. Such situation is rather natural for very tall and slender structures.

9.2.1. Stability analysis

Buckling of columns and lateral torsional buckling of beams are determined through stability analysis in FEM-design. The results for both models are displayed in table 9.1 and 9.2. The critical parameter is determined by the critical buckling force divided by the actual load (Bjergø, 2022). In other words, if the derived critical parameter is above 1, it indicates that it is safe for buckling. The values derived from the analysis based on quasistatic load case, suggest that buckling is not going to occur for given loads for the structure, both globally and locally, as the values are greater than 1.

Table 9.1: Stability analysis for pinned connection model.

Combination	Shape	Critical parameter
LC1ULS	1	8.631
	2	8.637
	3	9.566

Table 9.2: Stability analysis for rigid connection model.

Combination	Shape	Critical parameter
LC1ULS	1	10.287
	2	10.599
	3	11.914

9.2.2. Natural frequencies and modes

The results of the natural frequency and modal analysis is depicted in table 9.3 and 9.4. Lowest frequencies of the structure are 0.188 for pinned model and 0.172 Hz for rigid model. Mode shapes 1 and 2 in figures 9.19 and 9.20, display a bending motion in one direction of a fixed beam, which is the usual motion of first mode shape as seen in literature (Chopra, 2011). The lowest mode shapes are the most relevant because they can be easily excited by any wind subjected perpendicular to the surface.

In figures 9.23 and 9.24, mode shape 4 and 5 are displays bending in one axis as in the first mode shape, but forming a shorter wavelength as seen in the result. The frequencies associated with these mode shapes are higher, which indicate that the amount of excitation force required to initiate this bending is greater compared to the first mode shape. Mode shape 7 and 8 in figures 9.27 and 9.28 display bending with even shorter wavelength compared to the previous mode shapes. Natural frequencies are higher compared to the previous mode shapes and has a low occurrence probability as these are too energetically unfavourable, similarly to the higher buckling modes in the Euler bar analysis, figure 9.18.

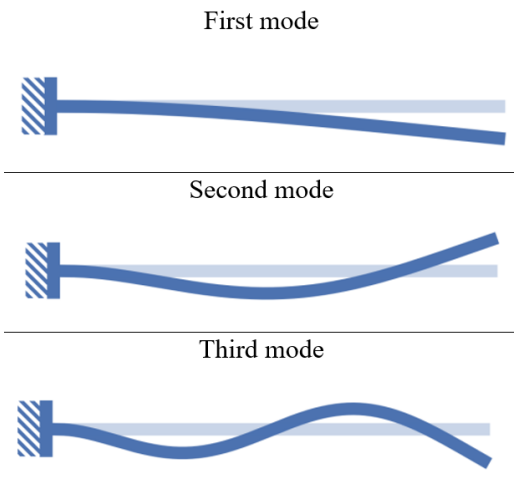

Figure 9.18: Buckling modes in the Euler bar analysis.

Both the pinned and rigid connection models exhibit torsional deformation at mode shapes 3 and 6, with frequencies of 0.504 Hz and 1.475 Hz for the pinned connection, and 0.486 Hz and 1.432 Hz for the rigid connection, as shown in figures 9.21, 9.22, 9.25 and 9.26. The occurrence of these mode shapes can be attributed to uneven loading inconsistent wind loading on the along-wind surface which create a torsional moment or uneven shear forces on the sides of the structure. The first torsional mode shape has a lower frequency, therefore less stiffness. Mode shape 6 depicts more complex deformation and has a higher frequency compared to previous one. Based on illustration from figures 9.25 and 9.26, it can be observed that to initiate this particular deformation, it requires two dominant excitation forces located at the top and bottom of the structure which are acting in opposition, which as mentioned earlier, will have a low occurrence probability. Based on the literature, the usual mode shape that can occur after the first mode is another bending mode, which is mode shapes 4 and 5 in our case. Since torsional deformation is the third mode shape, this suggests that the structure has somewhat low torsional stiffness.

The natural frequencies are determined by structural mass and stiffness. The square shape of the structure provides a symmetrical vibrational system with respect to 90-degree rotation that ensures an equivalent distribution of mass and stiffness in both the x and y directions, resulting in almost identical natural frequencies for the aforementioned modes. The bending mode shapes 1 2, 4, 5 ,7 and 8 are symmetrical and have almost identical natural frequencies for both pinned and rigid model, while torsional mode shapes are different. Both torsion modes correspond to two different torsional deformations that are not rotationally symmetrical. The small difference in natural frequencies for symmetrical shapes are due to limitations of the accuracy of the numerical model.

The results for pinned and rigid are quite similar. The difference between the models is the mass distribution and stiffness of the structure. Although the mass of both models is nearly the same, the only distinguishing factor is the mass from the horizontal bracing. The rigid model has some bracing necessary to limit max displacement but much less than the pinned model. The stiffness of the rigid model is provided in a quite different way due to full moment in the joints. Therefore, the differences in natural frequencies between the two models are primarily due to their stiffness. The local stiffness of the rigid model should be higher due to the moment-bearing joints but the overall structural stiffness of the pinned model in this case is higher, which can be seen in max displacement in static case. Thereby the main lowest frequencies are partially higher for the pinned structure. For these lowest modes, the details of the structure are irrelevant, only global stiffness is relevant.

Table 9.3: Natural frequencies of pinned connection model.

Shape	Frequency (Hz)	Period (s)	Modal mass	mx' %	my' %
1	0.188	5.319	1.000	65.779	0.000
2	0.188	5.305	1.000	0.000	65.780
3	0.504	1.986	1.000	0.000	0.000
4	0.757	1.320	1.000	17.031	0.000
5	0.759	1.318	1.000	0.000	17.036
6	1.475	0.678	1.000	0.000	0.000
7	1.765	0.566	1.000	6.512	0.000
8	1.768	0.566	1.000	0.000	6.512

Table 9.4: Natural frequencies of rigid connection model.

Shape	Frequency (Hz)	Period (s)	Modal mass	mx' %	my' %
1	0.172	5.818	1.000	65.154	0.000
2	0.174	5.747	1.000	0.000	65.286
3	0.486	2.059	1.000	0.000	0.000
4	0.720	1.388	1.000	17.348	0.000
5	0.725	1.379	1.000	0.000	17.260
6	1.423	0.703	1.000	0.000	0.000
7	1.716	0.583	1.000	6.679	0.000
8	1.722	0.581	1.000	0.000	6.656

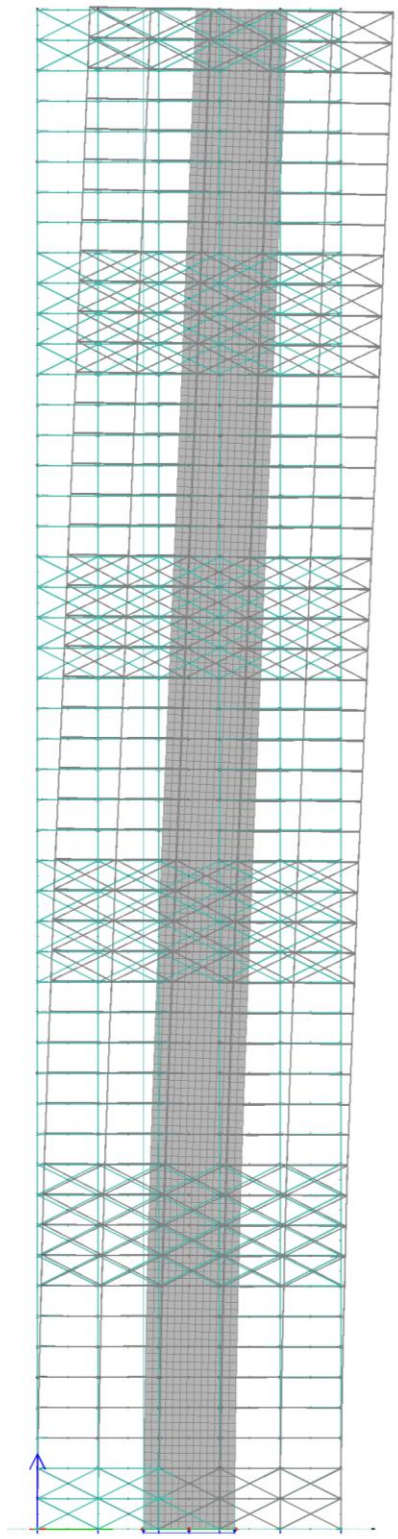

Figure 9.19: Mode shapes 1 and 2 in the x- and y-axes for a pinned connection model.

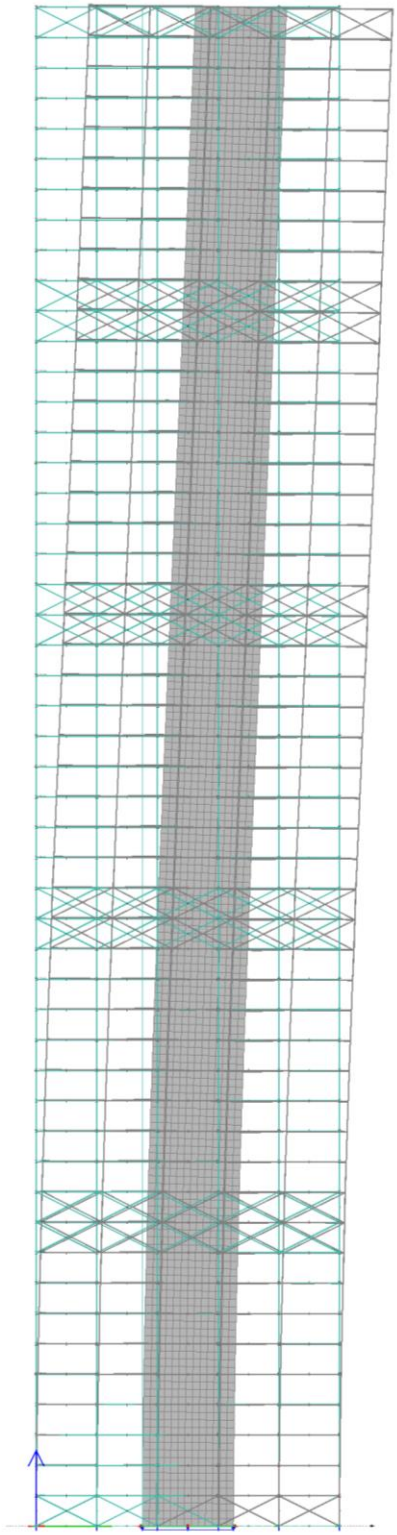

Figure 9.20: Mode shapes 1 and 2 in the x- and y-axes for a rigid connection model.

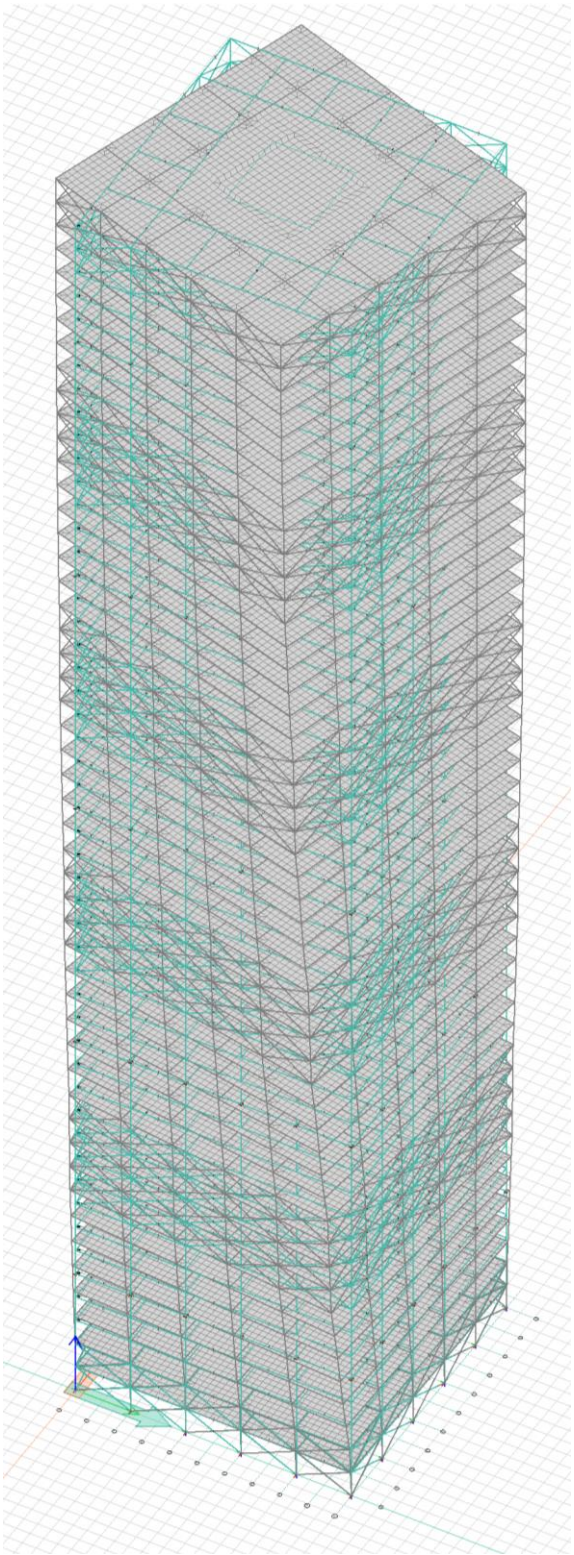

Figure 9.21: Mode shape 3 for pinned connection model.

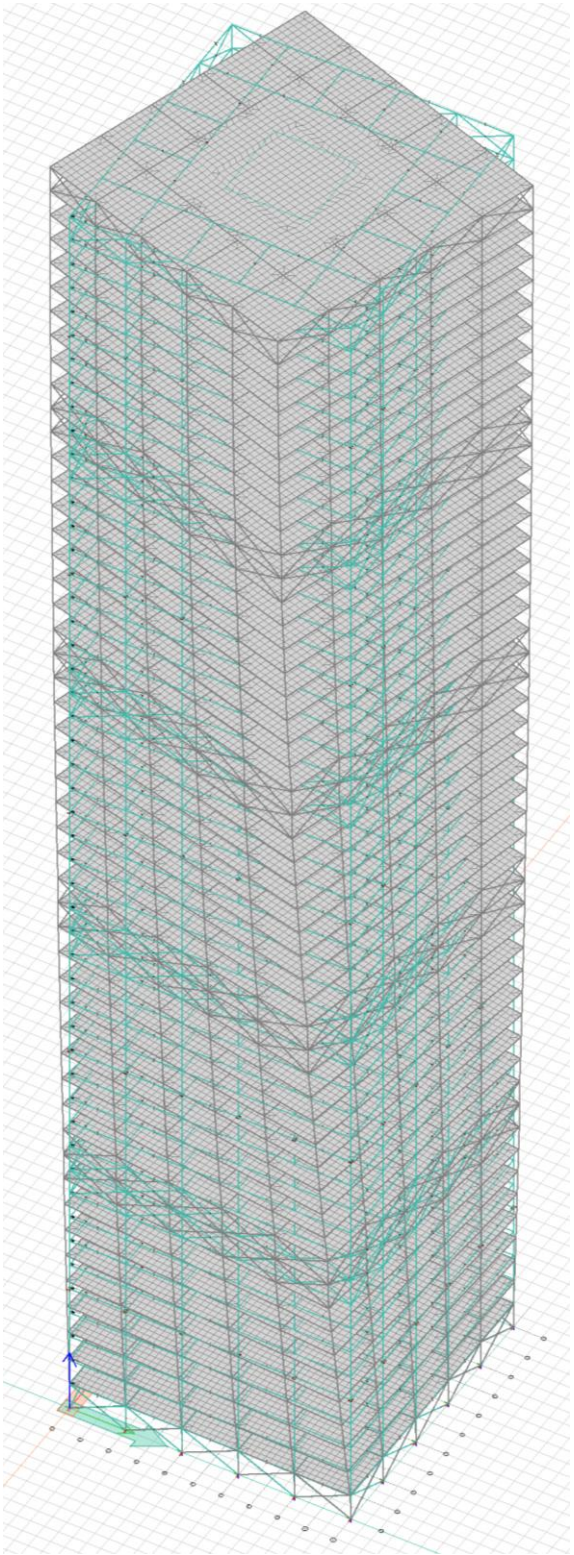

Figure 9.22: Mode shape 3 for rigid connection model.

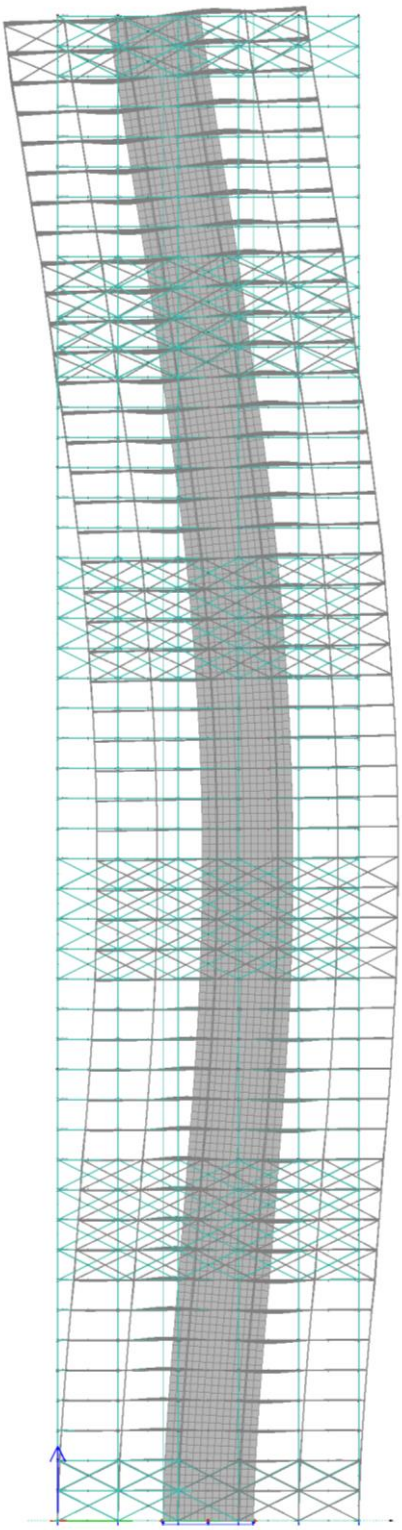

Figure 9.23: Mode shapes 4 and 5 in the x- and y-axes for a pinned connection model.

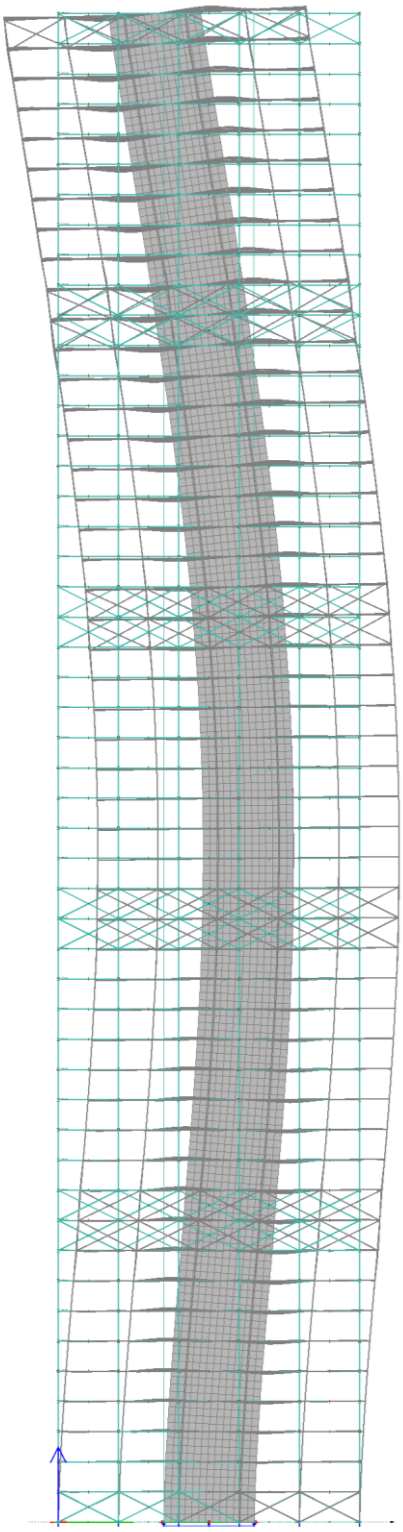

Figure 9.24: Mode shapes 4 and 5 in the x- and y-axes for a rigid connection model.

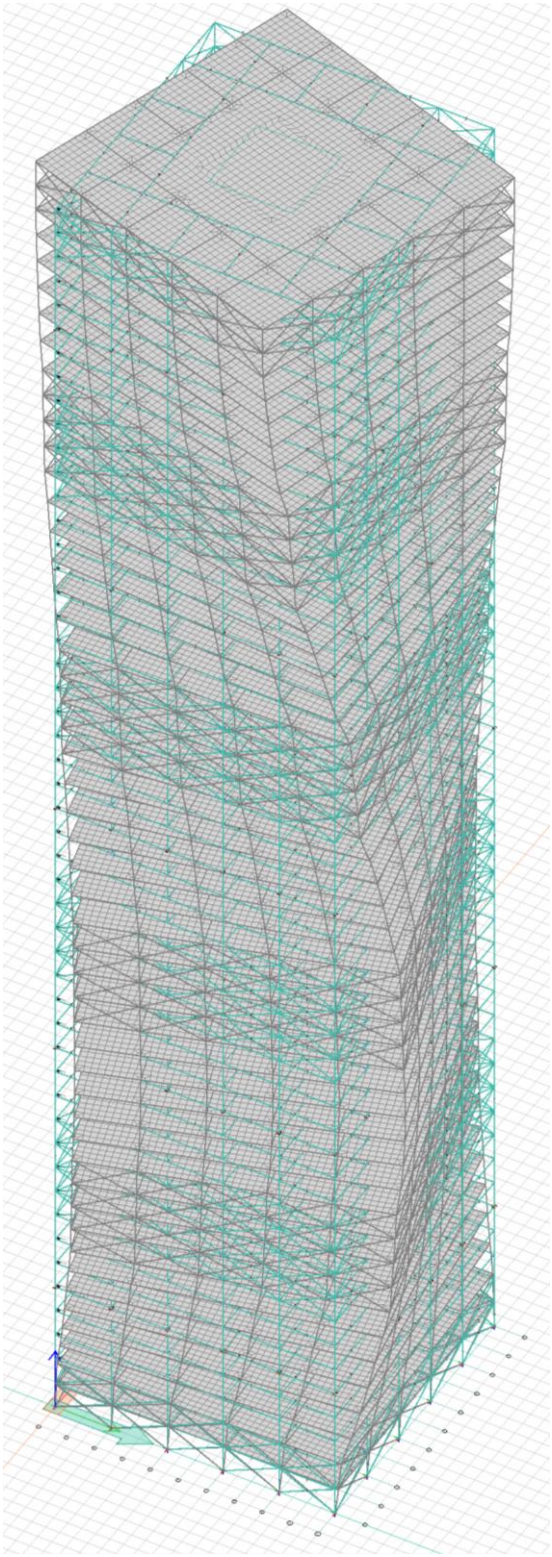

Figure 9.25: Mode shape 6 for pinned connection model.

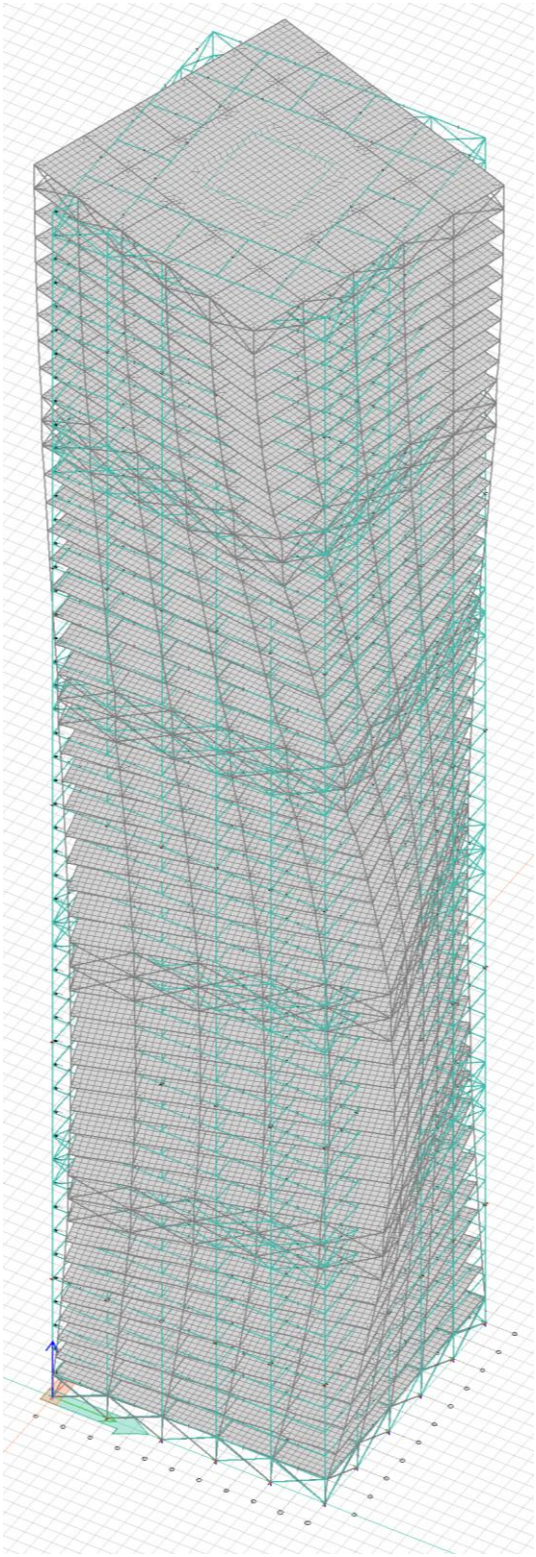

Figure 9.26: Mode shape 6 for rigid connection model

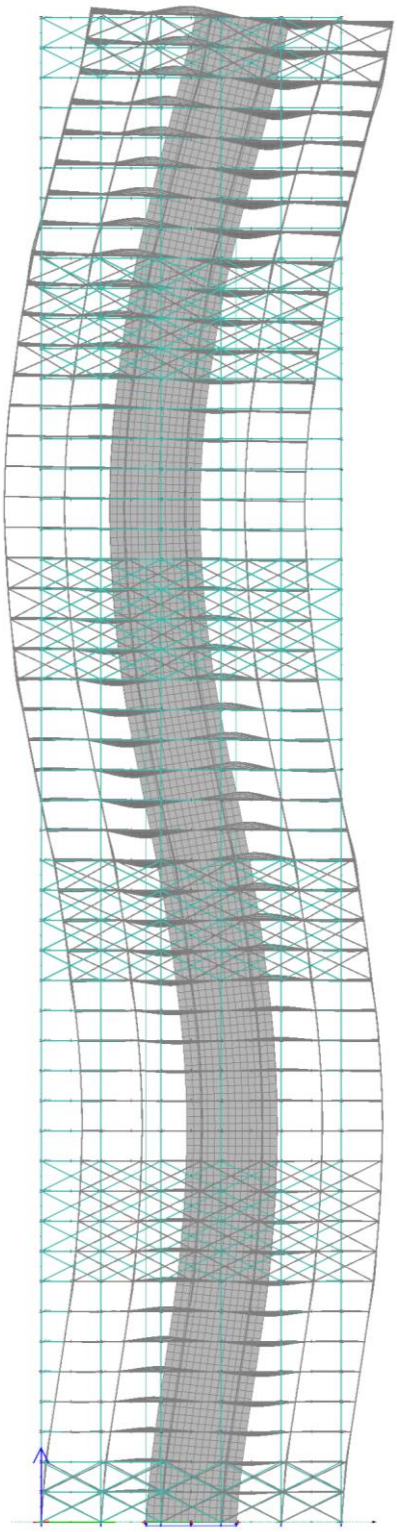

Figure 9.27: Mode shapes 7 and 8 in the x- and y-axes for a pinned connection model.

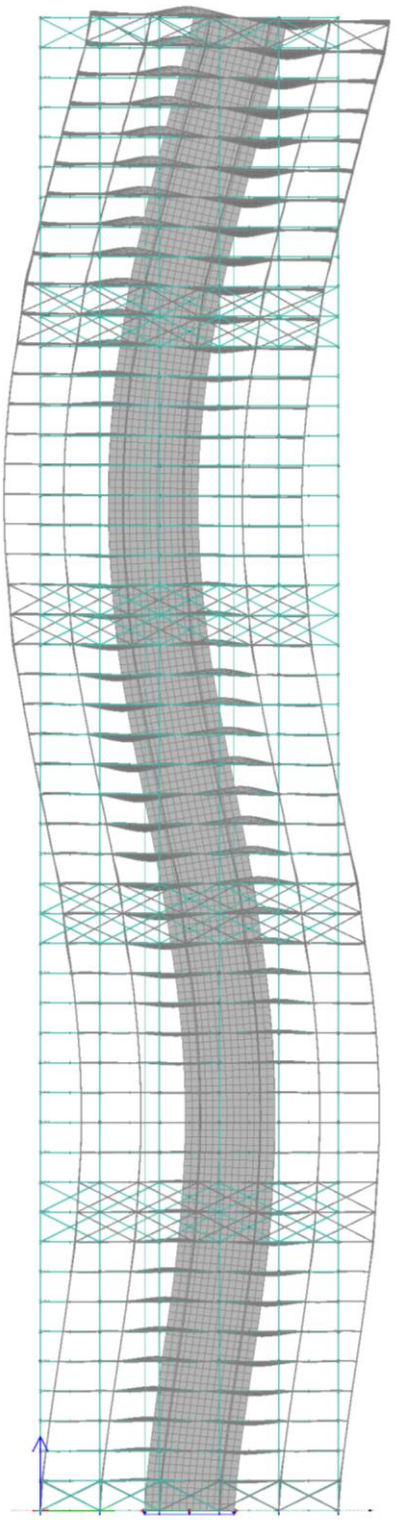

Figure 9.28: Mode shapes 7 and 8 in the x- and y-axes for a rigid connection model.

9.3. Dynamic load and response of models

Figures 9.29 and 9.30 display the motion of the building in response to the dynamic load generated by the simulation. The displacement has peak initial value at 178.3mm for pinned model, and 214.7 mm for rigid model. The vibration of the structure is displayed in figure 9.31 for pinned model and figure 9.32 for rigid model. The curves include two lines which represent the static and dynamic results. The static result depicts the displacement for a force in that specific time point as a static load. The purpose is to assist the user to comprehend and visualize the difference between the dynamic and static results, and to better understand the dynamic amplification factors.

The observation of 5-seconds period of vibration in the displacement versus time diagram indicates that the dynamic wind has excited the first natural frequency of the structure. The gradually decreasing amplitude of the structure illustrates damping in the structure, which implies that the supplied energy is insufficient to sustain the vibration. Conversely, had the wind maintained the same frequency, the amplitude could have sustained and gradually increased over time, hence causing the building to resonate.

The curves for both models can be segmented in three distinct zones. The first zone displays the initial strong transient vibration of the first mode shape is excited by wind force growing from zero to max within the first few seconds and gradually decreases as the structure initiates its damping effect. Oscillation of the structure is partially dissipated and stabilized in the second zone. Low amplitude of vibration with little damping were observed. In the third zone, it is apparent that vibration is still present, but the dynamic effect has mostly disappeared. Hence, the dynamic and static curves are the same. Frequency distribution in the PSD does not match the eigenfrequencies of the structure, thereby the wind load is insufficient to initiate more forced vibrations in the structure.

The dynamic analysis in the FEM design software does not display von Mises stresses directly as an analysis result. Based on the previous results, the structure is still linearly elastically deformed since the displacement in the dynamic case is lower compared to the quasistatic loading. This implies that the stress is proportional to the displacement. Therefore, the stresses of dynamic case can be evaluated from comparison with quasistatic case. Since the displacement of static case is almost double as high compared to dynamic case, the stresses occurred in the static case then are approximately twice as high as von Mises stress in dynamic load case.

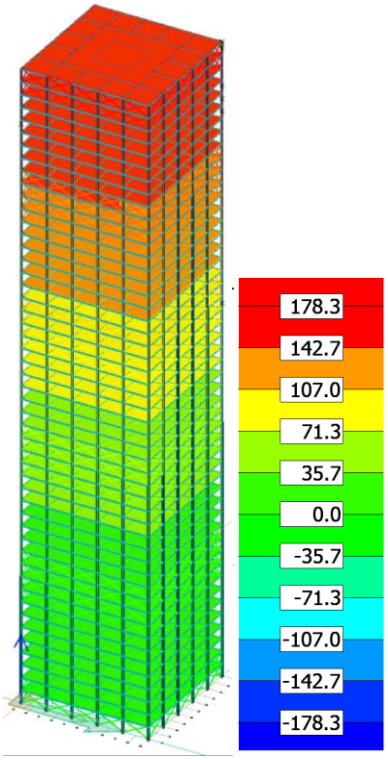

Figure 9.29: Horizontal displacement of pinned connection model subjected to dynamic wind load.

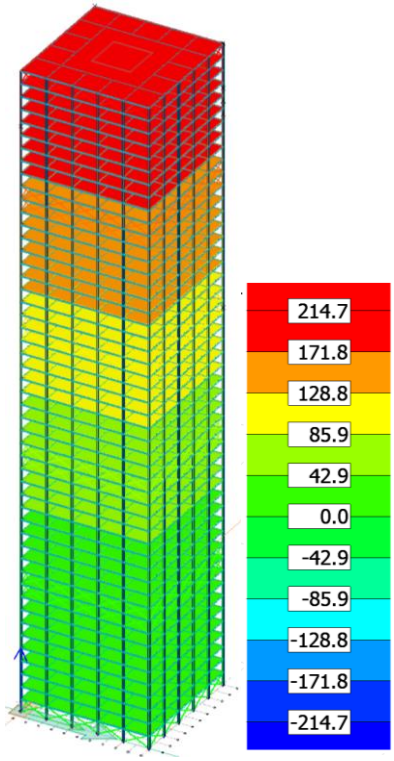

Figure 9.30: Horizontal displacement of rigid connection model subjected to dynamic wind load.

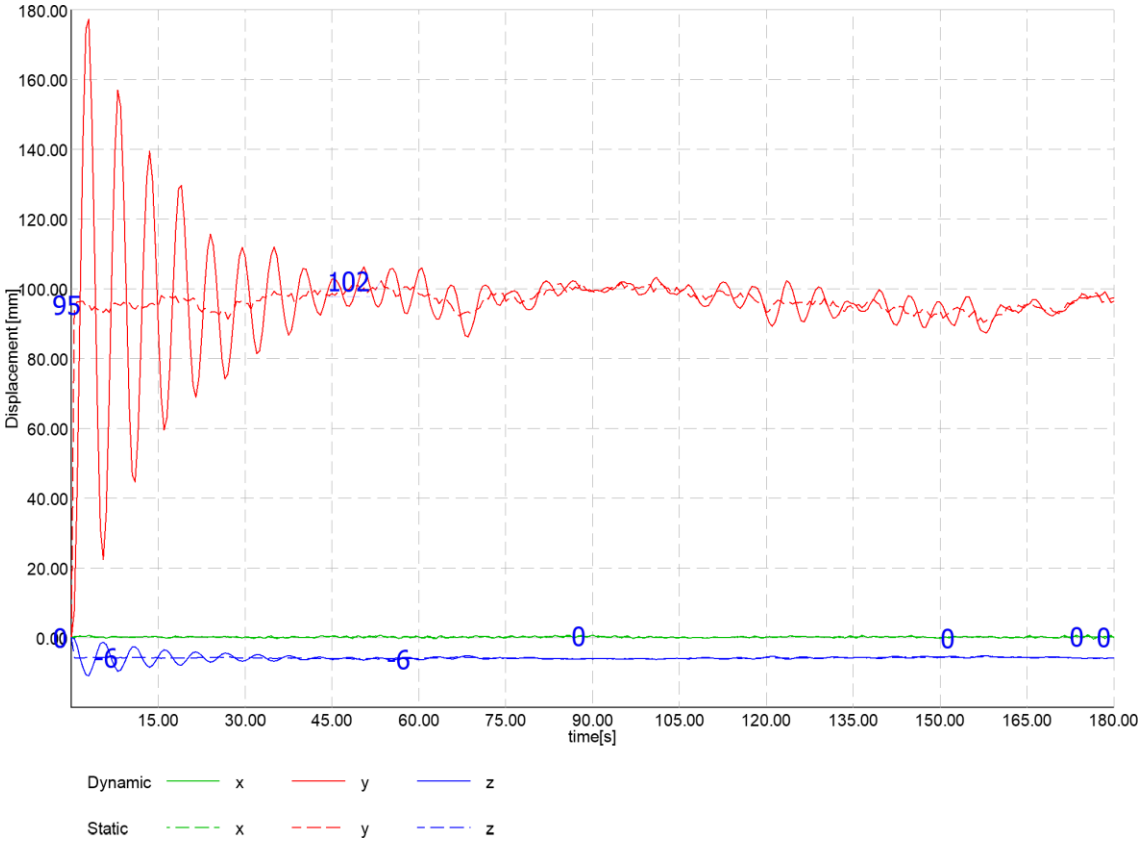

Figure 9.31: Dynamic and static displacement for pinned connection in x-, y- and z-axis with respect to time.

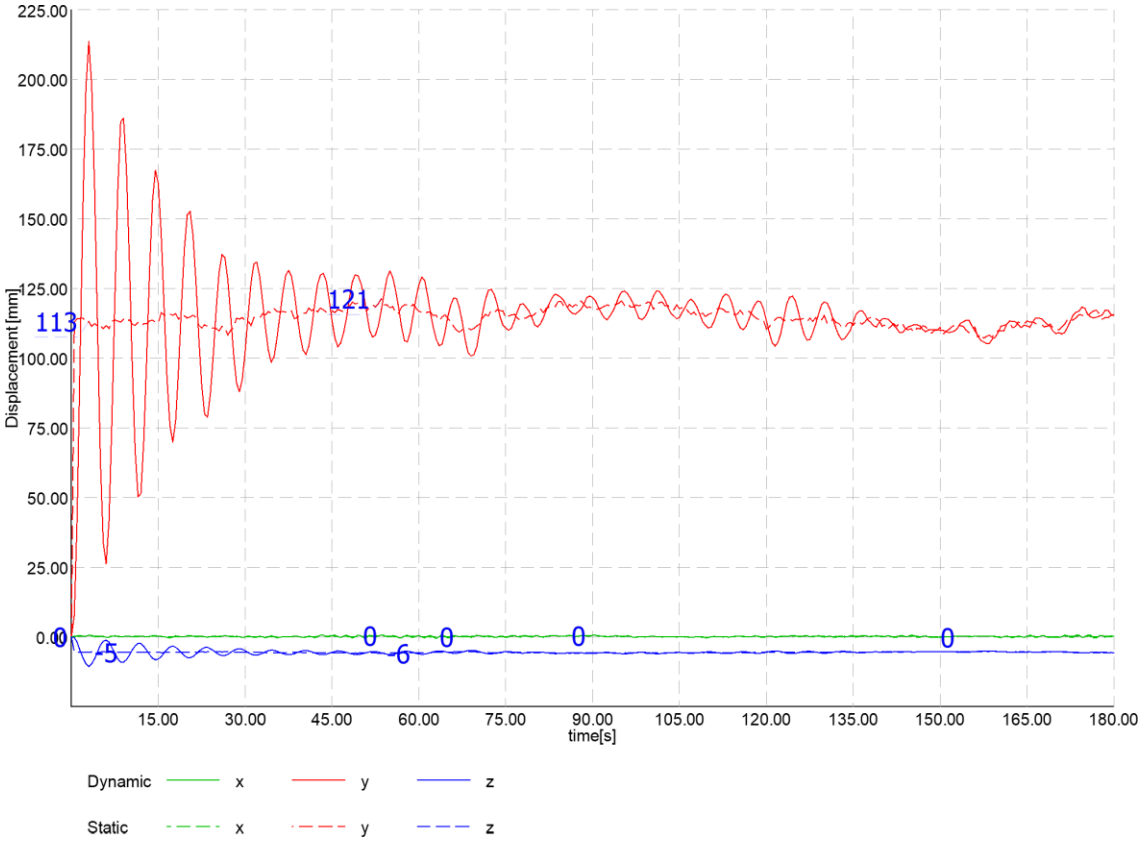

Figure 9.32: Dynamic and static displacement for rigid connection in x-, y- and z-axis with respect to time.

Based on the assessment of displacement for both models, it is observed that deformation is within the elastic range and did not exceed the yielding limit. However, the rigid model demonstrated better utilization of material capacity as it was subjected to higher stresses compared to the pinned model. Moreover, the rigid model required less bracing, which resulted in a reduction of materials used. Despite this, assembly of rigid connection on site is time consuming and challenging as it requires precise alignment and fitting of the connection plates and bolts. Both models have advantages and disadvantages, thereby which connection configuration should not be based solely on these observations.

9.4. Comparison of quasistatic wind and dynamic wind

In analysing the effects of quasistatic wind load, it was found that pinned connection model experiences a maximum displacement of 377.5 mm at the top of the structure. In contrast, rigid model exhibits an even higher displacement value of 434.4 mm. Under dynamic wind load, the pinned connection model displays a top displacement of 178.3 mm, whereas the rigid connection model experiences a displacement value of 214.7 mm. The results indicated the same trend in displacement

for both static and dynamic analysis. One noteworthy observation is that the rigid model without any bracing was tested but found not stiff enough to resist deflection and was well outside of deflection criteria. Therefore, the belt trusses were implemented in the model, but in smaller quantity.

When analysing the displacement of a model under quasistatic and dynamic wind load, it was observed that the quasistatic wind load resulted in a higher horizontal displacement compared to the dynamic wind load for both the pinned and rigid model. Several factors may have contributed to this difference. Firstly, the calculation of quasistatic wind load is based on NS-EN 1991 standards, while dynamic wind load is generated using the ASCE standards, which involve different values based on different datasets. According to NS-EN 1991, the height factor yields wind pressures at the top that are three times higher than those located at the bottom of the structure. This is evident from the calculation outlined in appendix x. Notably, the dynamic wind derived from the simulator and subsequently converted into wind pressures is significantly lower than the quasistatic wind. NOWS is based on mathematical modelling of measured data and the variation of windspeed in height is a model approximation. The relevant height of 200 m could be outside of the heights that the simulator was designed for and there was no information regarding this in the description of the simulator, hence it is assumed that the wind speed is an extrapolation. The height factor in NS-EN 1991 is also an extrapolation, as demonstrated in the methodology section. Based on the given information, it can be assumed that NS-EN 1991 adopts a highly conservative approach, while NOWS offers a more realistic wind. It is important to be critically when utilising the simulator in extreme instances where structures exceed a certain height, such as 200 meters.

9.5. Acceleration and comfort

The results in figures 9.33 and 9.34 indicate that the structure exhibits a swaying motion, given the range of positive and negative acceleration values. The maximum acceleration values occur at the top levels and decrease in magnitude at lower levels, with a maximum value of 0.111 m/s2. There is no significant difference in acceleration values between the two models. Since acceleration is correlated with natural frequencies, and there was a small difference in natural frequencies, hence the results displayed similar acceleration values for both models, as seen in figures 9.35 and 9.36.

Humans can perceive motion within a certain range, and for office buildings, the comfort criteria for acceleration ranges from 0.02 to 0.2 m/s2 as shown in table 7.1. Based on the acceleration values obtained from the analysis, both models demonstrate that they can with maintain acceptable acceleration levels, particularly at the critical section at the top of the building where high acceleration

can occur. These results suggest that discomfort and unease resulting from wind-induced vibrations are minimized and fall within the acceptable acceleration criteria.

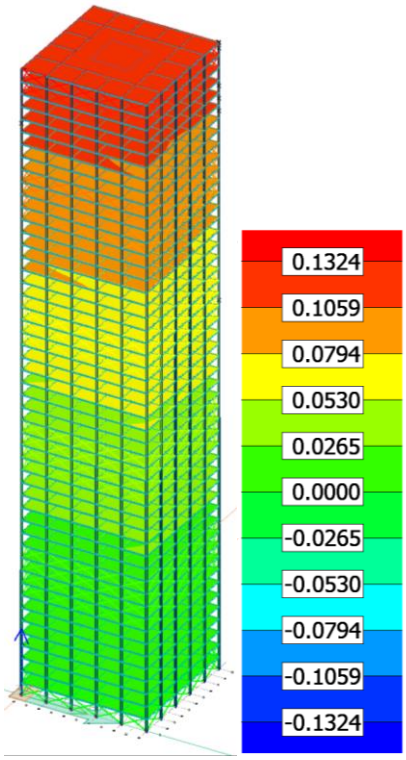

Figure 9.33: Horizontal displacement of pinned connection model subjected to quasi-static wind load.

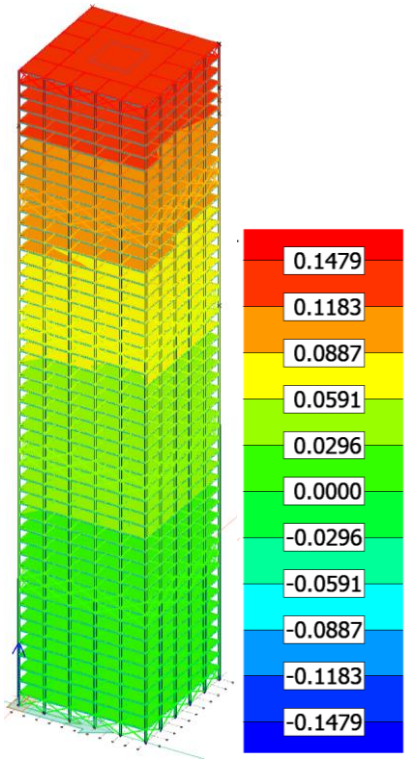

Figure 9.34: Horizontal displacement of rigid connection model subjected to quasi-static wind load.

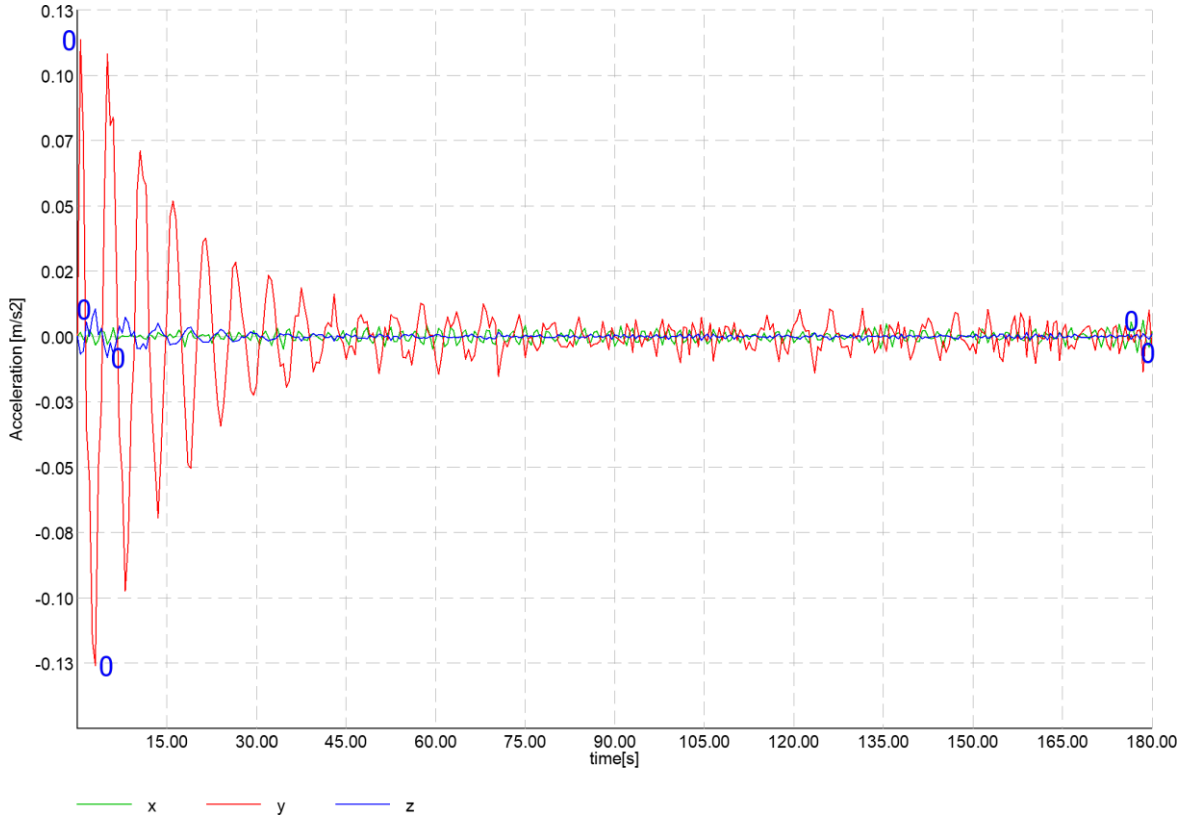

Figure 9.35: The acceleration of the highest column for pinned connection along the x-, y-, and z-axes with respect to time.

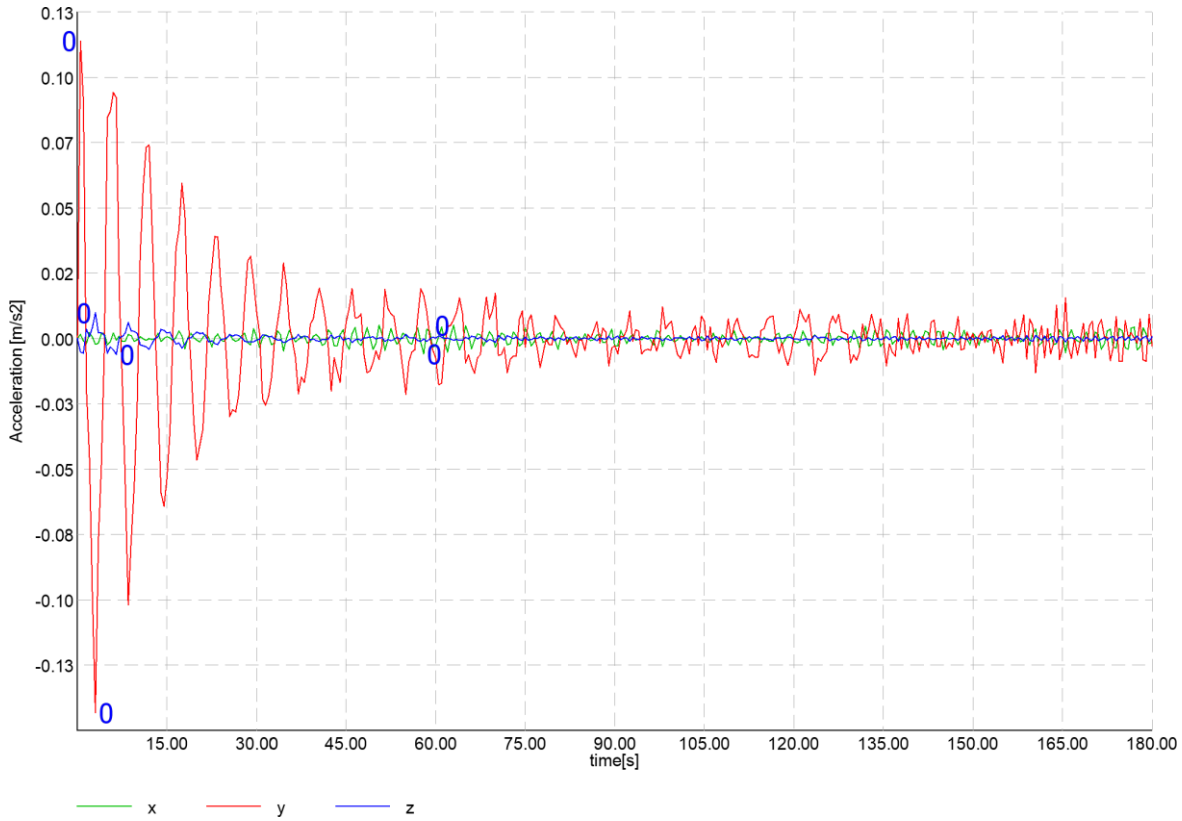

Figure 9.36. The acceleration of the highest column for rigid connection along the x-, y-, and z-axes with respect to time.

Chapter 10

Conclusion

Based on the analysis results, both models met the top displacement criteria in the wind dynamic case. While the pinned model also satisfied the criteria for the quasistatic wind load case, the rigid model only partially exceeded the limit. The implementation of belt truss bracing in the models increased their stiffness, resulting in a significant reduction in top displacement. It should be noted, however, that the top displacement criteria are a conservative approach that needs to be considered individually for each structure.

In terms of stress values, the maximum values in concrete elements were found locally at the interface between elements, which is insignificant for the overall behaviour of the structure and can be disregarded. The stresses in concrete elements were relatively small and did not exceed the yielding limit for both load cases. To better utilize the concrete core capacity, an outrigger system should be implemented in the model. The maximum stresses in steel elements were found between the transition of column profiles. The von Mises stress displayed remained in the elastic deformation zone and did not exceed the yield limit. The rigid model experienced higher stresses than the pinned model, indicating better utilization of the material capacity.

According to the acceleration analysis, acceleration in all cases was within the acceptable limit from the literature. These findings indicate that the occurrence of discomfort and unease caused by wind-induced vibrations are minimized.

Symmetrical geometry of the structure resulted almost identical natural frequencies for bending mode shapes due to equivalent distribution of mass and stiffness in both the x and y directions. When subjected to dynamic wind, first mode shape of the structure was activated and gradually decreases with time and dynamic effect almost disappeared from the system. This suggests that the frequency distribution in the PSD does not match the eigenfrequencies of the structure and thereby could not initiate more forced vibrations in the structure. Based on the results in wind design, wind model generated by the NOWS resulted less wind pressure compared to the quasistatic wind calculated based on NS-EN 1991. Thus, it can be concluded that wind design based on NS-EN 1991 is conversative.

Further work

Field measurements should be conducted to acquire more accurate wind profile due to NS-EN 1991 contains outdated wind data, in addition to inadequate calculation inputs when the buildings exceed a certain height. NOWS offers an efficient approach to generate approximated wind but does not guarantee complete reliability. Furthermore, wind tunnel testing and numerical wind analysis by CFD should be performed to have a more precise representation regarding the effects of wind pressure, shear drag, turbulence, and cross wind.

As mentioned earlier, the model constructed was simplified representation and the model may not accurately illustrate the actual behaviour of tube in tube system. Implementation of outrigger system and detailed design of connection will significantly improve the stiffness and mass distribution of the structure. Thereby, to better assess the behaviour and response of the structure when subjected to wind, a more detailed and optimized structure is needed.

Modelling of aerodynamics effect using to assess how fluid flow interacts with structures CFD is essential in designing high-rise. Further work should include assessment of aeroelastic effect such as flutter on high-rise buildings to ensure structural safety and comfort of occupants.

References

American Society of Civil Engineers Staff. (2021). Minimum Design Loads and Associated Criteria for Buildings and Other Structures. In.

Australian/New Zealand Standard. (2021). Structural design actions, Part 2: Wind actions. In.

Barbero, E. J. (2013). *Finite Element Analysis of Composite Materials using Abaqus™* (1 ed.).

Binck, C., Cao, A. S., & Frangi, A. (2022). Lateral stiffening systems for tall timber buildings–tube-in-tube systems. *Wood Material Science & Engineering*, *17*(4), 309-316.

Bjergø, I. B. (2022). *Analysis*. Retrieved May 10 from https://wiki.fem-design.strusoft.com/xwiki/bin/view/Manuals/User%20Manual/Analysis/

Burton, M., Kwok, K. C. S., Abdelrazaq, A. (2015). Wind-Induced Motion of Tall Buildings: Designing for occupant comfort. https://global.ctbuh.org/resources/papers/download/2311-wind-induced-motion-of-tall-buildings-designing-for-occupant-comfort.pdf

Chopra, A. K. (2011). *Dynamics of Structures: Theory and Applications to Earthquake Engineering* (4 ed.). Pearson.

Fiskum, J. (2012). Verification of the Wind Induced Dynamic Response of the Svinesund Bridge in the Time Domain by the use of Autoregressive Simulations. https://ntnuopen.ntnu.no/ntnu-xmlui/handle/11250/237136

Flickr. (n.d.). *One World Trade Center construction site, New York City*. Retrieved April 04 from https://www.flickr.com/photos/jag9889/8021188047

Fu, F. (2018). Design and Analysis of Tall and Complex Structures. (1)

Kim, N.-H. (2014). *Introduction to Nonlinear Finite Element Analysis* (2015 ed.).

Kontrollbetong. (n.d.). Ulike typer betong. https://kontrollbetong.no/aktuelt/ulike-typer-betong/

Kurowski, P. M. (2016). *Finite Element Analysis for Design Engineers* (2 ed.). December 1.

Mendis, P., Ngo, T.D., Haritos, N. (2017). Wind Loading on Tall Buildings. https://www.researchgate.net/publication/270162977_Wind_loading_on_tall_buildings#fullTextFileContent

Nair, S. R., Rooby, J., & Branesh, R. J. (2020). A Comparative Study of Aerodynamic Coefficients on Tall Structures using Experimental Studies with International Codes and Standards. IOP Conference Series: Materials Science and Engineering,

NatHaz, N. H. M. L. a. t. U. o. N. D. (n.d.). Brief Summary of NOWS Theoretical Backgrounds. Retrieved 2023 April, from http://windsim.ce.nd.edu/doc/Theo_backg1.pdf

Norsk Standard. (2009a). Eurokode 1: Laster på konstruksjoner - Del 1-4: Allmenne laster - Vindlaster. In.

Norsk Standard. (2009b). Eurokode 3: Prosjektering av stålkonstruksjoner - Del 1-8: Knutepunkter og forbindelser. In.

Norsk Standard. (2015). Eurokode 3: Prosjektering av stålkonstruksjoner - Del 1-1: Allmenne regler og regler for bygninger. In.

Orcina. (n.d.). Rayleigh damping: Guidance. https://www.orcina.com/webhelp/OrcaFlex/Content/html/Rayleighdamping,Guidance.htm

P.A., K. (n.d.). Mechanics Lecture Notes: An introduction to Solid Mechanics. http://homepages.engineering.auckland.ac.nz/~pkel015/SolidMechanicsBooks/index.html

Simiu, E. (2011). *Design of Buildings for Wind: A Guide for ASCE 7-10 Standard Users and Designers of Special Structures* (2 ed.).

Smith, R. J. (2011). Deflection Limits in Tall Buildings—Are They Useful? https://www.researchgate.net/publication/269083259_Deflection_Limits_in_Tall_Buildings-Are_They_Useful

Sun, J., Lee, K., & Lee, H. (2000). Comparison of implicit and explicit finite element methods for dynamic problems. *Journal of materials processing technology*, *105*(1-2), 110-118.

Thue, J. V. (2019). Betong. https://snl.no/betong

Wikipedia. (2023). Stress–strain curve. https://en.wikipedia.org/wiki/Stress%E2%80%93strain_curve

Appendix A

Case 1

$$\Sigma M_A = F * 3{,}5m - B_z * 3{,}5m$$
$$B_z * 3{,}5m = F * 3{,}5m$$
$$B_z = F \rightarrow B_z = 20$$

$$\Sigma F_Z = A_z + B_z = 0$$
$$A_z = -B_z$$
$$A_z = -20$$

$$\Sigma F_x = A_x + F = 0$$
$$A_x = -F$$
$$A_x = -20$$

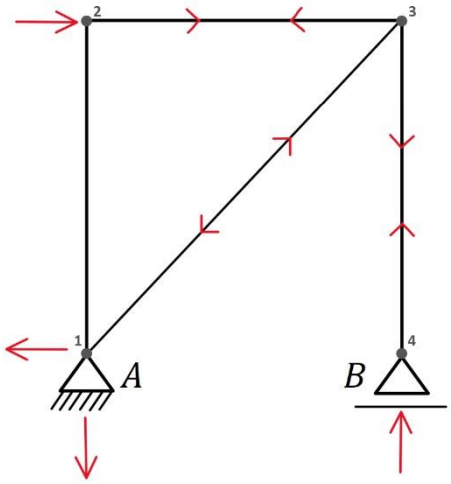

Shear force:

A_x	= 20 kN	A_z	= -20 kN
B_x	= 0 kN	B_z	= 20 kN

Internal force:

1-2	= 0 kN	2-3	= 20 kN
3-4	= 20 kN	3-1	= 28 kN

Case 2

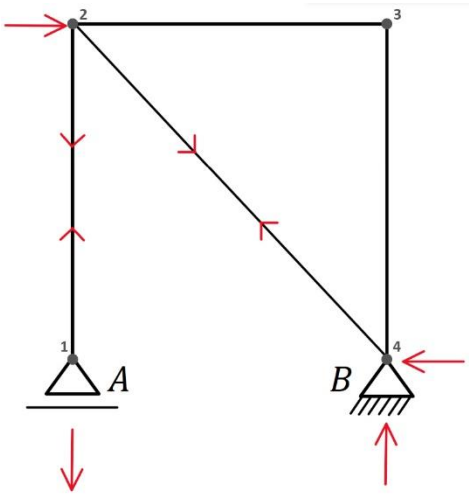

$$\Sigma M_A = F * 3{,}5m - B_z * 3{,}5m$$
$$B_z * 3{,}5m = F * 3{,}5m$$
$$B_z = F \rightarrow B_z = 20$$

$$\Sigma F_Z = A_z + B_z = 0$$
$$A_z = -B_z$$
$$A_z = -20$$

$$\Sigma F_x = B_x + F = 0$$
$$B_x = -F$$
$$B_x = -20$$

Shear force:

A_x	= 0 kN	A_z	= -20 kN
B_x	= 20 kN	B_z	= 20 kN

Internal force:

1-2	= 20 kN	2-3	= 0 kN
3-4	= 0 kN	2-4	= 28 kN

Case 3

$$\Sigma M_A = F * 3{,}5m - B_z * 3{,}5m$$
$$B_z * 3{,}5m = F * 3{,}5m$$
$$B_z = F \rightarrow B_z = 20$$

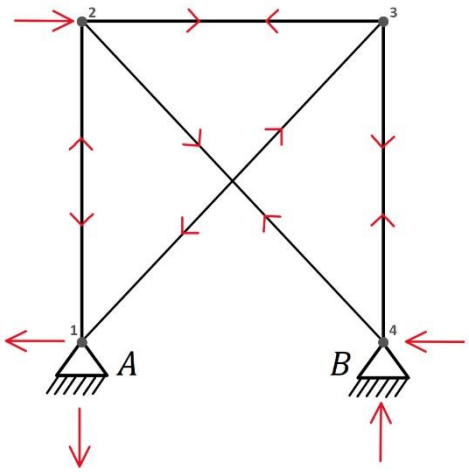

$$\Sigma F_Z = A_z + B_z = 0$$
$$A_z = -B_z$$
$$A_z = -20$$

$$\Sigma F_x = A_z + B_x + F = 0$$
$$B_x = -F/2 = -10$$
$$A_x = -F/2 = -10$$

Shear force:

A_x	= 10 kN	A_z	= -20 kN
B_x	= 10 kN	B_z	= 20 kN

Internal force:

1-2	= -10 kN	2-3	= 10 kN
3-4	= 10 kN	3-1	= -14 kN
2-4	=-14 kN		

Appendix B

$\lambda_1 = 2350{,}18$

$$\begin{bmatrix} 3926204 - 319{,}2 * 2350{,}18 & -1963102 \\ -1963102 & 1963102 - 319{,}2 * 2350{,}18 \end{bmatrix} \begin{bmatrix} \emptyset_{11} \\ \emptyset_{21} \end{bmatrix} = \begin{bmatrix} 0 \\ 0 \end{bmatrix}$$

$$\begin{bmatrix} 3176026{,}544 * \emptyset_{11} - 1963102 * \emptyset_{21} = 0 \\ -1963102 * \emptyset_{11} + 1212924{,}544 * \emptyset_{21} = 0 \end{bmatrix}, if\ \emptyset_{21} = 1, then\ \emptyset_{11} = 0{,}618$$

$$\emptyset_1 = \begin{bmatrix} 0{,}618 \\ 1 \end{bmatrix}$$

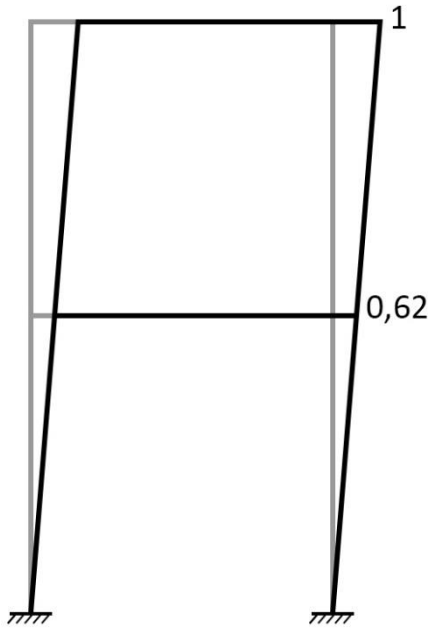

$\lambda_1 = 16103{,}88$

$$\begin{bmatrix} 3926204 - 319{,}2 * 16103{,}88 & -1963102 \\ -1963102 & 1963102 - 319{,}2 * 16103{,}88 \end{bmatrix} \begin{bmatrix} \emptyset_{12} \\ \emptyset_{22} \end{bmatrix} = \begin{bmatrix} 0 \\ 0 \end{bmatrix}$$

$$\begin{bmatrix} -5136932{,}496 * \emptyset_{12} - 1963102 * \emptyset_{22} = 0 \\ -1963102 * \emptyset_{12} - 3177256{,}496 * \emptyset_{22} = 0 \end{bmatrix}, if\ \emptyset_{22} = 1, then\ \emptyset_{12} = -1{,}618$$

$$\emptyset_2 = \begin{bmatrix} -1{,}618 \\ 1 \end{bmatrix}$$

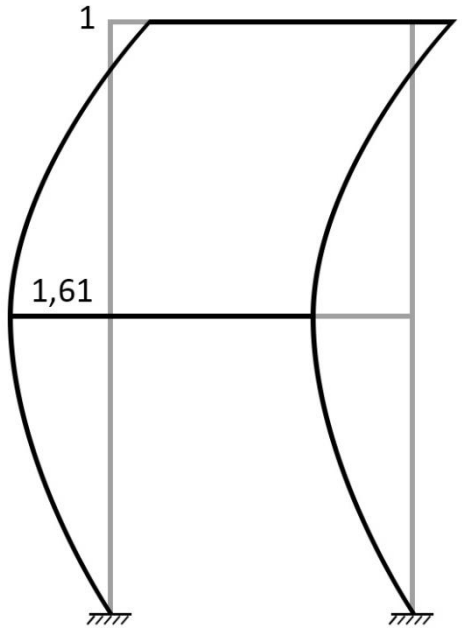

Appendix C

1. Basisvindhastigheten

C_{dir}	1	-
C_{season}	1	-
Vb,0	26	m/s
V_b	26	m/s

$$v_b = c_{dir} \cdot c_{season} \cdot v_{b,0} \quad (4.1)$$

der

v_b er basisvindhastigheten, definert som funksjon av vindretning og årstid for høyden 10 m over bakken og terrengkategori II

$v_{b,0}$ er referansevindhastigheten, se (1)P

c_{dir} er retningsfaktoren, se merknad 2

c_{season} er årstidsfaktoren, se merknad 3.

MERKNAD 2 Verdien av retningsfaktoren c_{dir} for forskjellige vindretninger kan angis i det nasjonale tillegget. Anbefalt verdi er 1,0.

MERKNAD 3 Verdien for årstidsfaktoren, c_{season}, kan angis i det nasjonale tillegget. Anbefalt verdi er 1,0.

2. Basisvindhastighetstrykket

ρ	1,25	kg/m3
Vb	26	m/s
qb	422,5	

$$q_b = \frac{1}{2} \cdot \rho \cdot v_b^2 \quad (4.10)$$

MERKNAD 2 Verdiene for ρ kan angis i det nasjonale tillegget. Anbefalt verdi er 1,25 kg/m^3.

3. Vindkasthastighetstrykket

Z, m	Ce (z)	qb	qp
10	1,2	422,5	507,00
20	1,65	422,5	697,13
30	1,95	422,5	823,88
40	2,15	422,5	908,38
50	2,35	422,5	992,88
60	2,5	422,5	1056,25
70	2,65	422,5	1119,63

80	2,75	422,5	1161,88
90	2,85	422,5	1204,13
100	2,95	422,5	1246,38
110	3,02	422,5	1275,95
120	3,1	422,5	1309,75
130	3,18	422,5	1343,55
140	3,25	422,5	1373,13
150	3,32	422,5	1402,70
160	3,39	422,5	1432,28
170	3,45	422,5	1457,63
180	3,5	422,5	1478,75
190	3,57	422,5	1508,33
200	3,63	422,5	1533,68

$$q_p(z) = \left[1 + 7 \cdot I_v(z)\right] \cdot \frac{1}{2} \cdot \rho \cdot v_m^2(z) = c_e(z) \cdot q_b \qquad (4.8)$$

der

ρ er lufttettheten, som avhenger av høyde, temperatur og barometertrykk som kan forventes i området når det er sterk vind

$c_e(z)$ er eksponeringsfaktoren gitt i ligning (4.9)

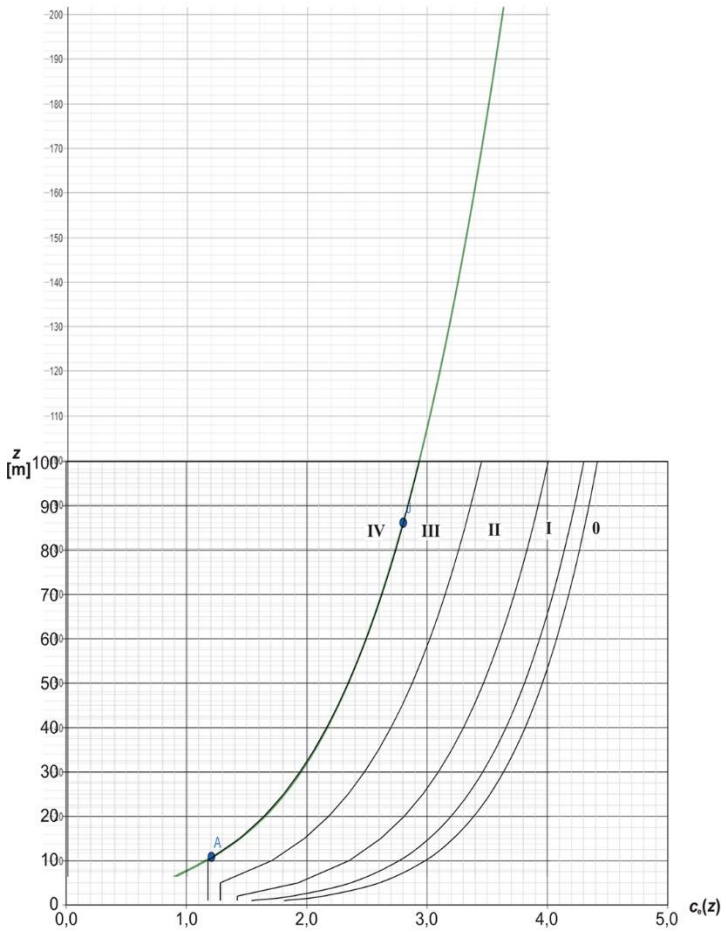

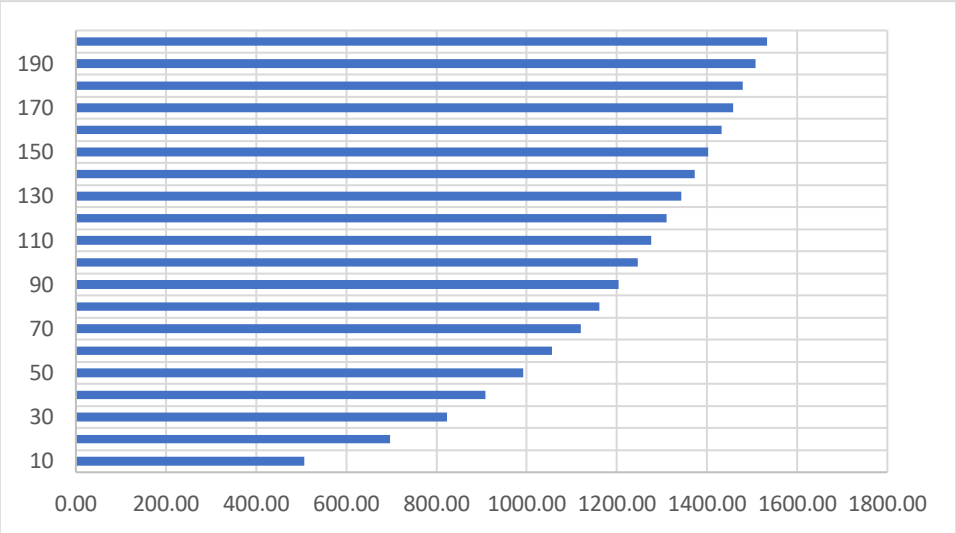

4. Utvendige formfaktorer, Sone			
A	B	D	E
-1,2	-0,8	0,8	-0,7

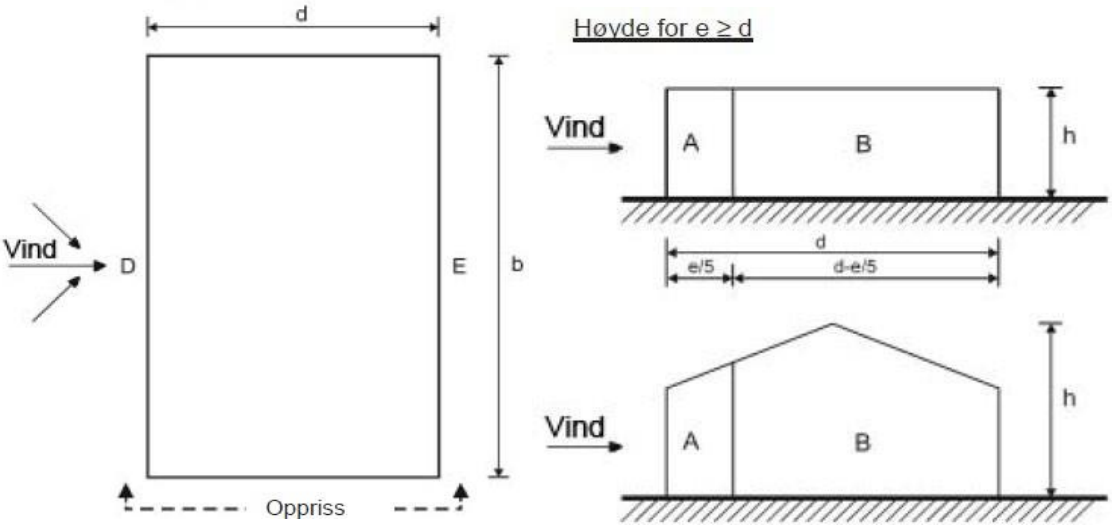

5. Vindtrykk på overflater

Z, m	A	B	D	E
10	-608,40	-405,60	405,60	-354,90
20	-836,55	-557,70	557,70	-487,99
30	-988,65	-659,10	659,10	-576,71
40	-1090,05	-726,70	726,70	-635,86
50	-1191,45	-794,30	794,30	-695,01
60	-1267,50	-845,00	845,00	-739,38
70	-1343,55	-895,70	895,70	-783,74
80	-1394,25	-929,50	929,50	-813,31
90	-1444,95	-963,30	963,30	-842,89
100	-1495,65	-997,10	997,10	-872,46
110	-1531,14	-1020,76	1020,76	-893,17
120	-1571,70	-1047,80	1047,80	-916,83
130	-1612,26	-1074,84	1074,84	-940,49
140	-1647,75	-1098,50	1098,50	-961,19
150	-1683,24	-1122,16	1122,16	-981,89
160	-1718,73	-1145,82	1145,82	-1002,59
170	-1749,15	-1166,10	1166,10	-1020,34
180	-1774,50	-1183,00	1183,00	-1035,13
190	-1809,99	-1206,66	1206,66	-1055,83
200	-1840,41	-1226,94	1226,94	-1073,57

(1) Vindtrykket som virker på de utvendige flatene, w_e, bestemmes fra ligning (5.1).

$$w_e = q_p(z_e) \cdot c_{pe} \qquad (5.1)$$

Ulike variabler for å finne dynamsik faktor										
s (meter)	Ih	gv	Bs	Lh	Hs	na	gR	N	S	Et
10	0,342	3,4	0,641	179,75	1,0025	0,121	3,126	1,809	0,04761	0,0606
20	0,342	3,4	0,653	179,75	1,01	0,121	3,126	1,809	0,04761	0,0606
30	0,342	3,4	0,664	179,75	1,0225	0,121	3,126	1,809	0,04761	0,0606
40	0,285	3,4	0,676	179,75	1,04	0,121	3,126	1,647	0,05469	0,0644
50	0,27	3,4	0,689	179,75	1,0625	0,121	3,126	1,604	0,05682	0,0656
60	0,248	3,4	0,702	179,75	1,09	0,121	3,126	1,542	0,06018	0,0673
70	0,248	3,4	0,715	179,75	1,1225	0,121	3,126	1,542	0,06018	0,0673
80	0,233	3,4	0,729	179,75	1,16	0,121	3,126	1,499	0,06264	0,0685
90	0,233	3,4	0,743	179,75	1,2025	0,121	3,126	1,499	0,06264	0,0685
100	0,233	3,4	0,757	179,75	1,25	0,121	3,126	1,499	0,06264	0,0685
110	0,233	3,4	0,771	179,75	1,3025	0,121	3,126	1,499	0,06264	0,0685
120	0,233	3,4	0,786	179,75	1,36	0,121	3,126	1,499	0,06264	0,0685
130	0,233	3,4	0,800	179,75	1,4225	0,121	3,126	1,499	0,06264	0,0685
140	0,233	3,4	0,815	179,75	1,49	0,121	3,126	1,499	0,06264	0,0685
150	0,233	3,4	0,828	179,75	1,5625	0,121	3,126	1,499	0,06264	0,0685

160	0,196	3,4	0,841	179,75	1,64	0,121	3,126	1,394	0,06942	0,0719
170	0,196	3,4	0,852	179,75	1,7225	0,121	3,126	1,394	0,06942	0,0719
180	0,196	3,4	0,861	179,75	1,81	0,121	3,126	1,394	0,06942	0,0719
190	0,196	3,4	0,867	179,75	1,9025	0,121	3,126	1,394	0,06942	0,0719
200	0,196	3,4	0,869	179,75	2	0,121	3,126	1,394	0,06942	0,0719

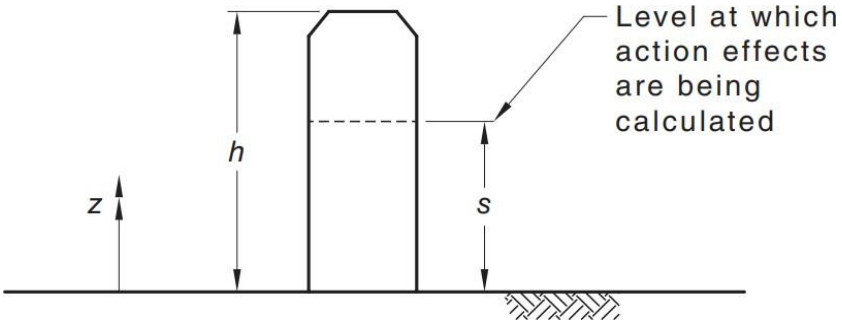

s = height of the level at which action effects are calculated for a structure

h = average roof height of a structure above the ground, or height to the top of a tower

I_h = turbulence intensity, obtained from Table 6.1 by setting $z = h$

g_v = peak factor for the upwind velocity fluctuations, which shall be taken as 3.4

B_S = background factor, which is a measure of the slowly varying background component of the fluctuating response, caused by low-frequency wind speed variations, given by Equation 6.2(2):

$$B_S = \frac{1}{1+\frac{\sqrt{0.26(h-s)^2+0.46b_{sh}^2}}{L_h}} \qquad 6.2(2)$$

where b_{sh} is the average breadth of the structure between heights s and h

L_h = a measure of the integral turbulence length scale at height h in metres, given by Equation 6.2(3):

$$= 85(h/10)^{0.25} \qquad 6.2(3)$$

H_S = height factor for the resonant response which equals $1 + (s/h)^2$

g_R = peak factor for resonant response (10 min period) given by Equation 6.2(4):

$$= \sqrt{1.2+2\log_e(600n_a)} \qquad 6.2(4)$$

S = size reduction factor given by Equation 6.2(5), where n_a is first mode natural frequency of vibration of a structure in the along-wind direction in hertz and b_{0h} is the average breadth of the structure between heights 0 and h:

$$\frac{1}{\left[1+\frac{3.5n_a h(1+g_v I_h)}{V_{des,\theta}}\right]\left[1+\frac{4n_a b_{0h}(1+g_v I_h)}{V_{des,\theta}}\right]} \qquad 6.2(5)$$

E_t = (π/4) times the spectrum of turbulence in the approaching wind stream, given by Equation 6.2(6):

$$\frac{\pi N}{\left(1+70.8N^2\right)^{5/6}} \qquad 6.2(6)$$

where

N = reduced frequency (non-dimensional)

= $n_a L_h \left[1+\left(g_v I_h\right)\right] / V_{des,\theta}$

n_a = first mode natural frequency of vibration of a structure in the along-wind direction in Hertz

$V_{des,\theta}$ = building design wind speed determined at the building height, h (see Clause 2.3)

ζ = ratio of structural damping to critical damping of a structure

NOTE 1 For structural damping in structures for ultimate limit states, values of ζ should be—

(a) for steel structures: 0.015 to 0.02 of critical; and

Dynamisk faktor	
s (meter)	Ih
10	0,928
20	0,933
30	0,938
40	0,960
50	0,971
60	0,984
70	0,991
80	1,003
90	1,010
100	1,018
110	1,026
120	1,034
130	1,043
140	1,052
150	1,060
160	1,081
170	1,089
180	1,097
190	1,105

Vindtrykk med dynamisk faktor				
Z, m	A	B	D	E
10	-564,44	-376,29	376,29	-329,26
20	-780,21	-520,14	520,14	-455,12
30	-927,32	-618,21	618,21	-540,94
40	-1046,65	-697,77	697,77	-610,55
50	-1156,70	-771,13	771,13	-674,74
60	-1247,56	-831,70	831,70	-727,74
70	-1331,30	-887,53	887,53	-776,59
80	-1398,20	-932,14	932,14	-815,62
90	-1459,66	-973,11	973,11	-851,47
100	-1522,40	-1014,93	1014,93	-888,06
110	-1570,82	-1047,21	1047,21	-916,31
120	-1625,51	-1083,67	1083,67	-948,21
130	-1681,25	-1120,83	1120,83	-980,73
140	-1732,63	-1155,08	1155,08	-1010,70
150	-1784,74	-1189,82	1189,82	-1041,10
160	-1857,36	-1238,24	1238,24	-1083,46
170	-1905,18	-1270,12	1270,12	-1111,35
180	-1947,36	-1298,24	1298,24	-1135,96
190	-2000,24	-1333,50	1333,50	-1166,81

$$C_{dyn} = \frac{1 + 2I_h \sqrt{g_v{}^2 B_S + \frac{H_s g_R{}^2 S E_t}{\zeta}}}{(1 + 2g_v I_h)} \qquad 6.2(1)$$

Appendix D

The data given in this appendix is limited from 0 to 10 seconds.

$$\bar{q} = \frac{1}{2}\rho U^2(z)\, C_D$$

	25 m	75 m	125 m	175 m	
ρ	1,25	1,25	1,25	1,25	[kg/m^3]
U	16,4	21,6	24,5	26,7	[m/s]
C_D	1,4	1,4	1,4	1,4	
q	353,01	612,36	787,83	935,67	[N/m^2]

u (t) from the wind simulator "NatHaz On-line Wind Simulator"

Second	Section 1	Section 2	Section 3	Section 4	Section 5	Section 6	Section 7	Section 8
0	0,00	0,00	0,00	0,00	0,00	0,00	0,00	0,00
0,25	-6,75	-4,63	4,91	3,87	-1,69	-4,46	0,33	1,31
0,5	-6,96	-5,63	4,71	1,92	-1,37	-5,85	0,66	-0,25
0,75	-7,49	-4,05	4,52	1,50	-0,08	-3,94	1,27	-1,33
1	-6,55	-5,37	6,61	3,11	-1,37	-3,79	1,93	-1,09
1,25	-6,54	-5,15	6,41	3,15	-1,68	-3,87	1,05	-0,85
1,5	-6,90	-3,29	5,88	1,96	-1,04	-2,43	0,09	-0,35
1,75	-4,46	-4,13	6,51	0,98	-0,63	-2,96	0,39	0,06
2	-2,28	-3,37	7,15	2,29	-0,52	-3,98	0,06	0,06
2,25	0,23	-3,96	4,90	1,99	-0,16	-4,84	-1,04	-0,15
2,5	0,71	-5,83	5,30	2,04	-0,62	-4,85	-1,19	-0,84
2,75	0,22	-5,65	3,89	3,91	0,15	-3,90	-0,84	-1,57
3	-0,13	-4,40	3,68	4,11	0,51	-4,71	-0,75	-0,52
3,25	-1,70	-4,52	1,86	2,83	-0,49	-3,39	-1,01	-1,99
3,5	-1,99	-3,46	2,96	2,19	-2,20	-3,34	-2,56	-1,27
3,75	-2,12	-4,18	2,78	1,85	-1,68	-4,21	-2,53	-0,39
4	-2,02	-5,15	3,41	3,22	-0,82	-4,03	-1,18	-1,20
4,25	-1,95	-4,22	3,03	2,41	-1,96	-3,22	-2,33	-1,14
4,5	-1,50	-3,28	4,25	1,35	-2,53	-3,50	-1,57	-1,70
4,75	0,62	-0,90	2,66	2,62	-2,84	-2,75	-0,45	-2,04
5	1,70	-0,92	2,04	2,76	-3,93	-2,86	-0,33	-2,14
5,25	3,33	-1,37	1,99	2,86	-5,19	-4,37	-0,27	-1,08
5,5	2,74	-2,83	2,46	3,60	-6,36	-4,27	-0,76	-1,79
5,75	3,12	-3,33	3,16	3,09	-5,67	-4,09	-1,74	-2,50
6	1,97	-1,72	2,77	1,32	-4,04	-4,28	-1,24	-0,49
6,25	1,24	-1,17	0,81	2,85	-4,96	-4,57	-0,24	-1,40
6,5	4,02	0,68	-0,85	1,36	-5,94	-4,96	-0,44	-1,48
6,75	6,45	1,82	-0,12	1,72	-4,56	-3,96	0,37	0,00
7	5,02	2,98	-0,11	1,39	-3,66	-2,74	1,52	-1,00
7,25	4,38	4,11	0,01	1,14	-3,49	-3,91	1,97	0,88
7,5	4,49	3,94	-1,27	1,36	-3,93	-5,34	1,84	1,53
7,75	3,31	5,39	-0,25	-0,19	-4,01	-4,98	1,50	1,81
8	4,51	4,54	-0,36	-0,74	-4,01	-4,75	1,11	1,20
8,25	4,86	4,09	-0,16	-0,90	-4,92	-4,29	0,90	1,74
8,5	5,63	2,62	-0,68	1,25	-3,96	-3,30	-0,79	1,35
8,75	5,36	3,70	-1,01	0,66	-3,60	-2,73	-0,53	1,76
9	6,46	5,27	-0,84	1,08	-2,59	-3,70	0,22	1,42
9,25	4,64	5,79	-0,28	1,96	-1,78	-3,87	-0,04	2,38
9,5	5,38	4,20	-0,31	2,51	-1,72	-4,98	-0,40	0,29
9,75	4,92	4,89	-0,40	3,08	-1,36	-4,19	-0,04	0,94
10	3,59	6,09	-0,56	2,51	-1,58	-4,55	0,30	0,89

$$q = \frac{1}{2}\rho u\,(x, y, z, t)\,U\,(z)\,C_D$$

Second	Section 1	Section 2	Section 3	Section 4	Section 5	Section 6	Section 7	Section 8
0	0,00	0,00	0,00	0,00	0,00	0,00	0,00	0,00
0,25	-96,82	-66,42	70,39	55,56	-24,19	-64,04	4,74	18,82
0,5	-99,87	-80,75	67,63	27,49	-19,59	-83,92	9,44	-3,58
0,75	-107,49	-58,09	64,85	21,58	-1,08	-56,48	18,26	-19,05
1	-94,06	-77,01	94,88	44,63	-19,62	-54,40	27,75	-15,65
1,25	-93,87	-73,84	92,00	45,25	-24,05	-55,53	15,05	-12,24
1,5	-99,08	-47,24	84,43	28,12	-14,91	-34,86	1,29	-5,04
1,75	-63,98	-59,33	93,35	14,02	-9,03	-42,53	5,53	0,84
2	-32,66	-48,38	102,62	32,84	-7,45	-57,18	0,89	0,89
2,25	3,36	-56,82	70,27	28,52	-2,23	-69,49	-14,86	-2,21
2,5	10,12	-83,65	76,06	29,34	-8,86	-69,58	-17,01	-12,11
2,75	3,13	-81,08	55,81	56,17	2,09	-55,94	-11,99	-22,56
3	-1,83	-63,13	52,86	58,96	7,30	-67,57	-10,77	-7,48
3,25	-24,42	-64,88	26,68	40,64	-7,10	-48,58	-14,51	-28,62
3,5	-28,58	-49,58	42,52	31,38	-31,62	-47,91	-36,68	-18,28
3,75	-30,37	-60,02	39,91	26,61	-24,06	-60,45	-36,26	-5,65
4	-28,99	-73,92	48,90	46,24	-11,80	-57,84	-16,88	-17,28
4,25	-28,03	-60,51	43,54	34,57	-28,12	-46,18	-33,44	-16,30
4,5	-21,49	-47,11	61,01	19,31	-36,37	-50,25	-22,54	-24,42
4,75	8,95	-12,98	38,17	37,53	-40,79	-39,45	-6,49	-29,28
5	24,44	-13,23	29,24	39,64	-56,45	-40,99	-4,71	-30,68
5,25	47,82	-19,61	28,49	41,01	-74,41	-62,65	-3,91	-15,43
5,5	39,35	-40,66	35,29	51,65	-91,23	-61,32	-10,86	-25,69
5,75	44,76	-47,85	45,41	44,37	-81,39	-58,73	-24,94	-35,86
6	28,20	-24,70	39,70	18,88	-57,91	-61,36	-17,75	-7,02
6,25	17,80	-16,75	11,57	40,92	-71,22	-65,58	-3,39	-20,06
6,5	57,62	9,79	-12,24	19,57	-85,17	-71,23	-6,33	-21,25
6,75	92,55	26,12	-1,72	24,64	-65,41	-56,82	5,31	-0,01
7	71,98	42,77	-1,53	19,97	-52,54	-39,34	21,75	-14,37
7,25	62,92	59,03	0,08	16,38	-50,01	-56,13	28,30	12,63
7,5	64,46	56,56	-18,20	19,58	-56,45	-76,62	26,34	21,93
7,75	47,44	77,30	-3,57	-2,70	-57,54	-71,47	21,50	25,93
8	64,68	65,10	-5,22	-10,62	-57,61	-68,20	15,91	17,20
8,25	69,67	58,74	-2,27	-12,88	-70,55	-61,51	12,97	25,03
8,5	80,82	37,53	-9,76	17,93	-56,81	-47,39	-11,38	19,37
8,75	76,90	53,10	-14,48	9,43	-51,70	-39,17	-7,57	25,27
9	92,77	75,58	-12,09	15,55	-37,17	-53,06	3,10	20,38
9,25	66,57	83,06	-4,02	28,18	-25,50	-55,57	-0,52	34,17
9,5	77,18	60,25	-4,48	36,06	-24,63	-71,49	-5,78	4,12
9,75	70,58	70,22	-5,80	44,26	-19,48	-60,10	-0,53	13,51
10	51,58	87,44	-8,02	35,99	-22,61	-65,25	4,29	12,72

$$\bar{q} = \frac{1}{2}\rho U^2(z) C_D$$

+

$$q = \frac{1}{2}\rho u(x,y,z,t) U(z) C_D$$

Second	Section 1	Section 2	Section 3	Section 4	Section 5	Section 6	Section 7	Section 8
0	0,35	0,35	0,61	0,61	0,79	0,79	0,94	0,94
0,25	0,26	0,29	0,68	0,67	0,76	0,72	0,94	0,95
0,5	0,25	0,27	0,68	0,64	0,77	0,70	0,95	0,93
0,75	0,25	0,29	0,68	0,63	0,79	0,73	0,95	0,92
1	0,26	0,28	0,71	0,66	0,77	0,73	0,96	0,92
1,25	0,26	0,28	0,70	0,66	0,76	0,73	0,95	0,92
1,5	0,25	0,31	0,70	0,64	0,77	0,75	0,94	0,93
1,75	0,29	0,29	0,71	0,63	0,78	0,75	0,94	0,94
2	0,32	0,30	0,71	0,65	0,78	0,73	0,94	0,94
2,25	0,36	0,30	0,68	0,64	0,79	0,72	0,92	0,93
2,5	0,36	0,27	0,69	0,64	0,78	0,72	0,92	0,92
2,75	0,36	0,27	0,67	0,67	0,79	0,73	0,92	0,91
3	0,35	0,29	0,67	0,67	0,80	0,72	0,92	0,93
3,25	0,33	0,29	0,64	0,65	0,78	0,74	0,92	0,91
3,5	0,32	0,30	0,65	0,64	0,76	0,74	0,90	0,92
3,75	0,32	0,29	0,65	0,64	0,76	0,73	0,90	0,93
4	0,32	0,28	0,66	0,66	0,78	0,73	0,92	0,92
4,25	0,32	0,29	0,66	0,65	0,76	0,74	0,90	0,92
4,5	0,33	0,31	0,67	0,63	0,75	0,74	0,91	0,91
4,75	0,36	0,34	0,65	0,65	0,75	0,75	0,93	0,91
5	0,38	0,34	0,64	0,65	0,73	0,75	0,93	0,90
5,25	0,40	0,33	0,64	0,65	0,71	0,73	0,93	0,92
5,5	0,39	0,31	0,65	0,66	0,70	0,73	0,92	0,91
5,75	0,40	0,31	0,66	0,66	0,71	0,73	0,91	0,90
6	0,38	0,33	0,65	0,63	0,73	0,73	0,92	0,93
6,25	0,37	0,34	0,62	0,65	0,72	0,72	0,93	0,92
6,5	0,41	0,36	0,60	0,63	0,70	0,72	0,93	0,91
6,75	0,45	0,38	0,61	0,64	0,72	0,73	0,94	0,94
7	0,42	0,40	0,61	0,63	0,74	0,75	0,96	0,92
7,25	0,42	0,41	0,61	0,63	0,74	0,73	0,96	0,95
7,5	0,42	0,41	0,59	0,63	0,73	0,71	0,96	0,96
7,75	0,40	0,43	0,61	0,61	0,73	0,72	0,96	0,96
8	0,42	0,42	0,61	0,60	0,73	0,72	0,95	0,95
8,25	0,42	0,41	0,61	0,60	0,72	0,73	0,95	0,96
8,5	0,43	0,39	0,60	0,63	0,73	0,74	0,92	0,96
8,75	0,43	0,41	0,60	0,62	0,74	0,75	0,93	0,96
9	0,45	0,43	0,60	0,63	0,75	0,73	0,94	0,96
9,25	0,42	0,44	0,61	0,64	0,76	0,73	0,94	0,97
9,5	0,43	0,41	0,61	0,65	0,76	0,72	0,93	0,94
9,75	0,42	0,42	0,61	0,66	0,77	0,73	0,94	0,95
10	0,40	0,44	0,60	0,65	0,77	0,72	0,94	0,95

Factors utilised in FEM-design for excitation force

Second	Section 1	Section 2	Section 3	Section 4	Section 5	Section 6	Section 7	Section 8
0	0,75	0,71	0,84	0,85	0,89	0,89	0,88	0,91
0,25	0,55	0,58	0,94	0,92	0,87	0,82	0,89	0,93
0,5	0,54	0,55	0,93	0,89	0,87	0,79	0,89	0,91
0,75	0,52	0,59	0,93	0,88	0,89	0,82	0,90	0,89
1	0,55	0,56	0,97	0,91	0,87	0,83	0,91	0,89
1,25	0,55	0,56	0,97	0,91	0,87	0,82	0,90	0,90
1,5	0,54	0,62	0,96	0,89	0,88	0,85	0,89	0,90
1,75	0,62	0,59	0,97	0,87	0,88	0,84	0,89	0,91
2	0,68	0,61	0,98	0,89	0,89	0,82	0,89	0,91
2,25	0,76	0,60	0,94	0,89	0,89	0,81	0,87	0,91
2,5	0,77	0,54	0,94	0,89	0,88	0,81	0,87	0,90
2,75	0,76	0,55	0,92	0,92	0,90	0,82	0,87	0,89
3	0,75	0,58	0,91	0,93	0,90	0,81	0,87	0,90
3,25	0,70	0,58	0,88	0,90	0,89	0,83	0,87	0,88
3,5	0,69	0,61	0,90	0,89	0,86	0,83	0,85	0,89
3,75	0,69	0,59	0,89	0,88	0,87	0,82	0,85	0,90
4	0,69	0,56	0,91	0,91	0,88	0,82	0,87	0,89
4,25	0,69	0,59	0,90	0,89	0,86	0,84	0,85	0,89
4,5	0,71	0,62	0,92	0,87	0,85	0,83	0,86	0,89
4,75	0,77	0,69	0,89	0,90	0,85	0,84	0,88	0,88
5	0,80	0,68	0,88	0,90	0,83	0,84	0,88	0,88
5,25	0,85	0,67	0,88	0,90	0,81	0,82	0,88	0,89
5,5	0,84	0,63	0,89	0,92	0,79	0,82	0,87	0,88
5,75	0,85	0,61	0,90	0,91	0,80	0,82	0,86	0,87
6	0,81	0,66	0,89	0,87	0,83	0,82	0,87	0,90
6,25	0,79	0,68	0,86	0,90	0,81	0,81	0,88	0,89
6,5	0,87	0,73	0,82	0,87	0,80	0,81	0,88	0,89
6,75	0,95	0,76	0,84	0,88	0,82	0,82	0,89	0,91
7	0,90	0,80	0,84	0,87	0,84	0,84	0,90	0,90
7,25	0,89	0,83	0,84	0,87	0,84	0,82	0,91	0,92
7,5	0,89	0,83	0,82	0,87	0,83	0,80	0,91	0,93
7,75	0,85	0,87	0,84	0,84	0,83	0,81	0,90	0,93
8	0,89	0,84	0,83	0,83	0,83	0,81	0,90	0,93
8,25	0,90	0,83	0,84	0,83	0,81	0,82	0,90	0,93
8,5	0,92	0,79	0,83	0,87	0,83	0,83	0,87	0,93
8,75	0,92	0,82	0,82	0,86	0,84	0,84	0,88	0,93
9	0,95	0,86	0,82	0,87	0,85	0,83	0,89	0,93
9,25	0,89	0,88	0,83	0,89	0,87	0,82	0,88	0,94
9,5	0,92	0,83	0,83	0,90	0,87	0,81	0,88	0,91
9,75	0,90	0,85	0,83	0,91	0,87	0,82	0,88	0,92
10	0,86	0,89	0,83	0,90	0,87	0,81	0,89	0,92